Nanobiology:
Halting Steps into a Portion of Richard Feynman's Vision

Thesis by
Charles F. Spence

In Partial Fulfillment of the requirements
for the Degree of
Doctor of Philosophy

California Institute of Technology
Pasadena, California

2002
(Submitted May 2002)

Acknowledgements

No man walks alone, but trying to write your thesis in a month is a lonely experience. It is difficult to imagine how I would have gotten this far without the help of the people listed here. The most significant person in my life and who enabled me to earn a degree at this school is Bonnie. If she had not helped me face how important this was to me and encouraged me to apply to school I would not have the opportunity to write on these pages. I never thought I would be blessed with finding a true kindred spirit let alone such a wonderful one. Her help through all the terror of the graduate experience has been instrumental. I just wish we did not have so many miles to go before we sleep.

As for work colleagues and companions on this educational journey I have also been blessed. Now doctors Hou-Pu Chou and Anne Fu were wonderful to work with on the cell sorter and DNA sizer. Without their diligent and insightful effort these projects would not have even gotten off the ground let alone achieve the end results. I thank them for letting me share in the success. I am indebted to Robert Bao. Without him solving a significant amount of the biochemistry problems for the RNAP effort my candidacy would have been too entertaining. Vincent Auyeung continued this effort with much diligence and aplomb for which I am also grateful. I doubt this thesis would have happened in time if it were not for Heun Jin Lee. I am incredibly grateful for the sleepless two weeks we spent to get the potential shaping experiment to work. Your insights and quick-change optics were key even if I could not keep track of all of them. The education in recent physics history has also been incredibly useful.

I am also grateful and indebted to Dr. Regina Ragan and Deborah Santamore for the help with classes and studying till the wee hours. In this category I would also like to thank Steve Palm and Hou-Pu. It was very difficult to take classes again after all the years I had been away from school and their help was invaluable.

Finally I must thank professor Stephen Quake for giving me the opportunity to come to this school, tutoring me in quantum mechanics for the summer before I started classes

and the opportunity to work in and to help build up his lab. Along these lines I am also grateful to professors John D. Baldeschwieler and Leroy Hood for their recommendations. In a special category is Professor Scott Fraser. Thank you for the recommendation and the helpful counsel along the way.

Lastly is the broad category of old friends, coworkers, bosses, relatives and acquaintances along the long journey to get to this point. Their influence on me has been profound and hard to completely describe or understand. In an odd way my parents fit in this category. My father passed while I was half way through. Even though our relationship had deteriorated before I got here I wish he could have seen me graduate from this school. On a positive level I think it would have tickled him. Not bad for a kid from the wrong side of the tracks. I never thought I would miss him so much. I thank him for the brains, the freedom in my youth, his valiant fight with his own idiosyncrasies, his decision to do his best by me even though I was probably a problematic surprise to have so late in life, and inadvertently giving me so much fight.

Charles F. Spence
Pasadena, California
May, 2002

Abstract

The advancement of nanotechnology has slightly opened the door for significant applications in biology. These technologies offer the potential to analyze and manipulate biological systems on the single cell and single molecule scales. The ability to analyze biological systems on these scales provides a direct means to reverse engineer multi-cellular organisms by following gene regulation and protein expression from the point of embryo fertilization onward. The need for amplification for standard bulk assays would be eliminated. Significant diagnostic applications would also be possible especially for genetic disorders and viral based diseases. Unfortunately there are still significant hurdles to overcome so that this potential can be realized and the technology can be used in a more robust manner. This thesis describes a significant effort for advancing the state of the nanoscale art. Specifically: the design and development of microfluidic devices for manipulating and analyzing DNA and *E. coli* cells, and the design and development of a modular DSP based feedback controller for scanned probe microscope (SPM) and nanomanipulator applications. In addition two significant applications of the DSP controller are presented: controlling the Q of an SPM microcantilever and sculpting the force potential of optical tweezers on the nanometer scale. With the microfluidic devices described here single DNA molecules from 2-200 kbp were sized and sorted with equivalent or better resolution than gel electrophoresis methods and in less time. Using similar techniques a disposable fluorescent cell sorter was developed and demonstrated by sorting green fluorescent protein *E. coli* cells from wild type cells. Using the DSP electronics the Q of an SPM microcantilever was controlled over three orders of magnitude using force feedback techniques. The Q can be lowered to one, enabling high speed tapping mode scanning ten times faster than possible with the natural Q. Using the same basic DSP electronics the potential of optical tweezers was arbitrarily shaped with 10 nm edge resolution. Advisor: Prof. Stephen Quake.

Table of Contents

List of Figures

List of Tables

Preamble

Welcome to my thesis attempt. Welcome to the document that is part of my get out of jail free card. That at least five wardens of the institution at which I am a resident have the obligation of slogging through. No matter how hard I may try to make the subject matter interesting, unless you are really interested, it will be a bit of a chore to read through. A document that few other than the wardens or people who care will read. Nevertheless its purpose is to inform you, the reader, about the results of the work I have done which has hopefully contributed to expanding our knowledge of the world around us. It is also hoped that I have made some significant contribution to Science and specifically to the field of Applied Physics, more specifically to Applied Biophysics.

Chapter 1

Background and Motivation

1.1 Introduction

I think it can be said with little qualification that we have experienced an explosive growth of knowledge in the field of biology within at least the last 50 years. It could be argued that this pace of advancement goes back 90 years when the Rockefeller Foundation began to focus its philanthropic effort towards biological research [1]. A comparison between the discoveries and theoretical insights in physics at the first half of the last century and the rate of discovery in biology during the last half can be easily made. However, as with most increased understanding of things, with each new answer more questions are raised and the teasing of greater possibilities pushes the drive for more until you hit a wall. In physics, this has been manifested by what appears to me the dramatic difference between current theoretical work and the ability to experimentally verify theoretical insights some that are over 50 years old. Gravitational theory is an example. The need for instrumentation advances is continually needed in this field. Early on the instrumentation for physics appears to have developed in step with theoretical development. Much of the instrumentation seemed to be the direct result of the insight gained through the theory.

I argue that biology has always been plagued by the need for better instrumentation. However, early on a great deal of knowledge was gained by simple manipulations. Gregor Mendel's insightful and diligent work on inheritance with the garden pea is a great example. Unfortunately it seems that he set a standard and methodology that has been very hard to deviate from. Biology has advanced tremendously by methodical experiments performed with apparently crude tools (the petri dish will probably always be with us). Max Delbrück's work on the phage is another example. However, would the discovery or clarification of the bacterial basis for many diseases have happened without the microscope? If so, how much longer would it have taken? It would seem

that advances in instrumentation have greatly speeded the rate of discovery in biology. The difficulty is the divergence of interest and background needed.

Having been blessed with a profound interest in instrumentation development and its physical underpinnings and repeated stumbling into the biological community, I have the rare opportunity to make some contributions to both fields. This thesis is an attempt to elucidate some of these contributions for your review and more importantly, hopefully add to the knowledge base.

The problem with instrumentation is that on its own it is meaningless. Although the author has a strong interest in the design and development of instrumentation, he is keenly aware that it must be done in an applied context to merit the significant time of development. It otherwise becomes a monument. The laser initially was somewhat an example. The main drive of the development of the first lasers was mainly to demonstrate maser action at optical wavelengths. Dr. Maiman believed he had the correct insights to obtaining laser action with a flash lamp ruby rod [2]. The immediate interest was as a demonstration and to further elucidate the physics. The popular concept of using lasers as weapons was one of the earliest applications discussed but decidedly unrealistic. It is doubtful that Maiman believed his device would be capable of generating that amount of power. Because the obvious industrial and military applications were not possible with earlier lasers, it has been said the laser was a device looking for an application.

My thesis work has focused on three areas of instrumentation development and application towards biology and biophysical problems: microfluidics, optical detectors and methods, and the control and detection electronics needed for both.

Biology seems to continually need the ability to manipulate small things especially bio-molecules. Demonstrations such as spelling “IBM” with Xenon atoms inspire the imagination [3] (a high-tech atomic graffiti). One would like the ability to apply such tools to biological applications. Unfortunately, limitations exist such as the high vacuum required in the above experiment. Biological molecules tend to loose their shape and

functionality under such harsh conditions. However, microfluidics offers an advancement towards this end. Professor Quake's lab has been instrumental in advancing this technology towards biological applications. It demands an interdisciplinary approach to understand all the details involved to get it to work.

A more realistic tease offered by these tools of chemistry and physics is the possibility of picking, manipulating, and analyzing cells individually. The thought argument goes that you find the cell of interest and on that cell alone perform standard preparative techniques for analyzing its DNA or protein content. But where does the physics come into this? Well, how are you going to detect things? What can you detect? How much do you need? With what mechanisms can you manipulate these cells?

A great deal of biological knowledge has been derived from bulk assays. Sanger DNA sequencing and Edmund degradation protein sequencing, protein crystallography, southern blots, and an assortment of electrophoresis gel assays to name a few all rely on a relatively large number of hopefully similar molecules to obtain enough signal to make a measurement. Although a tremendous amount of information about the function of biological systems has been learned with these types of methods, they have two specific constraints, as viewed by this author, that seem to raise fundamental questions. The first is the requirement to either amplify the molecule you are looking for or require the synchronization of disjoint cellular machinery (such as colonies of *E. coli*) to obtain enough product so that the assay can be performed. It many ways this puts a tremendous constraint on experiment design and usually dramatically increases the time it takes to make a measurement. The other constraint is these techniques do not really let you see directly how cells differ. This is especially important during the first cell divisions in a developing embryo. What differences are significant? What are the cell by cell error rates? When is the average more important? Unfortunately we can only conveniently measure averages.

It has been shown [4] that many of the regulatory functions in a cell are controlled by proteins that exist in a rather low percentage compared to the rest of the cells chemical

machinery. These are the proteins that appear to provide us with the best tools to cure diseases and completely heal traumatic injuries. Obtaining a better understanding of even their mere existence as well as their interactions should greatly speed the rate of progress towards these medical ends. In addition, numerous industrial applications can be addressed. The metabolism of formaldehyde by methanogenic bacteria is an example. Elucidating and being able to manipulate that cellular mechanism could enable easier methods to cleanup formaldehyde waste sites. Other metabolic processes of these types of cells also offer promising methods towards handling other hazardous wastes.

The problem as mentioned above is that these molecules occur in relatively small numbers. Wanting to detect and analyze them on a single-cell basis may be a too aggressive initial approach, but developing techniques to achieve this end should still have immediate beneficial applications. You would need less product for analysis.

So where is this discussion going? Well, I am trying to tease you along the path and provide a relatively short background to the motivation for my graduate education and thesis work. Biology has benefited significantly from many advances in physics. Harold Varmus's talk at the APS Centennial meeting beautifully outlines the tremendous advances enabled by the many marriages of physics and biology [5]. The difficulty with the two fields is that they tend to attract a rather divergent talent pool. Besides the intellectual ego stroke that many who pursue physics desire, I believe an undercurrent motivating their interest in it as a field of study is its seeming tidiness. Reducing the workings of the physical world to a small number of equations is seductive. It affords an illusion of being able to significantly control the world around us.

Biology, on the surface, is a much more fluid animal. It could be argued that the theory of biology is even simpler than physics (DNA is transcribed into RNA, RNA is transcribed into protein). However, I feel that most who enter the field are keenly aware of the staggering complexity of biological systems. It can be argued that our efforts to manipulate have been modest at best. Even the relatively simple virus presents a staggering task to understand a fraction of its inner workings. An experimental

physicist's approach seems to be that of controlling every variable except one and then see how it varies by manipulating a single input at a time. A biologist may love to be able to do that but he is painfully aware that this is generally not realistic. Biology has usually adopts an observational approach. Vary one thing and then see if something stands out that seems to correlate. I believe this tends to attract people to the field that are more willing to shotgun in their experimental approach–a distasteful methodology for one interested in and trained in physics. Biologists seem to be more flexible.

It appears that we are at the crossroads in the many marriages of the fields of biology and physics. There seems to be two undercurrents pushing this. The current development of scientific instrumentation seems to enable a more systematic research in the understanding of biological systems. The ability to manipulate, detect, and analyze single molecules opens up a world of possibilities. It also appeals more to people interested in physics. "... they (physicists) brought to biological problems a quantitative, analytic approach..."[5]. The second, money. An undercurrent scientists seem to ignore or at least portray they are not contaminated by. The investment in biology/ biotechnology is staggering. As a field of research the only other areas that seem to compare at this time are the military, computers, and telecommunications. If you want funding or a job, you should give a serious consideration to how you can apply your talents and abilities in this arena.

The later may have a whiff of cynicism but I prefer to focus on the excitement of the former.

So where does this take us? The world of experimental physics has brought some tantalizing tools to be applied to problems in biology. There is also a world to be investigated regarding the physical characteristics of biological systems and biomolecules. I will not pursue this much. Scannned probe microscopes, optical tweezers, optical detection techniques, and microfluidics appear to be the advancing tools of the trade. I should also mention mass spectrometry and electron microscopy. I would prefer to focus on the first group of instruments because they seem to allow for the development of more affordable instruments. This is another functional problem of tool

development. The less expensive the instrument or technique, the more people can use it and the more opportunities for discovery. However, there is a staggering amount of work to be done to make them useful. The doors that can be opened, tantalizing. Hopefully the following thought experiment will elucidate, but first a little more personal background.

Several years before winning the Nobel Prize in physics, Steve Chu gave a lecture at Caltech on the work in his lab. I had the privilege to attend. Besides presenting what was to be his Nobel-winning work, he showed a video of what I later learned was portions of Steve Quake's work using optical tweezers on DNA. In addition Dr. Chu showed some video segments of capturing and manipulating bacteria with the tweezers. This really captured my imagination as well as the group of nuts that I worked with at the time. An early crude idea was to use a laser tweezers to capture a bacteria and then another to cut out a region of interest. This section of the bacteria could then, using the tweezers, be moved through a sequence of reaction chambers to prep it for some form of analysis such as DNA sequencing.

There are several holes (chasms would be more appropriate) in this idea. One is the resolution possible with lasers for cutting. Another, once you cut something out, the laser trap will probably not be able to contain it. It can also be argued that much of this has been tried with micro-pipettes after heroic effort [6, 7]. Not a robust technique that can be used to analyze large numbers of cells. However, the most significant hurdle appears to be detection limits. How do you sense or analyze the very small quantities of stuff extracted with this technique?

Life is an odd journey. Who would have thought I would be working on ideas and concepts discovered and inspired by that long ago lecture in the lab of the man directly responsible, Steve Quake. I had abandoned thoughts of further pursuits with my interest and abilities with instrumentation in biology when I had the courage to apply for graduate school in applied physics at Caltech. So here I am again pursuing a knowledge base to solve many of the problems with the single cell analyzer and hopefully making scientific

advances towards that end thanks to my advisor, Prof. Stephen Quake, and the applied physics department deciding to take advantage of my unconventional background.

Many of the pieces are falling into place. Photoactive tags could be incorporated into regions of DNA that would allow cutting out a specific stretch of DNA down to a few base pairs. This suggests similar techniques could be applied to proteins. Todd Thorsen in our lab has done extensive work on reverse micelles for containing biochemical reactions. This technique could be used to contain a single bacteria in a small droplet while material is excised from it. Mark Unger, Emil Kartalov, and Ido Braslavsky have pursued extensive work in single fluorescent molecule chemistries and detection which can be applied to detecting the minute quantities of material in a single cell. More importantly has been Dr. Quake's focus on a relatively simple means to produce a micro-chemical factory by combining integrated circuit fabrication techniques with soft lithography via silicone rubber credited to George Whitesides [8]. Lastly, was the development in our lab by Hou-Pu Chou and Mark Unger of a microfluidic valve also using silicone rubber. Other "micro" valves have been developed, but they used the more expensive micromachining methods of the semiconductor industry. But more significantly they could not be easily incorporated into an entire microchemical "chip" unless you designed the entire system using the same expensive fabrication techniques. As a separate unit, its small size would be lost because of the plumbing needed to connect it to anything.

To continue with the development of the thought experiment, I would like to introduce a methodology from the world of developmental biology. It would appear that if you could analyze the expression of genes at different times during embryonic development you could reverse engineer the orchestration of these genes and gain insight into how they could be manipulated. Take a mature cell and inject the proper set of proteins discovered in the developmental process to restart this cellular machinery to generate lets say, for example a liver. It would require the ability to manipulate single cells and isolate its mRNA and DNA. Using the technique of reverse transcription to make cDNA copies of mRNA has so far proved to be more functional than directly monitoring the proteins,

especially at the single-cell level. I believe that we almost have all the pieces for doing this and a portion of my thesis work extended some of these tools.

One of the early hopes of 2-D protein gels was that you could use them to identify proteins that were responsible for a given cellular response to external stresses by subtractive gel analysis. You would run a 2-D gel on a cell line prior to the external stress, apply the stress, and then see what protein spots appeared or disappeared. In the case of cellular development you would just take snap shots of the cell during different times in its development/cell cycle.

There have been several difficulties with this technique. One was getting the gels repeatable enough to easily observe the differences and preferably enable a computer to do it. More importantly the normal method for observing the protein is via silver staining. This tends to damage the protein so that if you want a sample for later analysis, you had to run a second nonstained gel and hope that the protein would be in the same spot as that of the stained gel. Another was even if you could see a difference the quantity of sample needed for analysis was significant. Some reviews of the state of protein analysis can be found in the references [9-11]. Several advances have been made. One is Matrix-Assisted Laser Desorption Ionization Time-Of-Flight Mass Spectrometry (MALDI-TOF MS) scanning of 2-D protein gels directly [12]. The amount of sample is significantly less and you do not need to do staining since it is possible to scan the entire gel in the mass spectrometer. However, this technique has signal limitations due to chemical background and internal calibration requirements in the sample in order to yield higher accuracy. In addition it does not yield any realistic sequence information.

Well, Charles, where does your work fit in all this? Detection and control electronics and the physics which set the limits. In addition, what can be done with existing devices in the profound libraries of the semiconductor manufactures and to a limited extent, determine if there is a semiconductor technology that should be improved or modified to better fit the needs for microchemical factories and detectors.

I am leaving chemistry out of this discussion. I feel safe in saying that much of the work done here is fairly well sequestered in the field of physics. Please do not misinterpret this. Our understandings and insights through chemistry are vital. However, I am pursuing a degree in applied physics. I feel these crossroads present a dramatic opportunity to greatly advance the already profound explosion of knowledge in biology. In some ways understanding the intricacies of biological systems dwarfs efforts to come up with a unified field theory in physics. There is a significant difference. There have been demonstrated techniques which tease us with the possibility of reverse engineering biological machinery enough to really mess around. More significantly, a variation of the more comfortable approach for a physicist, manipulate one variable at a time, seems realizable. How about being able to at least monitor all the variables?

Part II of this thesis describes devices and techniques developed using microfluidics, mechanics and electronics for the detection and manipulation of biological systems and molecules. Specifically a cell sorter, and a DNA sizer, and sorter. All were efforts towards developing technologies for single-cell analysis. The cell sorter is hopefully obvious. The DNA sizer developed techniques and pointed out difficulties in manipulating and detecting single molecules of DNA.

Proposed methods for reverse engineering protein regulation using PDMS microfluidic devices. Basic principle.

1. Need almost the complete genomic sequence of the organism.
2. Create a cDNA library of mRNA. If possible use directly in hybridization experiments. Do not clone. Poly dTs have fluorescent label.
3. Screen cDNA by either sequencing directly using the wonder sequencer or with hybridization array.
4. After exhaustive determination of everything in cDNA library, go back to the genomic database and see what compares with known proteins, intron elucidation, and upstream regulation sequences. How is the gene spread out across the genome. What is known to exist that was not found in cDNA library.
5. Repeat process again but vary cDNA creation conditions.

Tools needed that currently do not exist but seem possible to develop with known technology for achieving the above.

1. DNA sequence hybridization array. This would be large pieces of DNA for very specific hybridization that would cover the entire genome with 1 kbp pieces tethered to a substrate. Similar idea to pen based microarrayer [13] but without the time consuming automation expense.
2. High speed scanned probe based DNA sequencer would be preferred over hybridization array.
3. Fabrication techniques to make microfluidic devices from more chemically resistant materials such as Teflon™.

Using genomic data mining see if an NxM matrix of primers can be created that when every possible combination is mixed a reasonably complete coverage of the genome is made if the primers code 5 to 10 kbp fragments. If all the products were 10 kbp in length would theoretically need only ~1100 primers to cover the complete genome. The cost of primers (35 mers $20 x 1100 = $22000) is arguably a one-time cost and can be used on multiple arrays. Arrange in a microarray mixing matrix to generate every possible combination (550 x 550 = 302500) at 10kbp per copy could cover entire genome. One axis of primers would have a sticky end such as biotin or digoxygenin. This microchemical chip could be fabricated using PDMS. Appears that all reagents are compatible with material. Chip would be somewhat complex but reusable. Chip would be placed on a steptavadin or antidigoxygenin treated microscope slide which also rests on a thermoelectric heater/cooler. This heater/cooler could also be thermally segmented so that different regions could be at various temperatures to aide in determining optimum reaction conditions for the entire array. It would be advantageous to also include in the array a means to control the Mg+ concentration for the same reason. The genomic DNA would be added and then the PCR cycles begun. This could then generate an NxM hybridization array for screening cDNA libraries. Jian Liu is working on portions of this. He is currently just trying to get the PCR to work in an NxM array. The obvious extension of this is to create the above hybridization array.

Using large segments of DNA as hybridization probes from the same genome as that which the cDNA comes from should be more effective than short oligomers. Much more specific hybridization should be possible. Nonspecific binding is a major drawback to sequencing or other analysis by hybridization using short oligomers.

It is conceivable that the mRNA conversion to cDNA using just one cell is possible. The protocol by Invitrogen (Carlsbad, California) for their TRIzol™ reagent seems to indicate that many of the steps could be done in a microchemical device. Unfortunately the device needs to be made from something other than PDMS. Phenol extraction is one step. Centrifugation could be carried out on a chip that was placed in a centrifuge for purifying the DNA.

What am I trying to demonstrate by this outlandish example? That it is not that outlandish. Many of the pieces are very close to being a reality. Why would you want to go to the trouble of single cell analysis? I have alluded to it in the above discussions. One of the obvious pathways to reverse engineering the regulatory mechanisms of gene regulation and protein function is to follow the development phases of an embryo. However it seems that you really need to track each individual cell in the embryo to really track down how the proteins are turning on and off and following the cells as they differentiate to form the various organs and appendages of a complex organism. If you have a fast robust way of following this progression at the single cell level, it would appear that you have a significant chance of seeing how the puzzle pieces fit. You need to do the analysis steps a lot. What we seem to have now are many puzzles without the border pieces, let alone all the pieces. If you can isolate the border pieces, it greatly speeds the process of putting the puzzle together. Starting with the just fertilized embryo seems like a border piece, a corner in fact.

The ability to analyze single cells appears to offer a significant tool to elucidating the intricacies of gene regulation and protein expression. But this also pushes the bar towards single-molecule detection and analysis. Another possible tool for this seems

possible with scanned probed microscopes. Several years ago I pushed a couple of graduate students in Prof. John Baldeschwieler's group at Caltech to try imaging DNA with a scanning tunneling microscope (STM) [14]. Unfortunately even though their results lead to a cover of *Nature* there has always been significant controversy. No one that I know of has been able to reproduce this result. However, imaging of strands of DNA at lower resolution has been done repeatedly including images of polymerases bound to DNA and even transcribing [15]. If you can atomically resolve DNA with some form of scanned probe microscope (SPM) (not necessarily STM) it should be more straightforward to sequence cDNA from a single cell for the above analysis without having to resort to the complexity of the hybridization array methodology mentioned above. You would also get the sequence of the proteins you are looking for directly. It should also be a very rapid way to sequence DNA.

Another focus of my thesis effort has been improved control electronics with applications towards feedback control of instrumentation for single molecule work using Digital Signal Processors (DSP). The above application towards SPM's being just one example. An important emphasis in this work was cost and high performance. In addition I wanted to clearly determine why this readily available technology has not been widely used. What is currently available for SPM's is expensive and difficult to use. It also requires a significant amount of additional work to apply to a given experiment or instrument.

In Chapter 2 of this thesis I will do my best to demonstrate and offer an explanation for why this situation exists. I will present a modular DSP feedback controller reference design that is relatively straightforward to use. It is significantly more cost effective than commercially available systems and its basic architecture solves many of the fundamental electronic limitations of these same designs. The appendix contains detailed schematics of these circuits, parts lists and layouts of all the printed circuit boards that make up the system.

In the chapters that follow, two significant applications of these electronics demonstrate the incredible flexibility such a system offers. One application changes the Q of the

cantilever for a scanning force microscope (SFM). This allows for higher-speed scanning in "noncontact" mode SFM. The other application offers intriguing possibilities that the author feels are significant but not explicitly apparent. In this application, a particle is confined in a laser trap to a region with boundaries that can be defined with nanometer resolution. These control electronics provide one of the only ways by which arbitrary control of a potential on the nanometer scale can be obtained.

1.2 Commentary

During my journey in trying to get my faculties together and, focused on writing about all that was done to get to this point, I came across a review in the *LA Times* by Robert Hotz [16] of two books which try to discuss the ethical components of this type of research: *Our Posthuman Future* by Francis Fukuyama [17] and *Redesigning Humans* by Gregory Stock [18]. I feel it necessary to comment on this because I feel that most people just brush on the surface of what makes this mostly a mute point. As an example the discovery and manipulation of atomic fusion was not by itself a destructive thing. It has taunted us with free electrical power. This has definitely proved to not be the case. It threatens us with mass destruction. This still remains to be seen. It definitely has been used to destroy.

The ramifications of applications of discoveries that could be made by the research in gene regulation are pretty much dwarfed by human nature. I feel that the focus on the ethics of this type of work is an unfortunate means to avoid what I feel is a more significant issue. How people choose to interact with each other and treat themselves and the powerful consequences of these choices are much more significant. You can go off on a tangent and debate the minutia of how much choice people have and as a result again avoid the significance. Technology is just a tool. It does not appear to have an ethic attached to it. The people using it do. There is an argument for restricting the tools or even preventing their creation.

On the medical front, we know that several readily accessible drugs are greatly overindulged by a large segment of the population with known disastrous consequences to the individual and significant expense to the community: food, alcohol and tobacco. While significant strides have been made to curtail the consumption of tobacco, it seems to have been replaced by a dramatic increase in the consumption of fatty foods that has resulted in a corresponding increase in obesity. Obesity is a major contributory factor to numerous health problems, specifically heart disease and diabetes. Not much needs to be said about tobacco's connection to heart disease and lung cancer. Alcohol has significant health effects as well but has its most dramatic effect on society when combined with operating an automobile. These are all known results that can arguably be changed by choosing to cope with the stresses of life in a less physically harmful way. You do not need advanced medicine to make a significant change in the result. Those that choose otherwise then need the benefits of modern medicine to buy themselves more time.

These three "health" issues cost this country significantly on a financial basis alone. Their root cause seems to be around how individuals choose to cope with human existence and the fact that it ends and we don't know when. Unless there is a significant discovery in how the mind works and can be manipulated, it is doubtful that any of the potential advances in medicine through increased understanding of biological systems will make a dent in these problems. Using the health of the population as a yardstick it is humbling to consider that in spite of all the technological advances we have made they have not made anywhere near as much impact as just two, refrigeration and septic practices such as sewage treatment. While it is hoped that the research efforts here will benefit more than just the career goals of the author, the greatest contribution that can be made by anyone is just giving what you got and being mindful of the consequences of your actions. Any fool can easily destroy life or make someone's life miserable. Our very existence seems to defy entropy.

1.3 References

1. Kay, L.E., *The molecular vision of life: Caltech, the Rockefeller Foundation, and the rise of the new biology*. 1993, New York: Oxford University Press. 304.
2. Hecht, J., *Laser Pioneers*. 1991: Academic Press.

3. Eigler, D.M. and E.K. Schweizer, *Positioning Single Atoms with a Scanning Tunneling Microscope.* Nature, 1990. **344**(6266): p. 524-526.
4. Alberts, B., et al., *Molecular Biology of the Cell.* Third ed. 1994, New York: Garland Publishing, Inc.
5. Varmus, H., *The Impact of Physics on Biology and Medicine.* 1999, National Institute of Health.
6. Ludecke, H.J., et al., *Cloning Defined Regions of the Human Genome by Microdissection of Banded Chromosomes and Enzymatic Amplification.* Nature, 1989. **338**(6213): p. 348-350.
7. Schmutz, S.M., et al., *Gene-Mapping from a Bovine 1-29 DNA Library Prepared with Chromosome Microdissection.* Mammalian Genome, 1994. **5**(3): p. 138-141.
8. Xia, Y.N. and G.M. Whitesides, *Soft lithography.* Angewandte Chemie-International Edition, 1998. **37**(5): p. 551-575.
9. Griffin, T.J. and R. Aebersold, *Advances in Proteome Analysis by Mass Spectrometry.* The Journal of Biological Chemistry, 2001. **276**(49): p. 45497-45500.
10. Griffin, T.J., D.R. Goodlett, and R. Aebersold, *Advances in Proteome Analysis by Mass Spectrometry*. Current Opinion in Biotechnology, 2001. **12**: p. 607-612.
11. Rajagopal, I. and K. Ahern, *Protein Sequencing in the Post-Genomic Era.* Science, 2001. **294**: p. 2571-2573.
12. Müller, M., et al., *Visualization and Analysis of Molecular Scanner Peptide Mass Spectra.* Journal of the American Society for Mass Spectrometry, 2002. **13**: p. 221-231.
13. Shalon, D., S.J. Smith, and P.O. Brown, *A DNA Microarray System for Analyzing Complex DNA Samples using two-color Fluorescent Probe Hybridization.* Genome Research, 1996. **6**(7): p. 639-645.
14. Driscoll, R.J., M.G. Youngquist, and J.D. Baldeschwieler, *Atomic-Scale Imaging of DNA Using Scanning Tunneling Microscopy.* Nature, 1990. **346**(6281): p. 294-296.
15. Bustamante, C. and C. Rivetti, *Visualizing Protein-nucleic Acid Interactions on a Large Scale with the Scanning Force Microscope.* Annual Review of Biophysics and Biomolecular Structure, 1996. **25**: p. 395-429.
16. Hotz, R.L., *Homo perfectus*, in *Los Angeles Times.* 2002: Los Angeles.
17. Fukuyama, F., *Our Posthuman Future: Consequences of the Biotechnology Revolution*. 2002, New York: Farrar, Straus & Giroux, LLC. 272.
18. Stock, G., *Redesigning Humans: Choosing Our Children's Genes*. 2002, New York: Houghton Mifflin Company. 277.

Part I

Nanometer Control

Chapter 2

Digital Signal Processor-Based Feedback Control and Data Acquisition

2.1 Introduction

I will try to provide background for and answer the following questions.

1. What can you do with a Digital Signal Processor (DSP) that you cannot do another way?
2. What makes a processor a DSP? (It is really hard to program in assembly.)
3. A brief review of the architectures.
4. Why did I choose the DSP56300?
5. What are the unfortunate practical limitations that have greatly impeded using DSPs for scientific applications?

As we are hopefully progressing further down one of the many roads that Richard Feynman envisioned [1] that we call nanotechnology, the need for tools to manipulate objects, molecules, and even atoms with nanometer or better resolution becomes greater. More flexible large dynamic range and less proprietary feedback controllers for mechanical nanomanipulators, such as scanned probed microscopes and various flexure mechanisms, seem to be desperately needed. What seems to be available is expensive and not easily adapted beyond its original specific design [2-5]. In addition, improvements in signal to noise and dynamic range by Analog to Digital (A/D) and Digital to Analog (D/A) converters are not quickly or appropriately taken advantage of in many designs. Improvements in dynamic range made possible by advancements in digital converters offer an enormous practical benefit in operability. With 24-bit converters the transition from optical microscope resolution (micron) to subatomic manipulator resolution (picometer) is continuous. This enables the straightforward

optical observation of a sample and its' position with respect to a picometer resolved manipulator, a tremendous operational advantage. With true 24-bit resolution you can have 10 pm resolution over a 160 μm scan range. This is well within the optical coverage of typical microscope immersion lenses and easily observed with non-immersion lower magnification objectives. In addition, molecular interaction along large stretches of DNA can be observed.

It appears that applying digital feedback techniques has not been more widely used by the scientific community due to a number of factors: 1. Existing hardware implementations of Digital Signal Processors (DSPs) are focused towards telecommunication, which has contradictory requirements to feedback control. 2. Feedback control concepts are not part of a physical scientist's education. 3. Current DSPs are extremely difficult to program. 4. Current hardware, in addition to not being directly useable, is expensive. 5. Educational documentation is diffuse and often at a high level or poorly written. 6. The learning curve is extremely steep. 7. Only within the last three years has DSP processor speed attained a level which enables wider bandwidth feedback applications. Feedback applications in a way have more stringent requirements than current high volume applications of DSPs, such as telecommunication and image processing.

The part of my thesis work focused on here is the development of a design architecture for control electronics that is flexible, simple, modular, takes advantage of currently available state of the art electronics, enables quick implementation of advanced control techniques, and is low cost. Because a feedback control system monitors or measures the response of the parameter controlled, this controller also incorporates a means to record response and control signals via a data acquisition mode. The author has also tried to eliminate many of the problematic grounding issues observed with current commercial data acquisition hardware. It is hoped and intended that because the basics of the architecture is simple, flexible and modular, advances in electronics can be quickly incorporated in modest incremental upgrades. One such upgrade was needed for experiments presented in this thesis. It is also hoped that the cost of this hardware is low enough that a greater number of researchers can make use of these technologies.

Current hardware is just too expensive to enable this, even if you ignore their functional limitations addressed by this design. It is also intended that the design be an open design providing working examples to speed the learning curve for researchers whose experiments could benefit from these techniques, but were inhibited by the apparent complexity let alone the cost. The determined researcher can construct the complete system with a modest investment in electronics assembly tools. Hopefully a more time saving avenue for this design will be available in the future. What has enabled the development of this instrumentation are Digital Signal Processors (DSPs) and the continuous improvement in their performance thanks to advancements in semiconductor fabrication techniques as predicted by Moore's Law. Because of the speed improvements allowed by advances in semiconductor processing, these processors have seen almost an order of magnitude decrease in processor cycle time [6, 7]. This speed increase is critical for enabling the application of the flexibility of digital feedback techniques to higher bandwidth control problems. I shall now elaborate on this adnauseam.

General Purpose Digital Signal Processors (DSPs) started to appear around the early 1980's. Texas Instruments TMS32010 was introduced in 1982 [8]. Motorola's DSP56000 began shipping in 1987 [8]. They seem to offer us the same tease now that they did then. To beat an old horse but for completeness 'what makes them different from regular microprocessors?' Today the distinction is a little blurry. Initially what separated them from microprocessors was mainly that they could multiply two numbers and add that result to a third number in one clock cycle of the processor. Often referred to as a multiply and accumulate instruction or MAC. There is a certain amount of parallel processing required to do this and the single cycle operation is only achieved when a repeated sequence of MAC operations is performed. These processors usually incorporate a pipeline structure which performs several preoperations to the incoming data and instruction stream so that the effective throughput of the processor is an instruction or MAC per processor cycle. The MAC operation is the heart of most signal processing algorithms and if your processor has one, it magically seems to become a DSP (i.e., Intel's MMX addition to its processors). Today many of the functions that

previously only DSPs could do in real time can be performed on General Purpose (GP) microprocessors, like the Pentium based personal computer I am using to write this thesis. However as of this writing, DSPs still have a significant weight, power, and cost advantage. A cell phone would be an awkward device if it needed a Pentium to work.

Today a better definition for a DSP maybe: A microprocessor which includes a MAC, plus internal logic for doing matrix-based algorithms that sequences through tables and loads data in parallel with the MAC instruction. In addition, a DSP provides direct interfaces to Analog to Digital converters (A/D) and Digital to Analog converters (DAC) as well as other built in peripherals that minimize the need for external glue logic other than memory. DSPs are fairly self-contained needing little more than power, a clocking source and boot ROM to implement a fully functional system. They can now be considered a subset of microcontrollers or embedded processors. Microprocessors need significantly more support chips to form a functional system. However, embedded versions of several microprocessors could be considered DSPs.

Another seemingly significant requirement to be called a DSP is predictability of code timing. However this issue is also starting to blur as DSPs become more powerful and complex. However, most DSPs have multiple timed interrupt capabilities so that they clock the A/D and D/A converters at a crystal referenced rate. GP processors usually require an external device for interrupt management. The timing of DSP code is also reasonably predicted by just counting the assembly instructions. All of the vendors discussed here have software tools to more precisely analyze the timing of the code. High-performance microprocessors, such as Intel's Pentiums are geared towards multi-tasking. Tasks can interrupt each other making timing unpredictable. The blurring between the two processor types is happening because the more advanced DSPs have multiple processors such as Motorola's Star Core, and Analog Devices' AD14XXX. There is a form of task switching being performed on these devices.

The tease that DSPs offer for scientific applications is the ability to implement feedback controllers that are extremely flexible and easy to reconfigure. In addition, feedback

techniques for nonlinear systems can be more readily implemented as well as optimal control techniques. They also provide a means to self calibrate feedback parameters to accommodate changes in the operating parameters of a given system. Classical feedback controllers usually use op-amp-based circuits to implement the control algorithm. Changing operating parameters usually required changing resistors or capacitors. Making these circuits easily adjustable adds more burden and complexity to the design. DSPs taunt you with the possibility that changing these parameters only requires changing coefficients or slight modifications in the DSP code. The same basic hardware can be used for different applications. As experimental science pushes resolution limits, the need to compensate for nonlinearity, hysterisis, and thermal drifts to name a few becomes more critical. DSPs offer a very flexible way to do this using feedback or calibrated open loop control. This is next to impossible with classic analog feedback techniques.

In addition, DSPs allow the real time filtering of incoming data. This is not usually that significant an advantage since presently this is a straightforward operation that can be handled by post processing recorded data. However, if the initial data rate is very high filtering out hopefully irrelevant signal information can greatly decrease storage requirements.

I am afraid that my original understanding of the above possibilities was a little naive and partly explains why DSPs are not more readily applied. This has always puzzled me. However, DSPs are still an incredibly powerful tool. Unfortunately the learning curve is steep and for feedback applications they have inherent limitations due to their clocking speed and the rate at which the signal you want to control can be digitized. In this introduction I will attempt to clarify what they can realistically achieve and the realities of implementation. But first let us bring in that nasty constraint, money.

The first big market for DSPs is the same one that is with us today and probably will be for a long time, the telephone. It can be argued that communications has really been the driving force for DSPs. Echo is big problem with telephone lines. We do not experience

it much thanks to DSPs. The last time I heard it was on an overseas phone call. AT&T appears to have started installing DSP-based echo cancellers on their national toll switches in the late 70's [8] when they converted the system to a digital architecture. When you send and receive two signals on a variable transmission line (i.e., a typical phone line) you are definitely going to have reflection issues of the two signals back to their sources especially on weirdly terminated and varying impedance transmission lines like what your phone is connected to. DSP techniques enable measuring the send and receive signals and canceling their return echo. Even today's all digital phone switches have this problem as the signal is passed from switch to switch. Each one generates a source of echo. Previously, the phone system monitored the send and receive signal levels and would mute the lower one. This assumed that the higher signal was that of the person speaking. Many of the less expensive speakerphones available today still use this technique. But the circuits have a certain time delay and hysteresis requirement in order that they do not oscillate. It does make them annoying to use and the technique does not let you easily hear if the other person is trying to interrupt you. Now we can yell at each other simultaneously and still hear each other on the phone.

Unfortunately for the scientific instrumentation world this basic application and its extensions does not need speed or very high numeric resolution. Sixteen-bit precision appears to be sufficient when the digitization of phone conversations are 12 bits at 8 K samples per second rate. However, increased processor speed does allow handling more than one phone call with a single processor which helps lower the cost of switching equipment for the phone company and so this has been aggressively pushed. Then came cell phones. In order to get as many conversations as possible in a finite frequency space extensive application of multirate signal processing techniques are used. According to one source [9] wireless applications accounted for 55% of DSP revenues in 2001. But here again the application only needs 16 bits resolution. Fortunately for scientific applications cell sites are space constrained and processing speed is advantageous here.

The question that arises is why do we have anything other than high-speed 16-bit processors. To answer this and confirm my suspicions, I contacted Kevin Kloker of

StarCore (Atlanta, Georgia). Kevin Kloker was the chief architect of the Motorola DSP56000 [6]. When Motorola entered the market, the largest exiting application, echo cancellation, was captive. AT&T designed and made their DSPs for in-house use. In fact they never marketed this chip [8]. They did not need an outside source. The next biggest application was V.32 modems (9600 baud was a big deal). It needed 24 bits of resolution and the ability to do complex math. In addition audio applications needed more resolution than the 16 bits at which they were digitized when CD players were developed if you wanted to do any signal processing on these signals. Also, according to Kloker, they were trying to include as much as was reasonable to make the processor powerful enough for a broad range of potential applications. They effectively threw in the kitchen sink. It seems reasonable to extrapolate that similar thinking was behind the DSP designs of Texas Instruments and Analog Devices. One other potential big application was image processing. However, it needs floating point capability. The DSP56000 was a fixed-point processor as were the first DSPs from TI.

I will focus on some specific details of the processors made by Analog Devices, Motorola, and Texas Instruments. There are now many more players in this field and the assortment of devices is a bit overwhelming. A directory of some of the choices can be found in the references [10]. These three companies have been around for a while and basically established the market. The odds are good that their current product lines will be around for at least five years so the time invested in understanding their processors will probably not be wasted. But this is not always the case as two processors I know demonstrate. They have been discontinued. They have also focused some of their processors on higher resolution applications, which benefits feedback and data processing scientific applications.

Motorola's DSP56000 in order to address the potential audio and modem markets ended up designing a processor that performs FFTs extremely fast. As mentioned above their processor uses a 24-bit wide memory space for data. Unfortunately the power of this processor has resulted in a very complicated device to use from this author's viewpoint. They also probably wanted to keep the cost down so the initial processor was fixed point

with a 56-bit resolution (hence the 56 in DSP56000). A floating-point processor was more expensive to design and fabricate at the time (it still is). I will elaborate on the significance of the 56-bit resolution later. Later they did introduce a floating-point based processor, the DSP96000, but it was significantly more expensive. The demand for this processor appears to have been low, so it is no longer available.

Texas Instruments (TI) introduced a 32-bit resolution mantissa floating-point processor soon after the 16-bit fixed point TMS320C010. It was called the TMS320C30. For the author this floating-point processor is more intuitive to program even at the assembly level. However, the 32-bit mantissa is a severe numeric constraint for applications that require high resolution. Numeric noise introduced by rounding errors becomes significant for several algorithms when operating on 24 bit data [11]. This TI part also implements the exponent in a separate 8-bit memory which makes programming awkward. A lower resolution floating-point mode is available which includes the exponent in a 32-bit representation. This has a 23-bit mantissa plus sign and an 8-bit exponent, a “real” limitation. Fortunately TI seemed to have realized the limitations this imposed and more recently introduced the TMS320C67XX series of floating-point processors. As a result some of the TMS320C30s have been obsoleted. These new processors have a 64-bit double precision floating-point capability with some limitations to taking full advantage of the processors speed. TI’s major emphasis still appears to be towards 16-bit processors for communications. TI has one of the broadest DSP product lines.

Analog Devices offers four lines of DSPs: Two 16-bit fixed point, ADSP-21xx and Blackfin and two 32-bit floating-point, SHARC DSP and TigerSHARC DSP. All except for the SHARC DSP are geared towards telephone communication applications. The SHARC DSP has the same limitation as the TI TMS320C30 by only implementing a 40 bit extended floating-point format in hardware (i.e., 32-bit mantissa 8-bit exponent). However, this processor does implement 32 bit fractional with an 80-bit accumulator for multiplication. This effectively overcomes the floating-point limitation but at the same time would seem to make having the floating-point capability pointless. Its only

advantage is to assist in developing code. Programming using floating-point numbers is simpler. An application, which needs the numeric resolution, would not use this mode in the final code.

For my feedback controller, I chose the DSP56362. It is a member of the Motorola DSP56300 family of DSPs. This is the second generation of the DSP56000 line of processors. The performance of this processor is still one of the best. Unfortunately it is the most difficult processor the author has ever programmed. Its target market is audio applications. It stands a reasonable chance of being in production for the next five years so that the design presented here will be useable for a reasonable amount of time. Because it is targeted at consumer applications, its cost is significantly less than other processors in this product family. This processor is based on the first processor Motorola designed so software written on this processor should work on future upgrades. According to Kevin Kloker the design has also been synthesized so taking advantage of future semiconductor fabrication improvements should be easily implemented.

As of this writing, the Motorola and TI parts are readily available in 100 to 150 MHz processor speeds. Analog Devices' equivalent cost parts are readily available at 80 MHz. The higher end and more expensive Analog Devices processors run at 100 MHz.

2.2 DSP Lament

To this writer the problem with the current processors is multifold. Making appropriate use of digital signal processing techniques is not a trivial matter. Incorrect implementation of the algorithms can greatly compromise performance either in speed or numerical resolution. Some of the errors can be hard to catch because you will get some form of functionality. In some ways the same can be said of implementing these techniques using analog circuits. The concepts are deceivingly straightforward, but real world implementations quickly reveal the subtleties that the manufacturing documentation does not seem to clearly explain. Part of this is probably intentional. If

you really know how difficult it would be, you may not give the technique a chance. In some cases one wonders if they even know. A great example is using the FFT for measuring power spectra. The simple interpretation is that it will represent the amplitudes of the frequency components of the incoming signal. It is at best an indication. One must remember that it is a sampling algorithm and if a frequency component falls between two frequency bins, its amplitude will be split between them. Other subtleties of the windowing used make even this a problematic assumption. A little more than a basic knowledge of the signal processing techniques is needed to correctly use DSPs. Constant testing of the performance of an algorithm is mandatory.

The second major problem is coding. To really make full use of the processing power of these devices you still must code in the assembly language of the processor. What complicates this is their combination pipelined parallel architecture. It is a tremendous effort to get things right and arrange the instructions in the proper order. In addition the initial architectures used for this generation of processors do not lend themselves to higher-level language compilers. Analog Devices have made some inroads here in that the assembly language mnemonics is more intuitive. The other is just the nature of assembly programming. An “If Then Else” can be a major chore. Compilers do so much for us. (Do you know the details of calculating Cosine? A simple Taylor series is not exactly right.)

The last major problem is mainly an issue for feedback applications. A rule of thumb for implementing a feedback circuit using digital techniques is your sampling rate should be 10 times that of the controlled systems bandwidth [12]. The preference is 50 times. If you are very close to this limit, things get interesting. In addition, if you are running at a high sample rate, the number of things you can do with the processor becomes limited. This is probably why a significant number of digital feedback applications are for large mechanical systems. There you have a ton of processor time to do really interesting things. Large mechanical objects have a low bandwidth. The X-31 Enhanced Fighter Maneuverability (EFM) experimental plane is an incredible demonstration of these technologies [13].

However, the speed issue will become less of an issue as these same basic processor architectures benefit from advances in semiconductor fabrication density enabling them to operate at higher speeds. What has been a bottleneck from the beginning and has probably inhibited their widespread use is programming. They are absolutely horrible to program. The manufacturers are aware of this and all of the three mentioned here have made a significant effort to build next generation DSPs which can be programmed with higher level languages and almost achieve the performance of optimized assembly code. But they are focusing efforts on 16-bit product lines first because of the demand from wireless applications. Not much help for higher resolution applications.

2.3 Goals of the DSP Design

Besides the desire to learn how to build such a beast, the more rational reasons for building the DSP-based feedback controller and data acquisition system were multifaceted and may be a little too ambitious. There are several problems with existing commercial hardware that need to be addressed in order that the potential of a general-purpose DSP-based feedback controller can be realized. Before enumerating the design goals a discussion about the limitation of current hardware is needed.

The general purpose DSP and data acquisition hardware that is readily available is either expensive or compromised by its implementation most cases, it is both. The fundamental flaw most commercial designs share is residing inside the chassis of a personal computer or some other computer chassis such as used by compact PCI cards. This configuration presents an extreme compromise when trying to digitize analog signals with high fidelity (16 bits or better). I once observed a demonstration of an early PC plug in DSP card, which contained a TI DSP and two 16-bit consumer audio A/D converters. A real time FFT was running on the DSP and the results displayed on the PC monitor. The sales people being not well versed in the technology did not realize this was showing the card had at best 11 bits of resolution above the noise floor.

The grounding system of a personal computer has high current pulses constantly running through it. It is an ever-increasing problem for the processors themselves as their speeds increase and their operating voltages decrease. The initial 8086 based PC did not need the separate voltage regulators that the current Pentiums need. They drew less current and had wider voltage margins. These regulators are not just needed because the processors run at 3.3 V to 1.8 V instead of 5 V. The high peak currents these processor draw can cause the voltage level to drop if not properly regulated. This is difficult to do for high peak currents if the regulator is a significant distance from the processor such as in the main power supply. Cables and printed circuit board traces provide too much impedance to control the voltages effectively. Having the regulator as close as possible to the processor helps. The same rules apply to A/D converters with the signals they are measuring. The fidelity of the signal measured needs to be maintained up to the inputs of the A/D. The power to the A/D and its reference must be clean and stable; otherwise it will introduce artifacts into the measurement. This design provides a solution.

In addition, to make things even more entertaining, the digital ground of a PC is connected to the chassis. This is done for reasons of operator safety, electrical interference and protecting the computer from static electricity. Then for one last stake in the heart of trying to make a high sensitivity measurement, the chassis is connected to the grounding system of the AC mains. The PC goes from being a small to a giant antenna. Having a high-resolution data acquisition system card inside of it enables you to pick up the PC generated electrical noise and everything inside the building it gets its power from. In addition, grounding through the AC mains creates numerous opportunities for ground loops. It has been the author's experience that a poor understanding of signal grounding and shielding compromises many measurements. The PC based data acquisition cards make this even worse.

The cost and electrical noise issues are somewhat resolved by many of the stand alone development/ educational boards available from the manufacturers of DSPs. Many include built in A/D and D/A converters. However, getting data out of them still requires

connecting them to the chassis of a PC, again compromising signal fidelity. The data connection is further compromised by not being very high speed. In addition the converters use Delta-Sigma techniques (AKA., 1-bit converters) to measure or generate voltages introducing substantial group delay.

Because of the group delay Delta-Sigma converters are not useful for feedback systems which need a bandwidth greater than a few 100 Hz. Analog Devices has a good basic description of the technique [14]. Several Delta-Sigma based converters have a 1 ms or greater group delay. This is the time between when the input was at a given voltage and when the converter generates a number representing that voltage. This technology dominates the market for high-resolution A/D and D/A converters. It can be readily implemented in CMOS, takes relatively little silicon real estate, uses little power and 24-bit resolution at 192KHz sample rates can be readily obtained. It is a very cost-effective solution. The major application, playing and recording music, is not affected in most cases by the 1 ms group delay. You can hear 1 ms of delay; it sounds like a subtle echo. Only in professional studios would it not be tolerated when you are trying to playback to the engineers or performers what is being recorded in real time.

Delta-Sigma converters also appear to have greatly distorted one significant aspect of implementing A/D and D/A converters, the need for high-performance low pass anti-aliasing filters. Delta-Sigma converters do not require steep roll-off multipole filters for anti-aliasing of the input signal. A steep digital low pass filter is part of the Delta-Sigma conversion process. It is also why they have a significant group delay. This seems to have resulted in the virtual disappearance of inexpensive off the shelf passive or active anti-aliasing filters. What seems to be available is expensive or built to order. In addition, it appears that because digital filtering techniques are in many ways more powerful than analog techniques, currently available engineering texts do not cover the subject and one of the classic texts is out of print [15]. Digital filters are more flexible and better behaved in many cases. However, they become more difficult to implement as the bandwidth of the signal increases.

What I have tried to do. DSPs continue to offer the potential to implement a combination flexible feedback controller and data acquisition system. With the continuing improvements in A/D and D/A converters in terms of speed and resolution some real practical advancements can be made in scientific measurements and control. The two experiments and their results described in this section of the thesis provide a nice demonstration. For the potential shaping experiment, it is difficult to imagine another way to implement.

After extensive searching on the part of the author, there does not appear to be any commercially available hardware that is configured in the way needed:

1. High resolution (16-bit or above) and high speed (1MHz) successive approximation (SAR) A/D converters and R2R ladder D/A converters driven by a DSP.
2. Anti-alias filters for the A/D and D/A converters.
3. Housed in a metal chassis for shielding with shield electrically isolated from the electronics.
4. A galvanically isolated medium speed digital interface to the PC for data acquisition.
5. Powered by isolated, shielded and, floating linear power supplies with line filtering and low capacitive coupling to the AC mains. Separate supplies for the A/D, D/A and DSP electronics to eliminate ground loops and feed through noise from the digital electronics to the analog front ends.
6. Configured so that the signal sources to be measured define the ground of the A/D converters and indirectly the rest of the electronics.
7. Low cost.
8. Low cost development software tools.

2.4 The Design

As mentioned for this basic design the Motorola DSP56362 from the DSP56300 family was chosen. This was done over a year ago and the latest version of the TI product line was not available. Choosing any particular processor or architecture is trying to hit a moving target. A feeling that I always have when I buy a computer is that it is obsolete

by the time it arrives at my doorstep. It is more painful here because of the time involved to get the entire system designed, built, debugged and programmed (especially under the constraints of a research project). Even with the knowledge of the currently available processor as of this writing, the DSP56362 would still be the one chosen. It offers six serial ports that greatly simplify connecting to A/D and D/A converters from a design and electrical standpoint. In addition the software tools are free. It is also an incredible deal (approximately $20 in moderate quantities). As of this writing Texas Instrument's TMS320C67XX family of DSPs would be seriously considered because it looks like it has better performance and one DSP in the family has similar pricing. TI has also gone to great lengths to improve the programming tools. However it only has four serial channels and comes in an inconvenient package for prototype assembly (Ball Grid Array (BGA)). The current design can be assembled using conventional electronic tools (soldering iron, tweezers and an inexpensive dissection microscope).

I must make a comment about this processor. It is difficult not to develop a love/hate relationship with computer hardware on any level when you are trying to get it to carry out an idea that we envision it can implement. How many of us have muttered or screamed at our computer when using it? Come on, raise your hand, I know you are out there. The DSP56362 has caused me serious hair loss. Unfortunately it is a very powerful DSP architecture. After reviewing, yet again, the other manufactures' documentation for this portion of the thesis, I am still amazed by the insight of the design. Motorola took several years after TI to release this processor. It basically contains three separate processors, a Program Control Unit (PCU), an Address Generation Unit (AGU), and an Arithmetic Logic Unit (ALU), plus three separate internal memories and separate data buses for each. The other manufacturers share similar elements but not in this powerful but frustrating combination. I have written code for the TMS320C30 and reviewed the instruction set for the AD Sharc processors. It is easier to write code for these processors. However I would argue that you couldn't get the performance out of these processors compared to the DSP56362 on a clock cycle basis. What makes them easier to use is that they hide many of the internal workings from the end user and disable

the ability to manipulate them. The Motorola DSP56362 enables you to directly control things. Edward Lee provides a nice explanation in his early articles [8, 16].

However, the programmer ends up writing a form of microcode. This is tough. In addition, a critical focus of this design seems to be implementing an FFT as fast as possible on a cycle by cycle basis. The register structure has specific organization and features that can only be explained by this focus. From conversations with Kevin Kloker there was also a focus on doing complex math. The other DSPs do not implement the FFT algorithm this intricately or as fast. Unfortunately this structure does not lend itself to efficient compiling of higher level languages. It also makes programming the processor on the assembly level difficult if you want to take full advantage of the processors capabilities. The power of this architecture is born out by its longevity. Both TI and Analog Devices are now at second generations of their original DSPs that have departed from the first generation. In the case of TI many are not code compatible. The DSP56300 family is a second-generation design but the significant difference from the DSP56000 family is a deeper pipeline and added instructions. The architecture has changed little and the parts are code compatible. One last item is the fractional math used by this processor. This takes some getting used to. The other two manufactures use this format for fixed-point math so it is a curse of all of them. It causes confusion when trying to write branch routines that compare values or examine bits. The data is left- instead of right-justified.

After all this background, the basic design is a bit of a let down to describe. Figure 2.1 shows the block diagram of the design. Figure 2.2 is a picture of the actual hardware. Figure 2.3 is a placement diagram that shows where the various boards in the design are located. The initial intended application by the author uses a quad photodiode as a

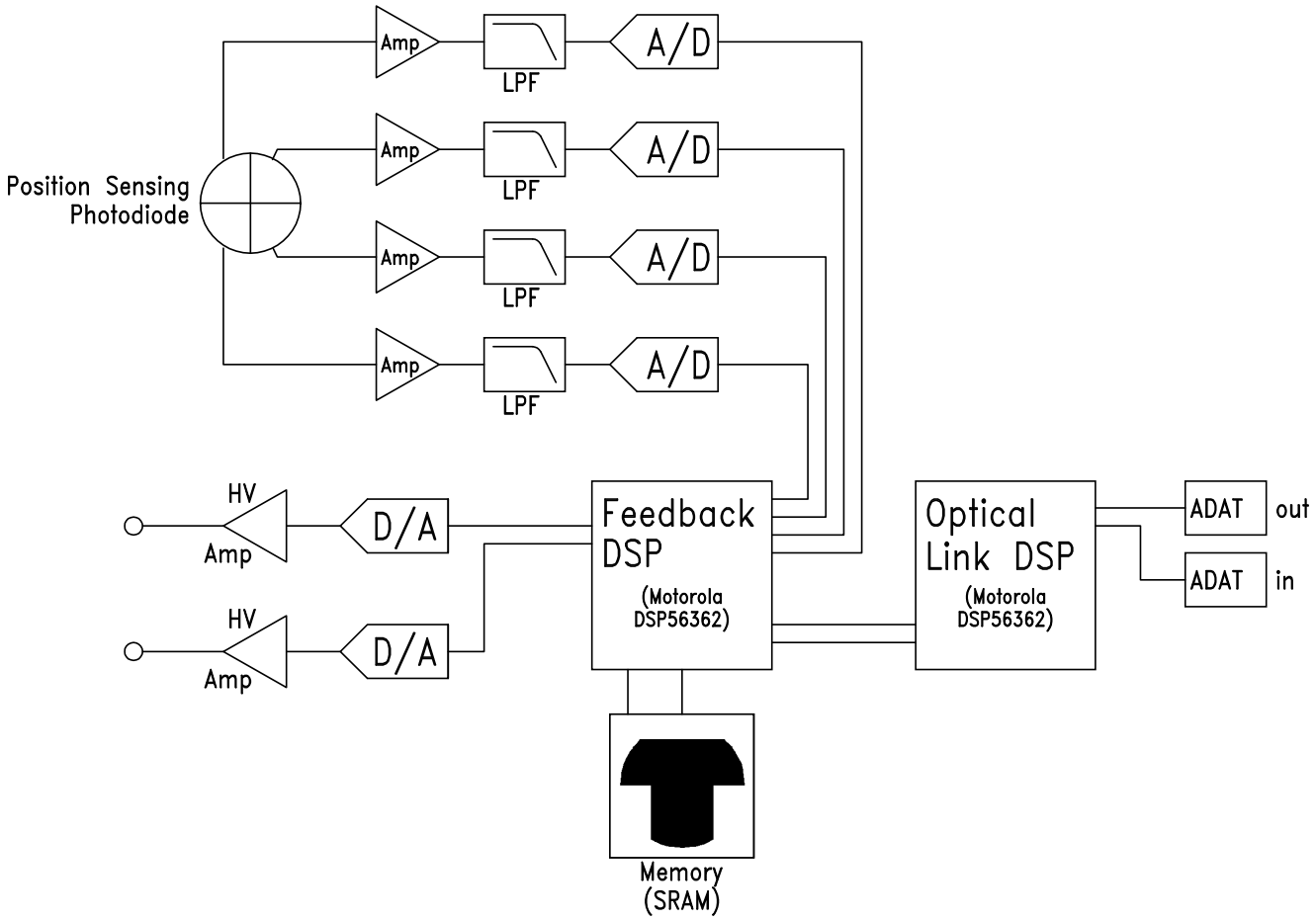

Figure 2.1. Block diagram of the Digital Signal Processor feedback controller.

33

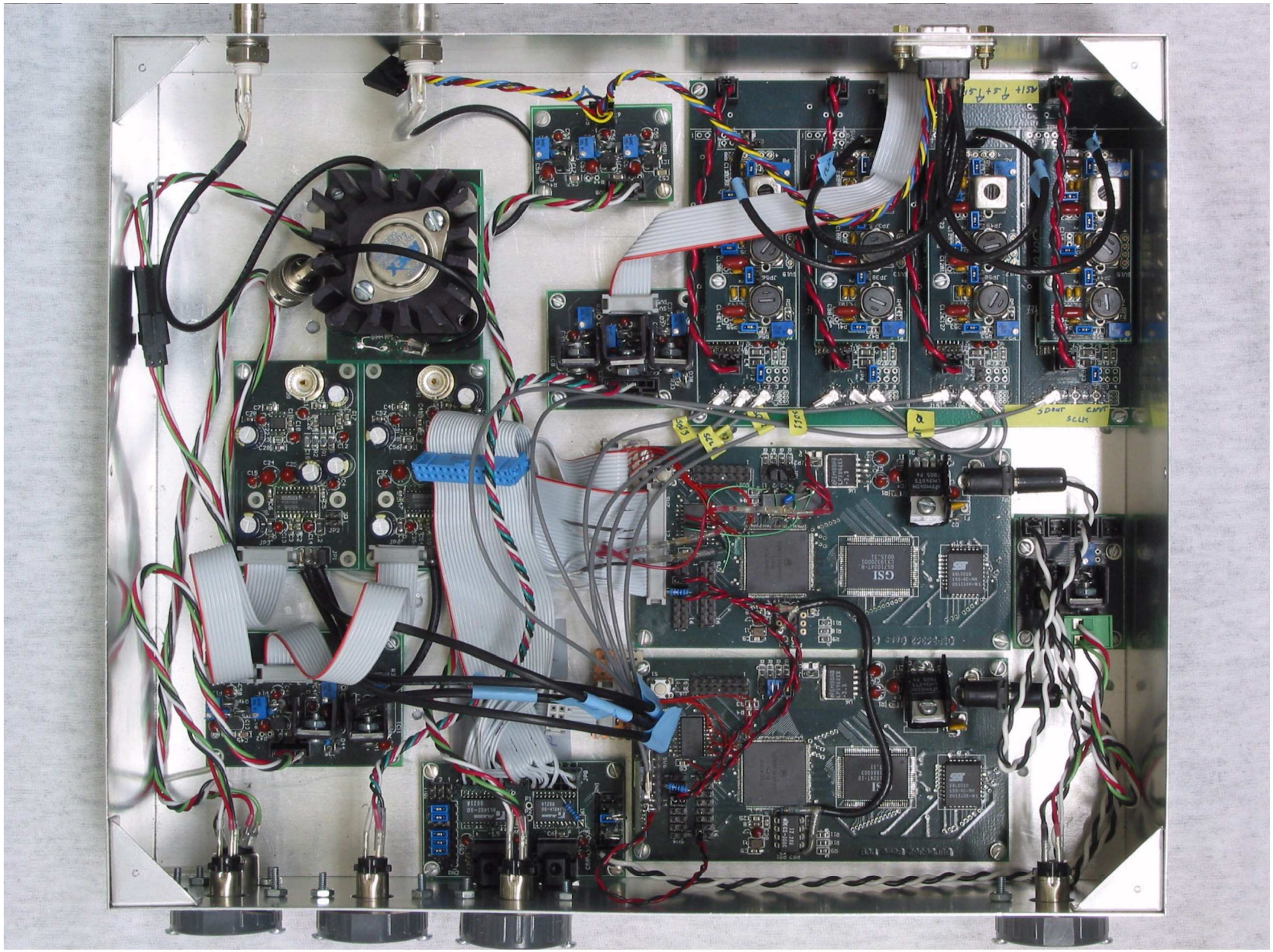

Figure 2.2. Digital Signal Processor feedback controller electronics.

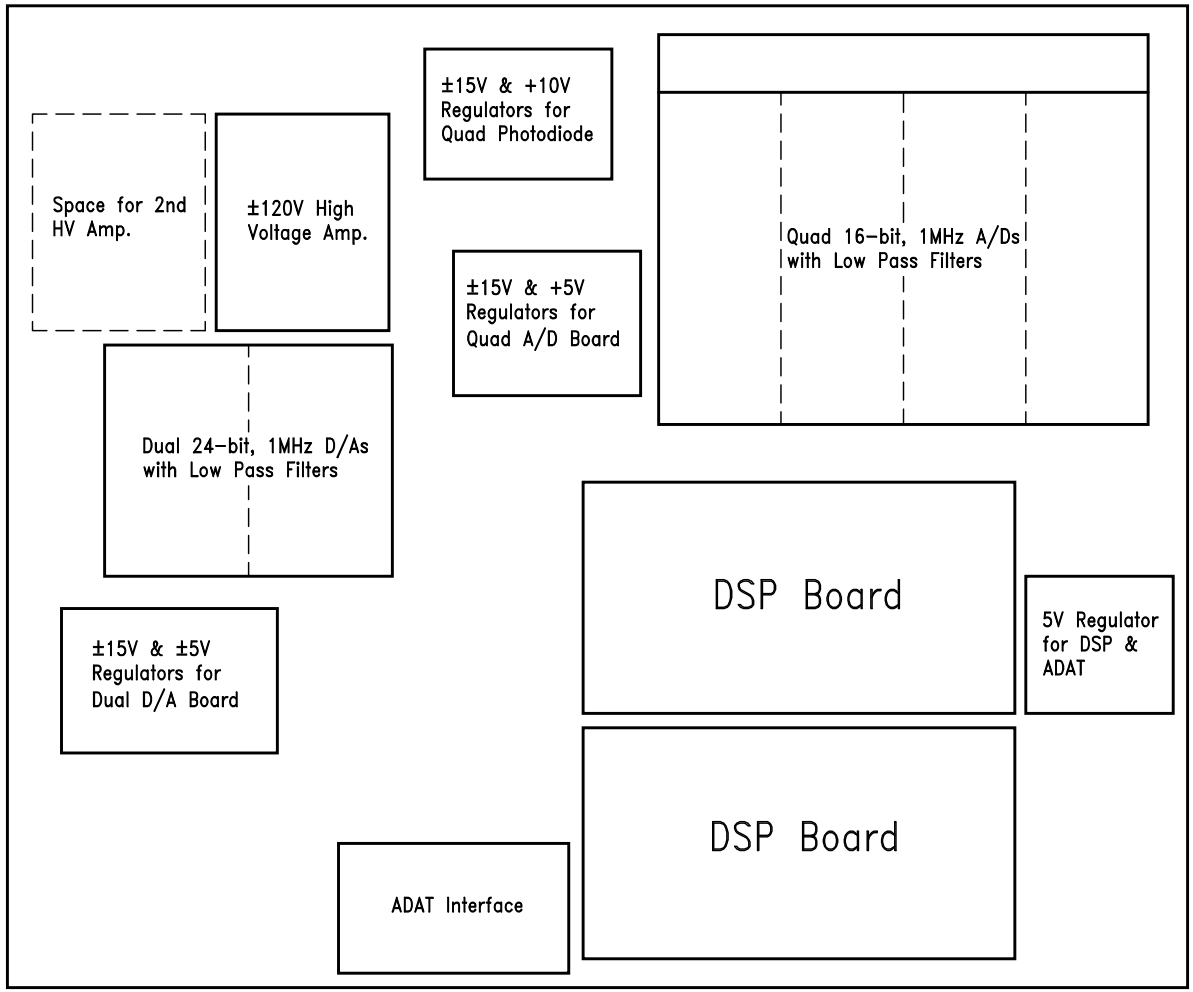

Figure 2.3. Placement diagram of DSP Feedback electronics shown in Figure 2.2.

35

position sensor for a x-y nanopositioning stage driven by piezo stack actuators. It is a nice fit to the six serial channels of the DSP56362. In the initial design, four of the serial channels are configured as inputs to control and receive data from four independent 16-bit A/D converters with a 100 kHz sample rate capability (TI/BurrBrown ADS8231) (See Figure 2.4). Each converter is preceded by a buffer amplifier and 5 pole low pass anti-aliasing active filter. The other two serial channels are configured as outputs to drive two 24-bit D/A converters (TI/BurrBrown PCM1704). These converters are intended to be driven at 8 times (or more) the A/D rate so that the output anti-aliasing filter is only a simple two-pole active filter with a roll-off at ~20 kHz. The D/A converters have a current output so a transimpedance amplifier converts the current to a voltage output. A capacitor is in parallel with the feedback resistor to limit gain peaking so the effective filtering of the voltage output of the entire circuit is that of a three-pole filter. Of significant importance the reader should note the significant number of bypass capacitors used in this circuit. This circuit is based on the reference design by TI/BurrBrown for implementing the PCM1704. The power lines need to be as quiet as possible to enable the part to achieve its performance potential of 24 bits.

The DSP circuit includes a 64 K x 24 bit SRAM and a 256 K x 8 bit Flash EEPROM. The flash can be enabled to load a boot program for standalone operation. The SRAM extends the memory internal to the DSP. It is mainly for limited lookup tables. Access to the SRAM has zero wait states but is still not as fast as using the on chip memories. The three on chip memories can be accessed simultaneously. The external memory cannot and has additional restrictions if it is configured to be extensions of all three internal memories. The DSP connected to the A/D and D/A converters is connected to a second DSP via a seventh serial port on these DSPs called an SPI interface. The second DSP serves as a communications controller for implementing the ADAT fiber optic interface to the data collecting personal computer. The ADAT interface uses two inexpensive plastic fiber optic cables for a 9.2M bit bidirectional data interface. The fiberoptic cables and drivers are the same ones used for the consumer S/PDIF interface for digital audio. Originally designed by Keith Barr [17] for implementing a digital audio recorder using PC computer hardware, the ADAT interface standard can accommodate 8

channels of 24-bit data at 48 K samples per second. Alesis Semiconductor (Los Angeles, California) manufactures a receive and transmit chip pair (AL1402 and AL1401A respectively) that implement the interface when combined with the appropriate optical transmitters and receivers. Unfortunately, because of the limits of the Motorola DSP56362 and the configuration of the Alesis chips this current design only uses six of the transmit channels and two of the receive channels for recording and playing back data to/from the PC. The interface is very flexible and various combinations of channels and data rate can be implemented such as combining all channels for a single channel to obtain a 576 K sample rate at 16-bit resolution.

Downloading code to the DSPs is accomplished via the DSP56362's built in On-Chip Emulator (OnCE™) interface. Besides offering the ability to program the DSP and its memory, it also offers limited real-time debugging capabilities critical to developing working code with the hardware. The interface is connected to the PC via a simple module plugged into the parallel printer port. Hardware and software breakpoints can be set as well as all memory and registers can be easily monitored and manipulated.

The entire system is constructed using separate boards for the DSPs, D/A and A/D converters as can be seen in Figure 2.2. However, the four A/D converter circuits are contained on one board. This modular approach eases debugging and changing of any section. Power to the entire system is provided by three ±18 V and one +8 V transformer isolated and linear regulated power supplies. These supplies are contained in two separate enclosed metal chassis and connected to the DSP electronics via shielded cables and connectors (mini-Din). Figure 2.4 shows the chassis containing the three ±18 V supplies and the typical arrangement of the three chassis boxes for the power supplies and DSP electronics. One ±18 V supply powers the A/D board, the second the D/A boards and the third the quad photodiode preamp circuit. The +8V supply powers the DSPs and optical transmit and receive board. Each supply powers a second set of regulators for the above circuits to improve noise performance and provide the multiple voltages that each circuit needs that cannot be meet by just the dual supplies. Because the supplies are floating and isolated (not connected to the chassis or the AC mains ground), a star

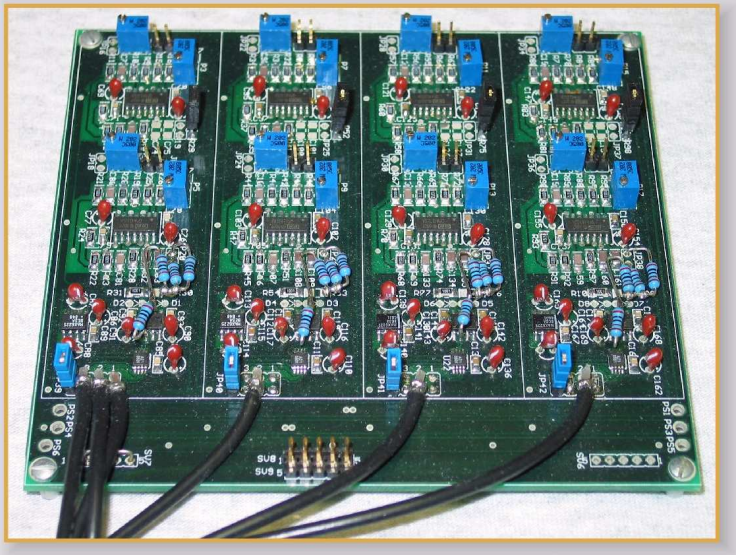

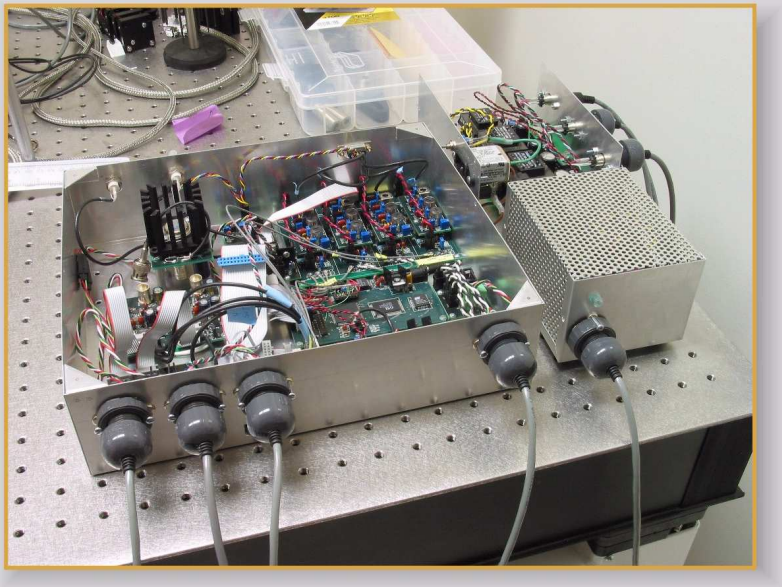

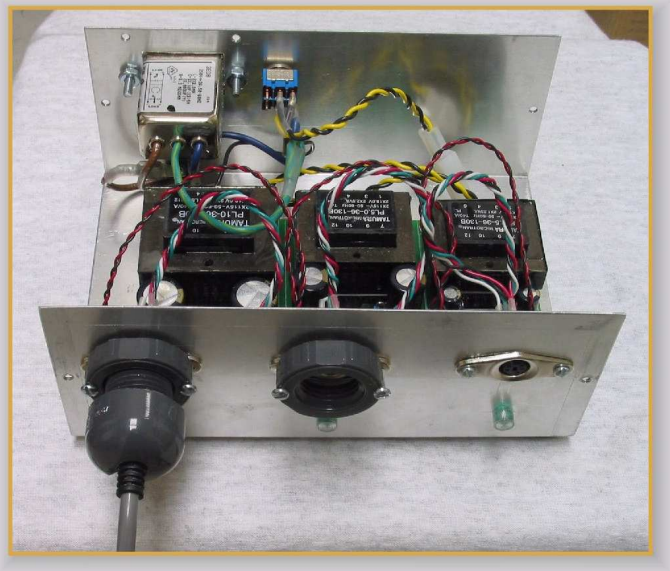

Figure 2.4. The top photo is of the 16-bit 100 kHz A/D board with active low-pass anti-aliasing filters. The bottom left picture shows the DSP electronics connected to the power supplies and the right hand picture is a close up of the three +/- 18V power supply chassis also showing the mini-DIN connector clamp solution.

grounding configuration is implemented. Unfortunately the DSP circuit acts as the hub. One other significant construction technique is using coax cables to connect the high-speed serial data, frame and data clock signals to/from the A/D and D/A circuits. It has been the authors experience that the radiated emissions of these signals routed with less care can feed through sensitive analog circuits. The signal drivers are connected to the coax via a resistor that matches the characteristic impedance of the coax to minimize or eliminate the reflections of the transmission line. A good review of this technique can be found in Texas Instruments' book on logic design [18].

The original quad A/D circuit was designed for lower bandwidth applications. It is also fairly inexpensive. A second A/D circuit was constructed for higher bandwidth. It is actually the converter shown in Figures 2.2. It uses Analog Devices' AD7671 1 MHz sampling 16-bit A/D converter. Because of the increased bandwidth, a passive 7-pole low-pass anti-aliasing filter was used instead of the active filter used in the other board. This filter was designed for a 140 kHz passband. The active filter was designed for a ~20 kHz pass-band. All boards were designed using Eagle printed circuit board layout software (CadSoft Computer GmbH, Pleiskirchen, Germany). All analog circuits make extensive use of copper ground planes surrounding all signal traces to provide a low impedance ground and limited shielding. Detailed schematics, parts lists and images of the board layouts can be found in the appendix. To keep the cost down all boards are 1/16" double sided, plated through hole, 1 oz copper except for the DSP boards. The DSP boards are 4-layer boards where the inner layers are the 3 V power plane and the ground plane. Gerber files for board fabrication can be obtained by request from the author.

The design solves all of the key electronic problems set out in the design goals. All electronics are shielded and electrically isolated from the AC line and the data collection Personal Computer. The electronics is powered by low noise isolated linear power supplies to further improve performance. This allows the near optimum connection to the signal source by enabling the signal source to determine ground. The connections between the DSP, A/D and D/A converters are designed to minimize any digital signals

feeding through and corrupting the analog inputs. A star grounding system enhances this feature. The multiple isolated and floating power supplies enable implementing a star ground. Digital currents do not flow through any analog section. The current implementation was designed for high resolution and uses state of the art 16-bit 1 M sample/sec successive approximation A/D converters and 24 bit 1 M sample/sec R2R type D/A converters. Both minimize the turnaround time of basic system to just 1 or 2 conversion cycles enabling a basic bandwidth of 250 kHz. Higher speed lower resolution converters can be implemented in a straightforward fashion if needed. The cost of the hardware is in the same range as a high end data acquisition card using 16-bit converters even if contract assembled . The software tools are free meeting another design goal for the expense of the end system.

2.5 References

1. Feynman, R., *There's plenty of room at the bottom.* Engineering and Science, 1960. **23**(5): p. 22-36.
2. Physik Instrumente (PI) GmbH & Co. KG, Karlsruhe/Palmbach, Germany
3. Newport Corporation, Irvine, CA
4. Digital Instruments (DI), Santa Barbara, CA
5. New Focus, San Jose, CA
6. Kloker, K.L., *The Motorola Dsp56000 Digital Signal Processor*. Ieee Micro, 1986. **6**(6): p. 29-48.
7. Motoroal, I., *DSP56362 24-Bit Audio Digital Signal Processor Datasheet DSP56362D*. 2000, Motorola, Inc.
8. Lee, E.A., *Programmable DSP Architectures: Part I.* IEEE ASSP Magazine, 1988: p. 4-19.
9. Dunn, D., *Big DSP suppliers chilled in market downdraft*, in *EBN*. 2002.
10. O'Leary, M., *DSP Directory*. EDN, 2002. **7**: p. 33-57.
11. Sohie, G.R.L. and W. Chen, *Implementation of Fast Fourier Transforms on Motorola's Digital Signal Processors*. Rev. 1 ed. 1989: Motorola Inc.
12. Lurie, B.J. and P.J. Enright, *Classical Feedback Control with MATLAB*. 2000, New York: Marcel Dekker. 456.
13. See NASA Dryden Flight Research Center website.
14. Kester, W., *Practical Analog Design Techniques*. Analog Devices Technical Reference Books, ed. W. Kester. 1995: Analog Devices. 428.
15. Williams, A.B. and F.J. Taylor, *Electronic Filter Design Handbook: LC, active, and digital filters*. 1988, New York: McGraw-Hill.
16. Lee, E.A., *Programmable DSP Architectures: Part II.* IEEE ASSP Magazine, 1989: p. 4-14.
17. Barr, K., et al., *Method and Apparatus for Providing a Digital Audio Interface Protocol*, in *US Patent Office Gazette*. US 5,297,181 (1994), Alesis: USA.
18. Instruments, T., *Design Considerations for Logic Products (SDYA002)*. 1997: Texas Instruments.

Chapter 3
Electronic Q Control of SPM Microcantilevers

3.1 Introduction

Since its initial invention by Binnig, Quate, and Gerber [1], atomic force microscopy (AFM) or scanned force microscopy (SFM) has taunted us with the potential to be a great investigative tool for molecular biology and biochemistry. In principle it should enable imaging of biological samples with almost atomic resolution. Much has transpired between now and when it was first introduced. The original "contact" method of using the technique proved problematic for imaging biological samples and molecules. In this method of imaging, the force probe is dragged across the surface of what is being imaged much like a phonograph needle was used to measure the audio signal of a vinyl record.

Unfortunately for biological applications this method introduces lateral forces onto the sample. This can greatly distort the sample or worse, wipe it away from the support substrate. To overcome this limitation, what is now called "tapping mode" or noncontact mode was devised [2]. This technique uses the resonance of the spring mass system of the AFM probe and its support to drive the probe up and down thus "tapping" the sample. Because the actual contact time is minimized or eliminated (depending on the sample tip interaction mechanism used), the amount of lateral force is also minimized or eliminated. In fact if the bandwidth is available in the translation mechanism of the microscope, the direct translation force resulting from the translation of the sample with respect to the probe tip could be eliminated. The translation would be stopped during the contact portion of the travel of the probe.

Currently the most commonly implemented noncontact method uses "slope detection" to monitor the surface effects upon the oscillating probe tip. In this method, the cantilever is driven slightly off its resonant frequency. For maximum sensitivity Martin, et al. have shown this is at $\omega_b(1\pm1/(8^{1/2}Q))$ [2]. This is where the slope of the cantilever response

curve vs. frequency is the steepest. External forces on the driven cantilever will cause a change in amplitude and frequency of the oscillation. Typical implementations convert the measured oscillations of the cantilever to a DC signal via some form of RMS to DC conversion.

They do not directly monitor the frequency. Unfortunately the method has shortcomings. The higher the *Q* of the cantilever, the longer it takes for the cantilever's resonance to stabilize to a new amplitude after it has been modulated by surface effects (which apply a force to the cantilever) especially those that represent step functions. This time constant dictates the rate at which a sample can be scanned and the bandwidth of the force detection. For biological and chemical applications, this compromises the ability to monitor real-time events. Image acquisition speeds tend to be on the order of minutes.

This time constant can be determined from *Q*, $\tau=2Q/\omega_0$ [3]. Albrecht et al. show that the transient response of the cantilever amplitude is given by the equation

$$A^2(t) = A_o'^2 + A_t^2 e^{-\omega_o' t/Q} + 2A_o' A_t e^{-\omega_o' t/2Q} \cos[(\omega_t - \omega_d)t + (\varphi_t - \varphi_o')], \qquad (1)$$

where A'_o and φ'_o are the new steady state amplitude and phase, A_t and φ_t are determined from boundary conditions and ω_d is the drive frequency [3].

Albrecht et al. [3] have also shown that increasing the Q of the cantilever allows using frequency modulation detection with an improved bandwidth. From this it can be seen that if you change the Q of the cantilever or its effective mass, you can increase the bandwidth of the detection system and therefore its scan rate without sacrificing sensitivity. In addition, Albrecht et al. have shown that the FM detection technique offers improved force sensitivity where the minimum detectable force is given by the equation

$$\delta F_{\min} = \sqrt{\frac{4kk_B TB}{\omega_o Q \left\langle z_{osc}^2 \right\rangle}}, \qquad (2)$$

where *k* is the spring constant of the lever, *T* is the temperature of the system, *B* is the bandwidth, ω_0 is the resonant frequency of the cantilever, *Q* is the quality of the system and $<z_{osc}^2>$ is the mean-square amplitude of the self-oscillating cantilever.

The ability to either increase or decrease the *Q* of a given cantilever should enable greater flexibility in using the same instrumentation for both imaging methods on the same sample as well as choosing the more applicable technique for a given set of observation/ experimental needs.

Two approaches to modifying a cantilevers *Q* have been demonstrated. One technique uses the damping effects of liquid to passively lower the *Q* [4]. The other method uses active feedback to modulate the response of the cantilever making it behave as though it has a lower *Q*. Image acquisition times of 1.7s [5] and 1.2s [4] have been reported for the passive method. Image acquisition times of 67ms have been reported for active Q damping [6].

Here we demonstrate increasing or decreasing the Q of a cantilever using a digital feedback controller based on a Digital Signal Processor (DSP) (Motorola DSP56300). A DSP-based controller provides a flexible means to implement this technique. In addition, conceptually the processor can measure its own loop response for calibration and optimization.

3.2 Description of Method

The fundamental *z* motion of a vibrating SPM cantilever can be simply described by the simple, driven damped harmonic oscillator [7]. The familiar equation is

$$m\ddot{z} + b\dot{z} + kz = F(t), \tag{3}$$

where *k* is the effective spring force, *m* is the effective mass of the cantilever mass spring combination, *b* is the damping coefficient and *F(t)* is an external driving force. The standard solution of this equation defines the following variables

$$\beta \equiv b/2m \tag{4}$$

the damping parameter and

$$\omega_o = \sqrt{k/m}, \tag{5}$$

is the resonant frequency of the spring mass system if the damping term is zero. The amplitude resonance frequency (the peak in the frequency response curve) can be calculated from the equation.

$$\omega_R = \sqrt{\omega_o^2 - 2\beta^2}\ , \tag{7}$$

From this the *Q* or "quality factor" of the spring mass oscillator is defined.

$$Q \equiv \frac{\omega_R}{2\beta} = \frac{\sqrt{\omega_o^2 - 2\beta^2}}{2\beta} = \sqrt{\frac{km}{b^2} - \frac{1}{2}} \tag{6}$$

From this we can see that by modifying *b*, the *Q* of the system can be changed. However it will also affect the resonant frequency. We can change the damping coefficient *b* by applying another force *f(t)* to the system via feedback. The equation of motion is rewritten.

$$m\ddot{z} + b\dot{z} + kz = F(t) + f(t) \tag{8}$$

which we have chosen

$$f(t) = b'\dot{z} \tag{9}$$

then equation (8) can be rewritten as

$$m\ddot{z} + (b - b')\dot{z} + kz = F(t)\,, \tag{10}$$

where we now have a new damping coefficient

$$\tilde{b} = b - b' \tag{11}$$

which allows us to rewrite equation (9)

$$m\ddot{z} + \tilde{b}\dot{z} + kz = F(t) \tag{12}$$

By measuring the velocity of the *z* displacement and applying a force proportional to this velocity on the cantilever, one should be able to suppress or enhance the *Q* of the system. For our experimental configuration, the forcing function *F(t)* is the ambient thermal energy. From the fluctuation dissipation theorem

$$\langle F(t)F(0)\rangle = 2bk_B T\delta(t) \tag{13}$$

Using the equation (11) for the new damping coefficient *b* this equation can be rewritten.

$$\langle F(t)F(0)\rangle = 2\tilde{b}k_B\tilde{T}\delta(t)\,, \tag{14}$$

where

$$\tilde{T} = \frac{b}{\tilde{b}} T \tag{15}$$

This implies that by varying the damping term we can change the effective temperature of the cantilever. From the equipartion theorem,

$$\left\langle z_{th}^2 \right\rangle = \frac{k_B \tilde{T}}{k} \tag{16}$$

Thus by changing the effective temperature you also change the mean square amplitude of the cantilever due to thermal fluctuations and improve the noise floor of the z measurement and hence the sensitivity. This is a simplification, because the other vibration modes of the cantilever are not completely orthogonal and do contribute to the motion in the z axis [8, 9]. However they do not appear to be the major component of the thermally induced motion we are trying to evaluate. The other difficulty with this simplification is, it does not properly account for the effects of the feedback circuit bandwidth. This is the delay between measuring the z position to outputting a voltage in response to this measurement. This delay is also present in analog circuits, but can be designed to be fairly small. It has not been until recently that DSP processors have become fast enough to minimize the turnaround delay. This enables the constructing a general-purpose feedback controller with its inherent flexibility for higher bandwidth applications such as the one presented here.

3.3 Experimental setup.

Figure 3.1 is a schematic representation of the experimental setup. Figure 3.2 shows pictures of the actual setup. It is based on the configuration for Q suppression

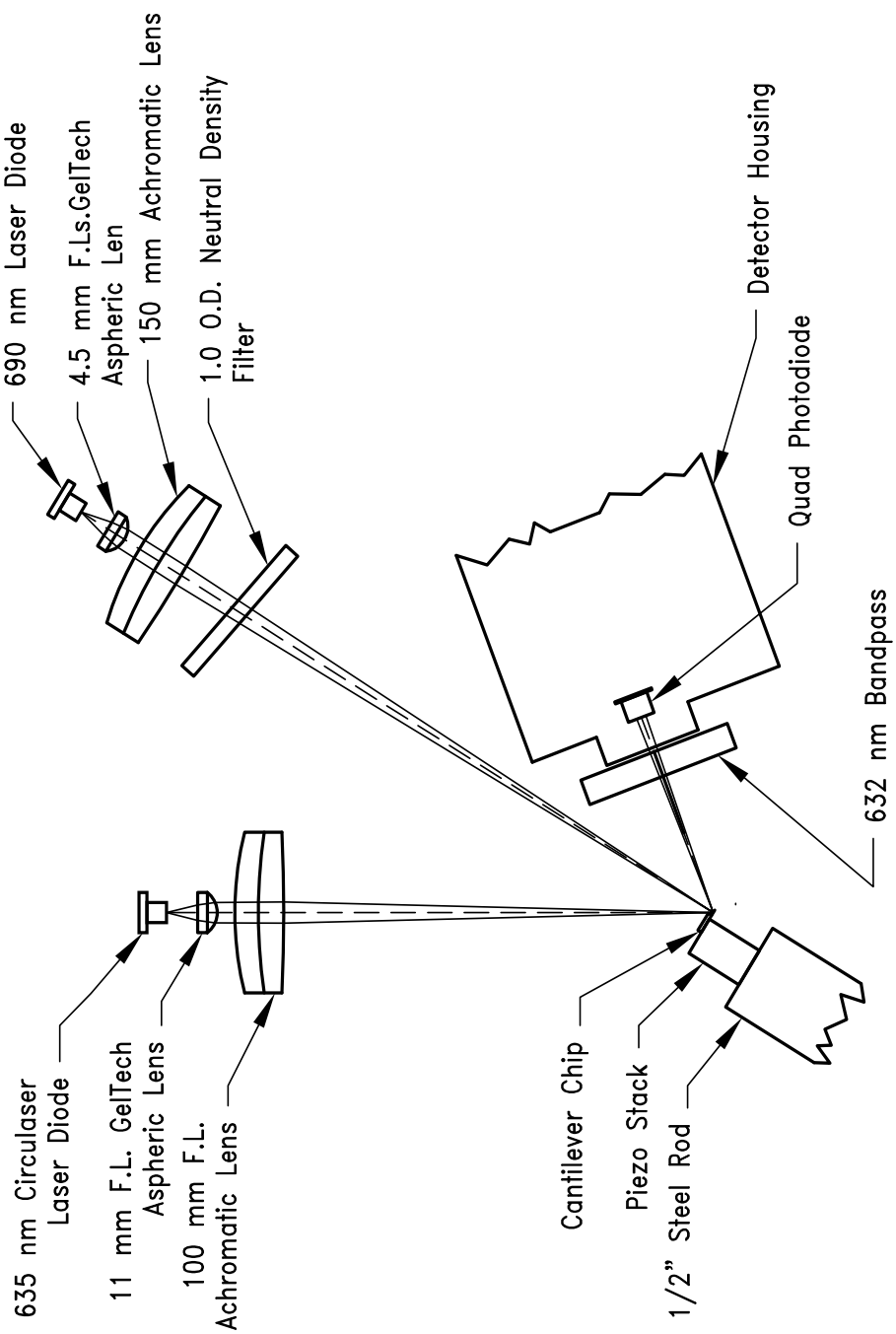

Figure 3.1. Schematic diagram of the optical arrangement used to implement the force feedback technique for actively changing the Q of an SFM cantilever. A second laser (the 690 nm laser diode here) heats the cantilever causing a differential expansion in a metal coated cantilever which applies a force to the tip of the cantilever that can be modulated by modulating the laser power. The 635 nm laser diode and quad photodiode implement a typical optical lever to measure the deflection of the cantilever tip.

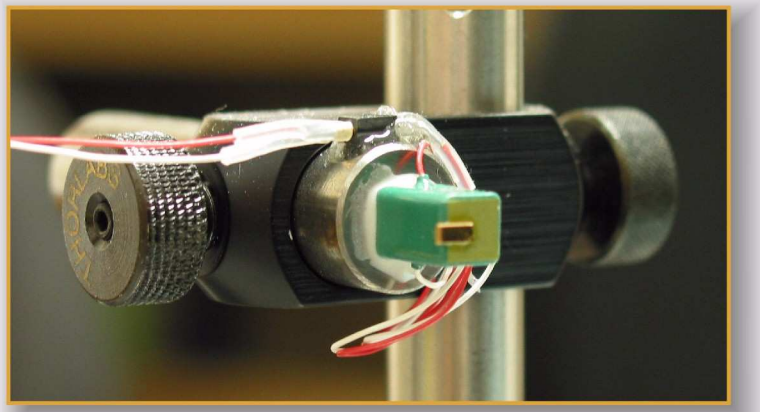

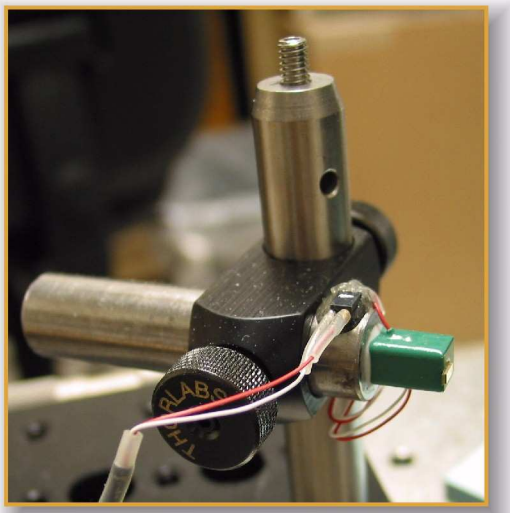

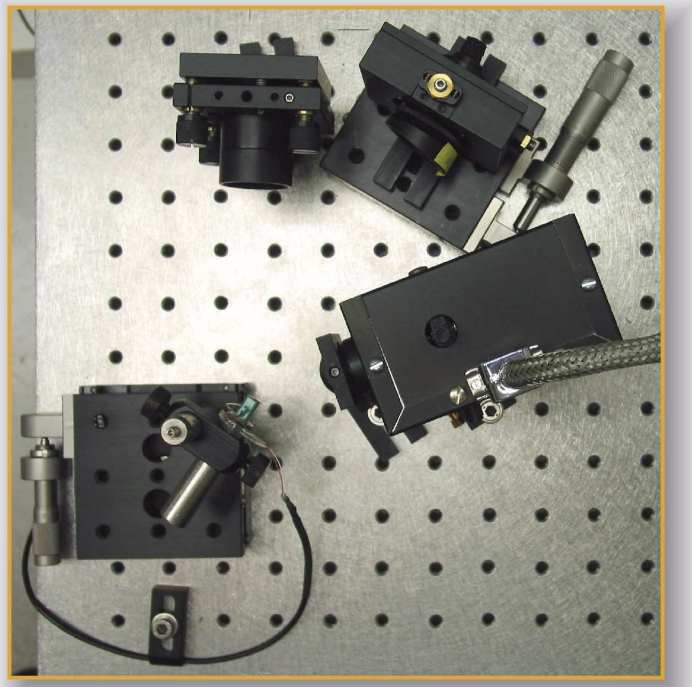

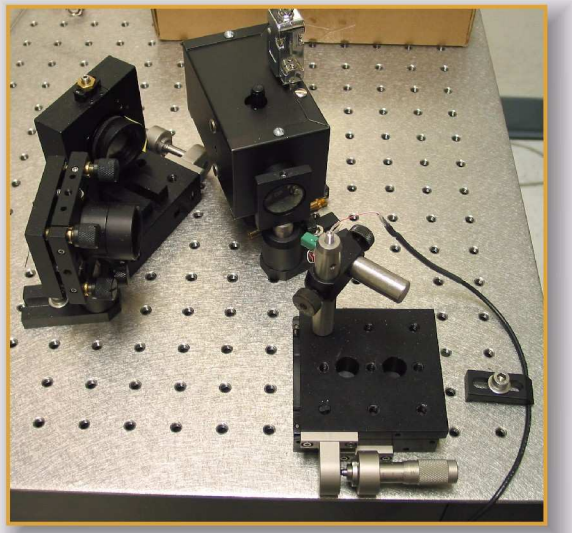

Figure 3.2. Q Modulation copto-mechanical configuration. Top two pictures show the mounting technique for the piezo and cantilever chip. Bottom pictures are the mechanical arrangement of the laser diodes and detector. See Fig. 3.1 for more detail.

demonstrated by Mertz et al. [10]. A laser diode and quad photodiode implement an optical lever to measure the *z* displacement of the cantilever. It should be noted that this does not directly measure the *z* displacement but the inclination at the end of the cantilever [8]. A second laser is then focused to a point in the middle of the cantilever to produce a force on the end of the cantilever by the differential thermal expansion of the reflective gold coating of the cantilever and its base material, silicon nitride. It has been shown that this technique can generate a reasonable force with relatively high bandwidth [10, 11]. The following paragraphs provide a more detailed description of the experimental apparatus.

The optical lever consists of a BlueSky Research (Milpitas, CA) Circulaser 635 nm 10 mW laser diode focused down to a spot on the cantilever. This spot is positioned to be as close as possible to the end of the cantilever. The reflected spot is imaged onto a CentroVision CD33H-4D quad photodiode with a 50 μm gap between the quadrants. The Circulaser contains a cylindrical microlens within the diode housing which is very close to the output of the laser diode. This lens substantially corrects the asymmetrical output of the laser diode which then only requires a simple lens to produce a reasonably circular collimated beam. An 11 mm focal length aspheric lens is used to produce this collimated beam. The collimated beam is focused onto the cantilever using a 100 mm focal length (f.l.) 25 mm diameter achromat (Edmund Scientific, Barrington, New Jersey). The laser diode power is adjusted so that the voltage output of one quadrant diode is ¼ the saturation limit of the electronics. This results in a laser diode output power level of approximately 3 mW. The laser diode is powered and regulated by a ThorLabs (Newton, New Jersey) LD1100 laser diode controller.

The output current of each photodiode in the quad photodiode is converted to a voltage by an op-amp (TI/BurrBrown OPA4130) in a transimpedance configuration. Schematics and drawings of the printed circuit board implementing this circuit can be found in the appendix. The feedback resistor is adjusted for a conversion gain of 1 V/10 uA (100 K ohms). This also coincides with the recommended power density limit for the photodiode of 10 mW/cm^2 when illuminated with a 1 mm spot. This means that the transimpedance

amplifier will reach its maximum output voltage when the diode is illuminated at its maximum recommended power density with a 1 mm spot (assuming uniform intensity across the spot). The quad photodiode and its amplifier circuit are in a black aluminum electronics box for EMI shielding and for minimizing scattered light hitting the photodiode. Also within the box is an x-y-z translation stage supporting the photodiode and its amplifier circuit to ease alignment.

The diode is positioned so that the reflected spot has a ~1mm diameter centered on the detector. It can be shown that the displacement sensitivity is somewhat insensitive to this exact diameter when implementing an optical lever for measuring the z displacement. The lever gain cancels the sensitivity decrease as the spot diameter increases. A 632 nm, 10 nm FWHM (Edmund Scientific) bandpass filter was placed in front of the detector to filter out scattered light from the forcing laser.

The quad photodiode and its amplifier were powered by the DSP electronics described in Chapter 2. Each amplifier output is connected to an individual 16-bit A/D converter circuit. Using the DSP's data output connection to a personal computer, these signal levels were used to align the optical lever laser spot with the center of the quad photodiode with a oscilloscope type program for displaying the data from the A/Ds. After this alignment, one of the amplifier outputs was disconnected from the DSP electronics and connected to the input of a Stanford Research SR760 FFT Spectrum Analyzer (Stanford Research Systems, Sunnyvale, California).

The forcing laser is a Hitachi 690 nm 35 mW laser diode. Its output is not corrected for its elliptical beam shape. This is actually desired so that both sides of the triangular cantilever can be illuminated without illuminating a significant portion of the whole cantilever. This laser diode's output was collimated using a 4.5 mm focal length aspheric lens. The collimated beam is then focused by a 150 mm focal length achromat (Edmund Scientific) onto the middle of the cantilever beam. A neutral density filter with an ND of 1.0 is placed after the achromat to lower the output power. This laser was chosen for wavelength not power. This allows using the bandpass filter to block its scattered light

onto the detector. The power needed for deflecting the cantilever is relatively low (300uW) [10]. This laser diode was powered and regulated by a ThorLabs IP500 laser diode driver board. It offers the capability of modulating the diode current via an external voltage signal with a bandwidth of 50KHz.

The DSP was programmed to take the derivative of only one of the photodiode quadrant signals. This made the code fairly simple. Performing the complete x-y position calculation is unnecessary for the basics of this experiment. In fact several optical lever configurations use just a dual photodiode. In this case taking the derivative of the difference of the signals on two of the photodiode is equivalent to taking the derivative on just one. Also, because of the desire to easily measure the response of the system independent of the controller, one of the diodes is disconnected from the DSP electronics and connected to the SR760 spectrum analyzer. The resulting derivative value is multiplied by a coefficient stored in memory that was set at different values to determine how much the technique could change the Q of a given cantilever. The resulting value is then transmitted to one of the output DACs whose voltage output was connected to the 690 nm laser diode driver.

Two cantilevers were used for this experiment, a rectangular cantilever with a typical resonant frequency of 15 kHz and a triangular cantilever with a typical resonant frequency of 6 kHz. These are two of the six cantilevers on a the single chip from TM Microscopes (MSCT-AUNM). Dimensions for the rectangular cantilever are 200um L x 20um W x 0.6um T. Dimensions for the triangular cantilever are 320um L x 0.6um T. The legs of the cantilever are 22um wide. The spring constants are 0.02N/m for the rectangle and 0.01N/M for the triangular cantilever. The cantilever chip was attached to a piezo stack (6.1 μm at 100V, ThorLabs) with cyanoacrylate adhesive (Loctite QuickTite). This enabled a fairly rigid attachment with the ability to remove the chip by soaking the adhesive joint with acetone. Several cantilever chips were attached and removed using this technique. The piezo stack was attached to the machined flat end of a ½” diameter steel rod with Torr Seal Epoxy (Varian No. 953-0001). This enabled using

standard optic mounts for holding and manipulating the cantilever chip and its support assembly (See Figure 3.2).

3.4 Results and Discussion.

The above mentioned mounting of the cantilever was a compromise between making a rigid structure without resorting to custom machined parts and was convenient to adjust. The piezo stack was added to enhance the ability to measure resonances and in case the ambient thermal noise was an insufficient driving force. To determine how stable the entire assembly was, three baseline measurements of the noise spectrum were made. One was just the signal output from one of the photodiode pre-amps with the photodiode covered so that it was not illuminated by any light. The second was recorded by focusing the optical lever laser onto the cantilever chip instead of the cantilever, adjusting the photodiode so that the reflected beam was centered on the detector and measuring the voltage spectrum output of the photodiode. The third baseline was made by driving the piezo in the above setup with a white noise voltage signal from an Stanford Research Systems DS335 function generator. The settings on the function generator were 5 V offset (the piezo cannot have its positive lead more negative than its negative lead) with an amplitude setting of 5 V_{p-p}. According to the manual for this instrument, "The rms value for NOISE is based on the total power in the output bandwidth (about 3.5 MHz) at a given peak to peak setting." It is left to the reader to figure out what that means. Measuring the resulting voltage spectrum from the DS335 on the SR760, gives a noise density of ~850$\mu V_p/Hz^{1/2}$. This implies that if you take the peak to peak amplitude voltage setting, divide it by $(3.5x10^6)^{1/2}$ x $2^{3/2}$, you can approximate the noise spectral density output by the DS335. This yields 945$\mu V_p/Hz^{1/2}$ for the above setting. The piezo has an expansion coefficient of ~60 nm/Volt. This would have added ~5 to 6 nm (rms) of translational noise over a 10 kHz bandwidth.

The above calculation is somewhat simplified. Measuring the power spectrum with an FFT is problematic [12]. One critical issue is the windowing function used by the FFT. In the case of the above measurement and all that follow, the Blackman-Harris (BMH)

window was used. A correction factor must be used to account for the bandwidth of a given window function. The following discussion and the values calculated are estimates and are used here to make relative comparison of the noise sources. A more rigorous approach would require taking the autocorrelation of a reasonably long time period of data and then taking the Fourier transform of this result. Using the SR760 was more straightforward and allowed monitoring the experiment in real-time. It provides measurements that provide a fair representation of the effects on the system Q using the DSP feedback technique. However, it makes the following noise analysis only an approximation or comparison.

The results of these measurements are shown in Figure 3.3. The SR760 can only take spectrums with 400 points of resolution at a given frequency range. The graphs shown here were generated by taking 4 spectrums from 0-195, 0-1.5KHz, 0-12.5 KHz and 0-100 KHz for each of the above measurement conditions. The data was taken in the peak voltage mode per frequency bin (Volts peak to peak/ 2). The resulting data was then normalized for the width of the frequency bins by dividing each bin voltage value by the square root of the frequency bin width for a given frequency span (i.e., $250^{1/2}$ for the 0-100 KHz spectrum). If you divide again by 4 you get approximately the rms voltage. The zero frequency or DC value for each frequency span was plotted at the next factor of ten frequency point from the previous lower frequency span to help distinguish each group. Also plotted for comparison are spectrums for measurements of the two cantilevers with the feedback circuit disconnected for spans of 0-50 kHz. The forcing diode was on.

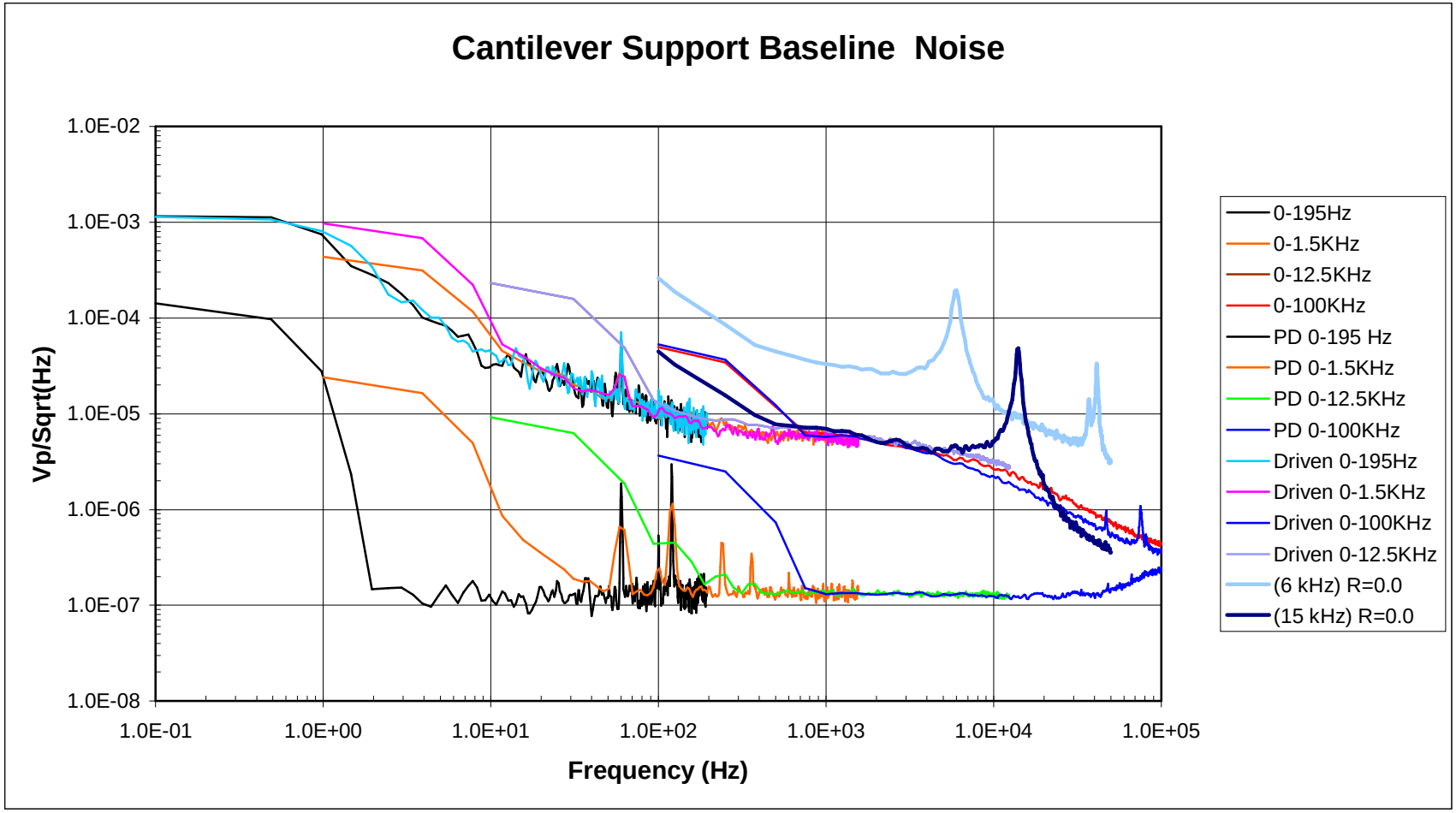

Figure 3.3. Spectrum of baseline noise of the covered photodiode, the photodiode illuminated by the optical lever laser reflected off the cantilever chip base and the same reflected illumination with a white noise source driving the piezo. Also included are spectrums of the cantilevers response with no feedback

The photodiode and its amplifier circuit do not appear to be a significant noise source. 60 Hz line noise is still present. These are the traces with the lowest signal levels. When applying the additional noise through the piezo, some higher frequency resonances in the support structure were excited but the rest of the noise floor is not very different from the undriven case. The reflected beam does show some significant noise. Based on the specifications of the 635 nm laser diode and the optics used for focusing it down to a spot on the cantilever, the spot on the cantilever can be from 43 to 19 μm $1/e^2$ diameter which should not overfill the cantilever tip too badly for the triangular cantilever at the worse case value of 43 μm. It will more than likely overfill the rectangular cantilever. The spot at the photodiode could then vary from 0.95 to 2.14 mm. The laser intensity was adjusted to be typically close to one fourth the maximum voltage output of any of the photodiode amplifiers or 2.5 volts. According to the noise spectrum graphs the system has worst case ~8 $\mu V_p/Hz^{1/2}$ in the region of interest for these experiments (1 to 20 kHz). Over a 10 KHz bandwidth, this is 800 μV_p of baseline noise. Using the simple approximation for the translational sensitivity of a quad photodiode $((\Delta V/V_{offset})*(\text{Spot dia}))$, the spectrum for the reflected beam suggests a translational noise of (0.0008/2.5)*1 mm = 320 nm_p. This is not too surprising. The laser diode drive is specified to have an output stability of <0.01%. There is no bandwidth given. In a simple interpretation this would equate to 250 μV_{rms} if the above value is an RMS value or ~750 μV_p on a 2.5V signal.

It needs to be restated that in order to make these measurements with a standard instrument (the SR760) that would be independent of the control electronics, the output of just one photodiode element in the quad was measured for these noise spectrums. Unfortunately this chosen method did not allow for a means to normalize this probable intensity noise from the measurements presented. Although it seems that the intensity noise floor of the LD1100 could account for the bulk of the baseline noise seen here, there is also the significant possibility of other intensity noise due to back reflected light into the diode causing instabilities in the pointing and intensity of the laser diode. Laser diodes, especially shorter wavelength like the one used here, are fairly notorious for these problems [13]. There is also a contribution from the motion of the mechanical system.

The author has seen similar apparent translation noise in a more rigid setup using a similar laser diode and quad photodiode.

The optical lever does provide amplification above the noise floor based on the following analysis. For an optical cantilever system such as the one used here, the deflection angle θ is related to the change in the z translation of the tip by the equation [14]

$$\delta(\theta) = 2A\delta z/(l\cos\phi), \tag{17}$$

where l is the length of the cantilever, ϕ is the angle between the surface being scanned and the cantilever, and A is a geometrical constant for the bending of the cantilever. For an unfilled triangular cantilever, A is ~1.8 and for a rectangular cantilever A is 1.5. If L is the distance from the cantilever to the detector (50 mm in this implementation), then

$$\begin{aligned} \delta z_{pd} &= L\tan\delta\theta \\ &\approx L\delta\theta \\ &\approx 2AL\delta z/(l\cos\phi) \end{aligned} \tag{18}$$

In this case ϕ is zero because the cantilever is not interacting with a surface. Plugging in the values for the two cantilevers used in the experiment, $\delta z_{pd}/\delta z$ or the optical lever gain equals 750 for the rectangular cantilever and 562.5 for the triangular cantilever. This means that the laser intensity noise equates to 427 pm_p for the rectangular cantilever and 569 pm_p for the triangular cantilever. Using equation (16) from the equipartition theorem, the expected Brownian type z translational thermal noise of the tip is 641pm_{rms} for the triangular cantilever and 453 pm_{rms} for the rectangular cantilever. The noise floor seems comparable. It should be noted that the equipartition theorem assumes an infinite bandwidth so these figures should be divided down by some amount. It should also be noted that the above are RMS values. Multiplying them by three is a reasonable approximation to peak amplitude.

The above noise is significant but is low enough to still see the resonances of the two cantilevers as the 0-50 kHz spectrums of these two cantilevers show. The 6 kHz cantilever does show an elevated noise floor. From the results of the equipartition theorem above it is somewhat expected but it seems a little higher than predicted by the simple calculation. It is a little problematic that several of the papers the author reviewed

do not discuss this noise source in their measurements. Laser diodes are one of the easier light sources to intensity stabilize but they still have a significant contribution to the measurement noise of optical cantilevers as demonstrated in the above analysis and measurement.

After the above measurements were made, the apparatus was readjusted to measure the motion of the cantilever and determine how much the above technique using the DSP electronics could change the Q of the two cantilevers evaluated. The 635 nm laser diode was focused as close as possible to the end of the cantilevers and achieved a reasonable spot on the quad photodiode. Similarly 690 nm laser was adjusted to illuminate the center of the cantilever. It was later discovered that a good way to find the optimum spot was to set the DSP electronics to increase the Q and adjust the position of the 690 nm spot for maximum peak.

The DSP generates the real *b'* coefficient in equation (8) by multiplying the value in a register called R by 16 and then outputting the result via a DAC to the laser diode driver board. Figure 3.4 shows the spectrums at three different R coefficient settings -0.180, 0.0, and 0.049 for the 6 kHz cantilever centered at resonance. The center curve is the natural resonance of the cantilever in air, i.e., the coefficient is zero. The solid black lines represent the least-squares fit to the equation for the amplitude response of the driven simple harmonic oscillator [7]

$$V = \frac{A}{(\omega_o^2 - \omega^2)^2 + 4\omega^2\beta^2} \tag{19}$$

for the three data sets. As can be seen the technique can dampen or increase the Q over a range of two orders of magnitude. The modulation depth of the forcing laser and the bandwidth of the electronics seem to be the limiting factors. The Q enhancement was the most obvious. The curve shown here was the maximum R could be set to before significant harmonics appeared. These were attributed to running into the maximum power level setting on the IP500 laser driver board and the nonlinear region of the laser

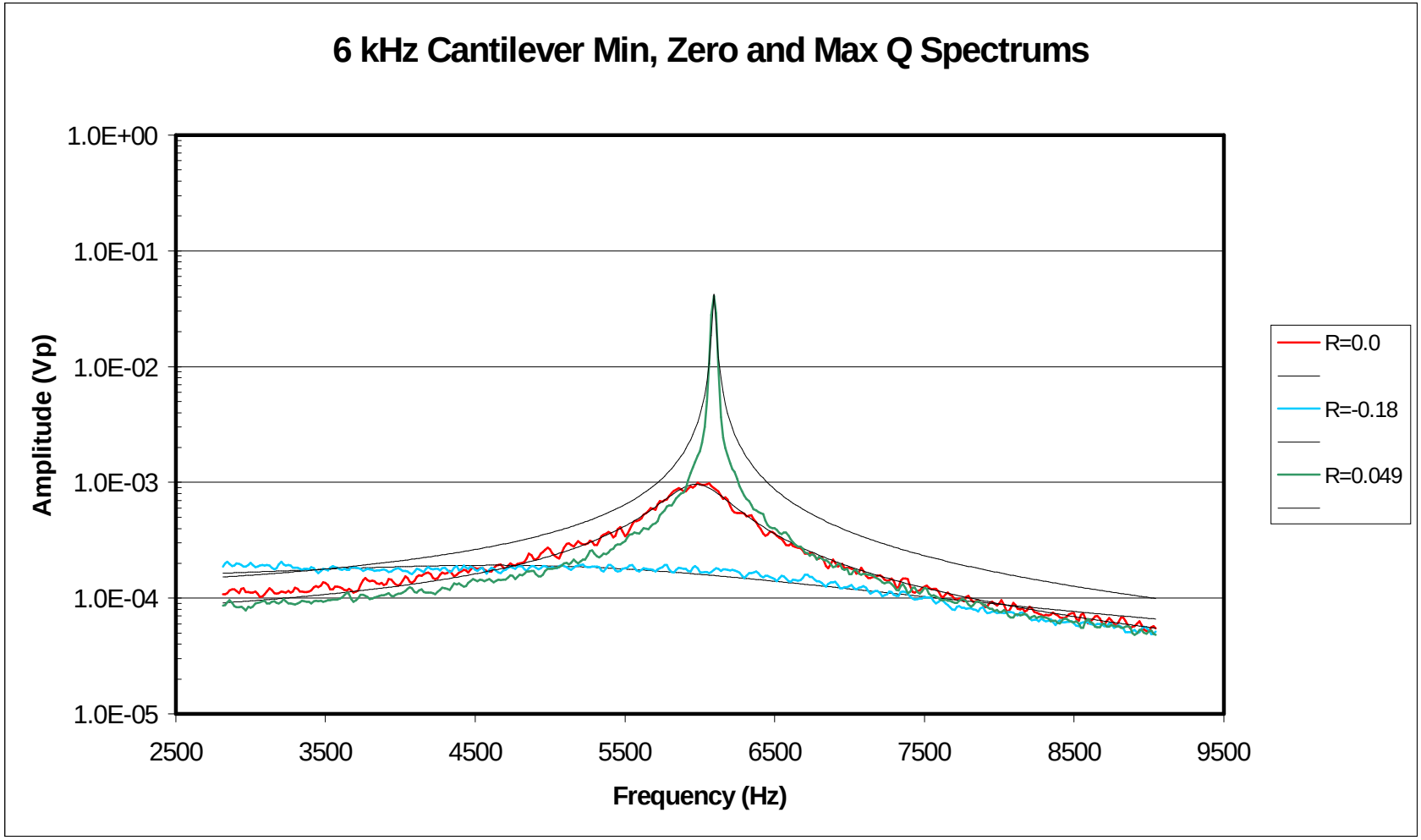

Figure 3.4. Spectrums of the 6 kHz cantilever response for the extremes of R centered at the cantilevers resonance. These are graphs of the minimum, maximum and zero R coefficient settings that could be obtained before harmonics were generated. The black solid lines are the best fit of the data to equation (19)

diode response at minimum power. This clipping generated significant harmonics. The curve for this response where harmonics were generated showed an even higher Q suggesting three orders of magnitude adjustment, but does not visually fit equation (19) as well. In addition the error for the Q derived from this data was significant. This response is shown in the later graphs.

Figure 3.5 shows similar spectrums for R coefficients of –0.260, 0.0, and 0.055 for the 15 kHz cantilever. The solid lines are the best fit curves for equation (19). This feedback technique was also able to change Q over two orders of magnitude. The bandwidth limit of the feedback electronics is more apparent. It can be seen by the substantial move of the center frequency and the inability to dampen Q as much as in the 6 kHz cantilever. There is also the appearance of a lower frequency peak when Q is damped in later figures. If the R coefficient is increased to the point where harmonics are generated a similar increase in Q is seen as in the 6 kHz cantilever suggesting being able to change Q over 3 orders of magnitude. However, the same poor fit to equation (19) is demonstrated and the corresponding large error in the derived Q.

Figures 3.6 and 3.7 are combined spectrums, centered at the resonance of the respective cantilevers, for several of the R coefficients tried on the two cantilevers. Fitted curves are not shown here. Figure 3.8 is a 0–50 kHz spectrums for the 6 kHz cantilever for several of the R coefficients tried. This graph demonstrates that a higher frequency resonance is affected as Q is increased or decreased by this method. It should be noted that this higher frequency effect was not noted by previous work on damping Q [3, 6, 10]. Figure 3.9 is a similar 0–50 kHz spectrum for the 15 kHz cantilever. This spectrum does not go out far enough to see the higher frequency effects. This effect on a higher frequency resonance was also observed on the rectangular cantilever. In both cases these peaks are probably due to the other vibrational modes of the cantilevers such as translation or rotation. They are not a harmonic of the fundamental resonance investigated here. Note that the harmonic peaks that do appear in these graphs are when the limits of the forcing laser are reached.

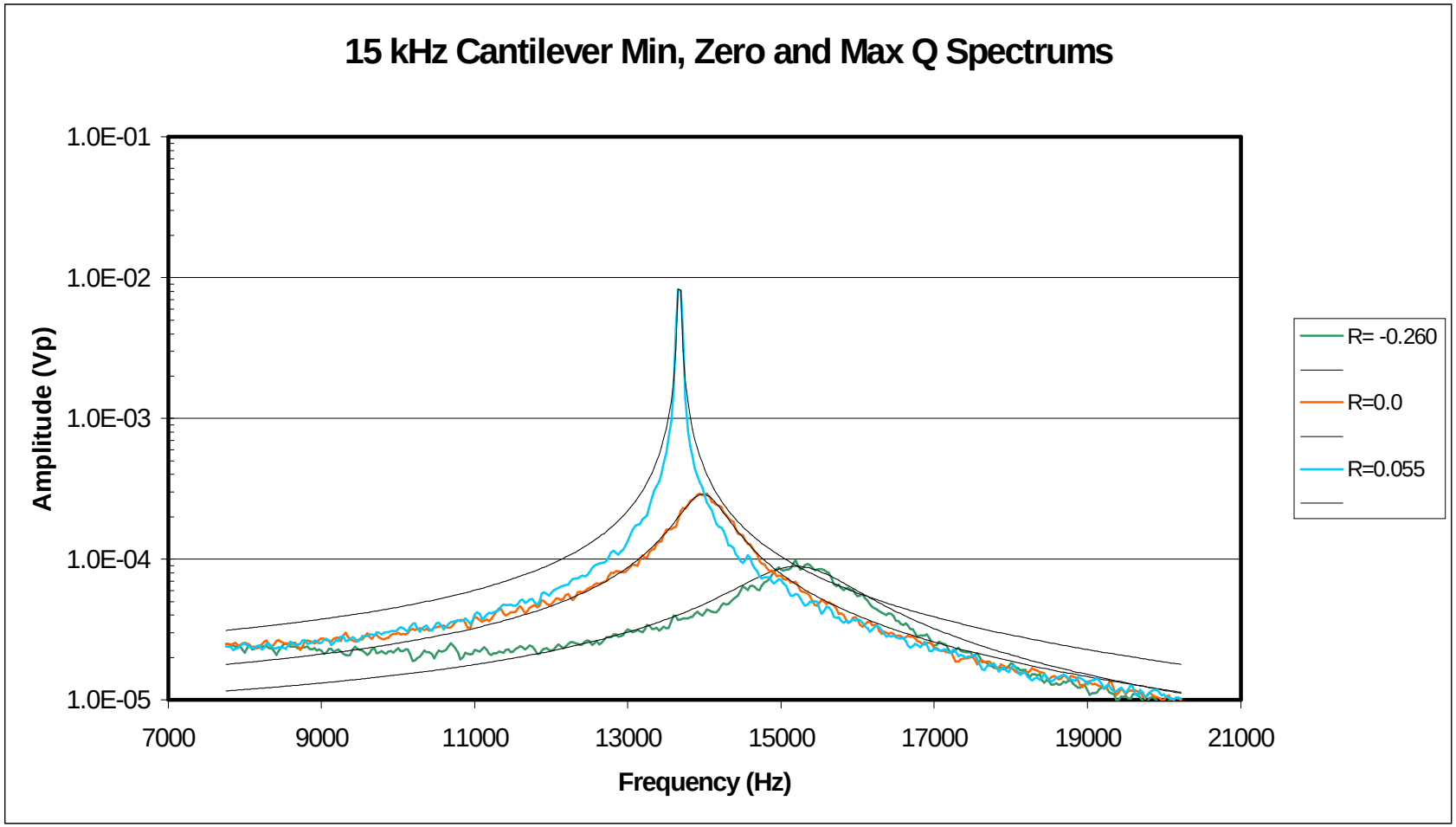

Figure 3.5. Spectrums of the 15 kHz cantilever response for the span of R centered at the cantilevers resonance. These are graphs of the minimum, maximum and zero R coefficient settings that could be obtained before harmonics were generated. The black solid lines are the best fit of the data to equation (19)

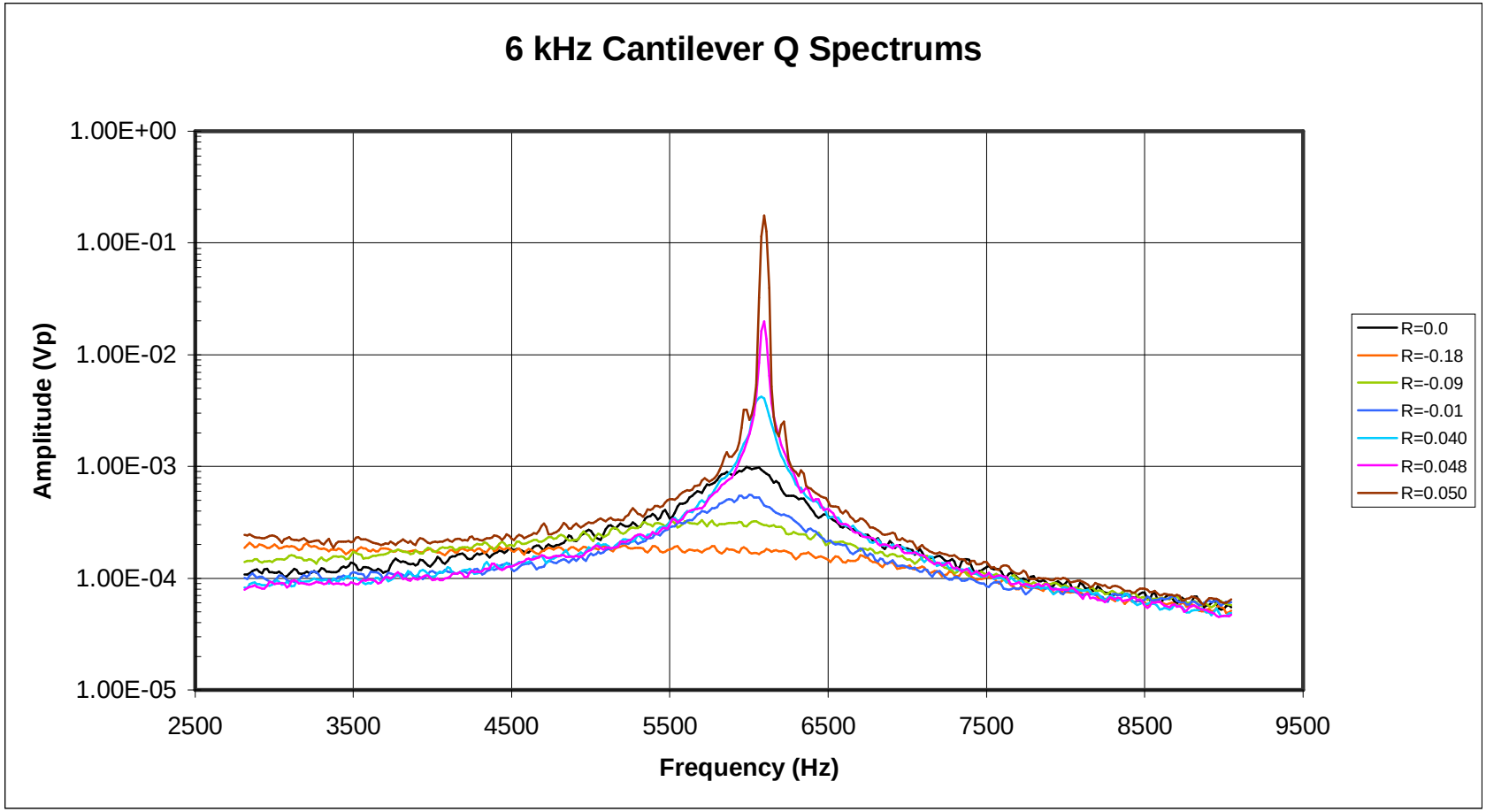

Figure 3.6. Combined spectrums of the 6 kHz cantilever, centered at the resonance frequency for several of the R coefficients tried on this cantilever. All the curves for all the R coefficients response measurements made are not shown for clarity.

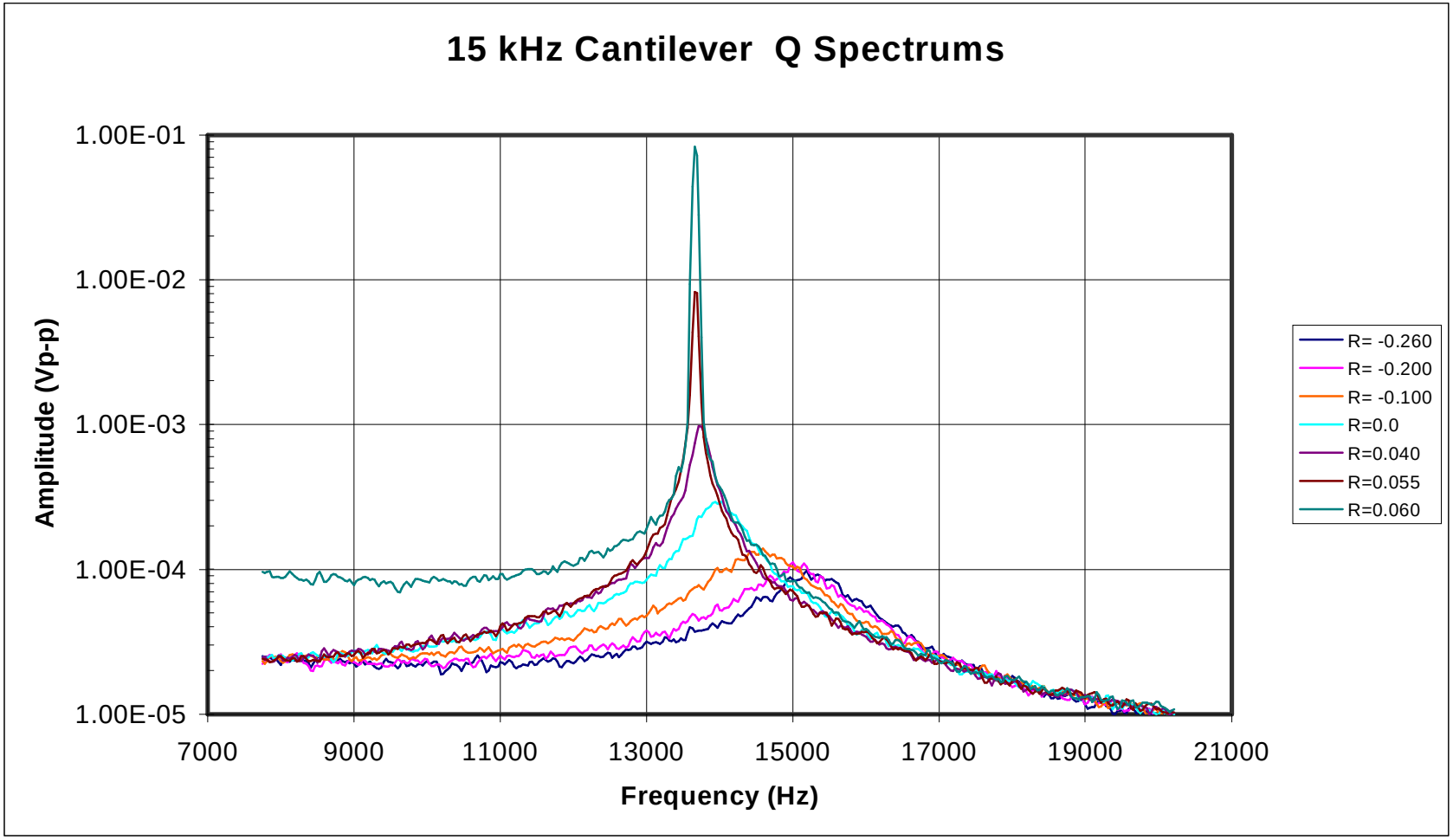

Figure 3.7. Combined spectrums of the 15 kHz cantilever, centered at the resonance frequency for several of the R coefficients tried on this cantilever. All the curves for all the R coefficients response measurements made are not shown for clarity.

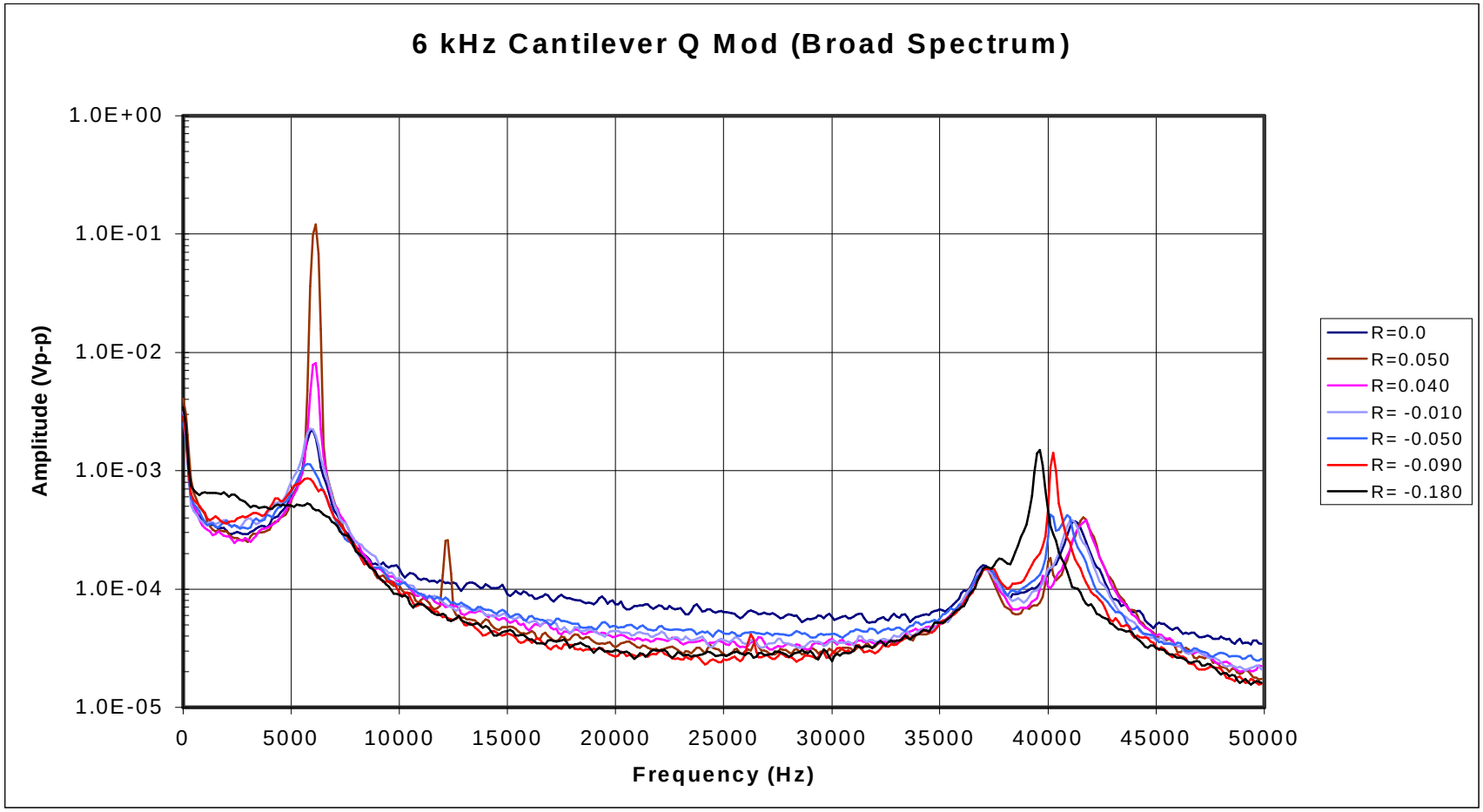

Figure 3.8. 0-50 kHz spectrums of the 6 kHz cantilever for several of the R coefficients tried on this cantilever. The graph demonstrates that a higher frequency resonance is affected as the Q is increased or decreased. Harmonic peaks are when the limits of the forcing laser are reached. All the curves for all the R coefficients response measurements made are not shown for clarity.

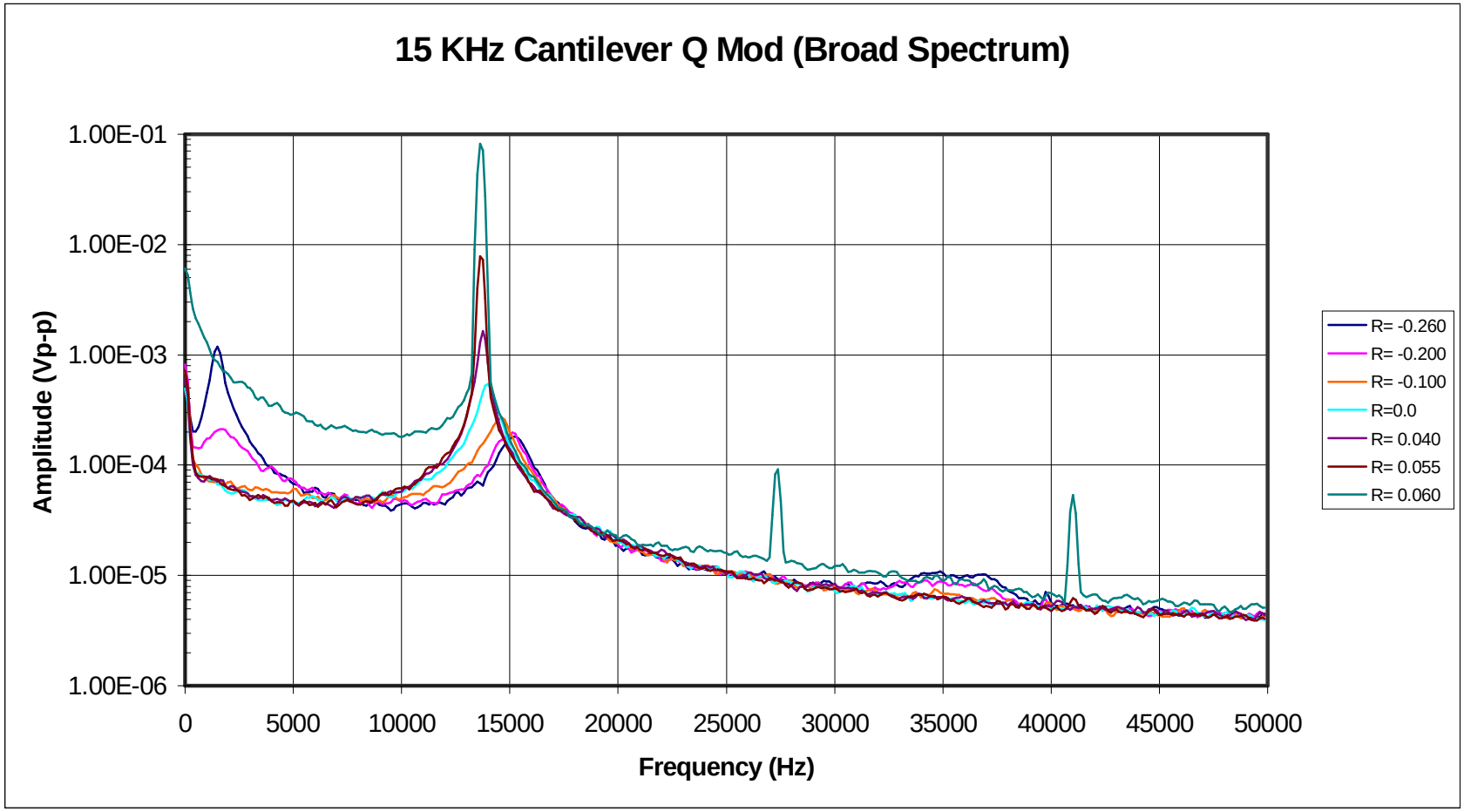

Figure 3.9. 0-50 kHz spectrums of the 15 kHz cantilever for several of the R coefficients tried on this cantilever. All the curves for all the R coefficients response measurements made are not shown for clarity. Harmonic peaks are when the limits of the forcing laser are reached.

Figures 3.10 and 3.11 plot the change in Q as a function of R. The extremely high Q values for the spectrums where significant harmonics are generated are not included in these graphs. The Q values were derived from the best fits of equation (19) to the frequency centered data. Figure 3.12 and 3.13 are plots of $<z_{th}^2>$ vs R for the two different cantilevers. The graphs are a composite of calculating $<z_{th}^2>$ over various bandwidths. These graphs show some of the expected change of the effective temperature to changes in *b'* as expected from equations (13) and (14), however, there is a significant non-linear increase as Q is increased beyond the natural Q of the cantilever.

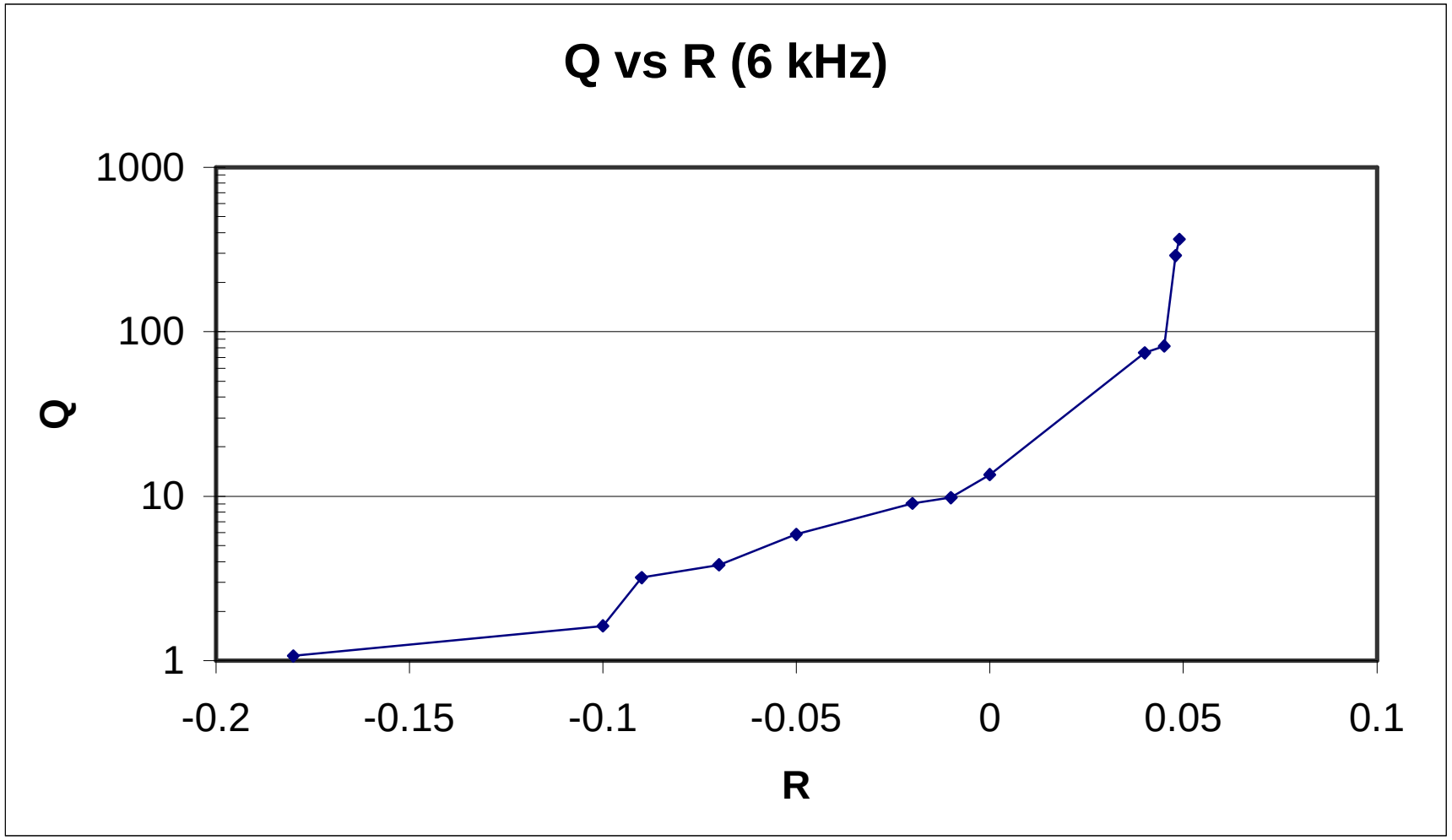

Figure 3.10. Graph of the change in Q as a function of R for the 6 kHz cantilever

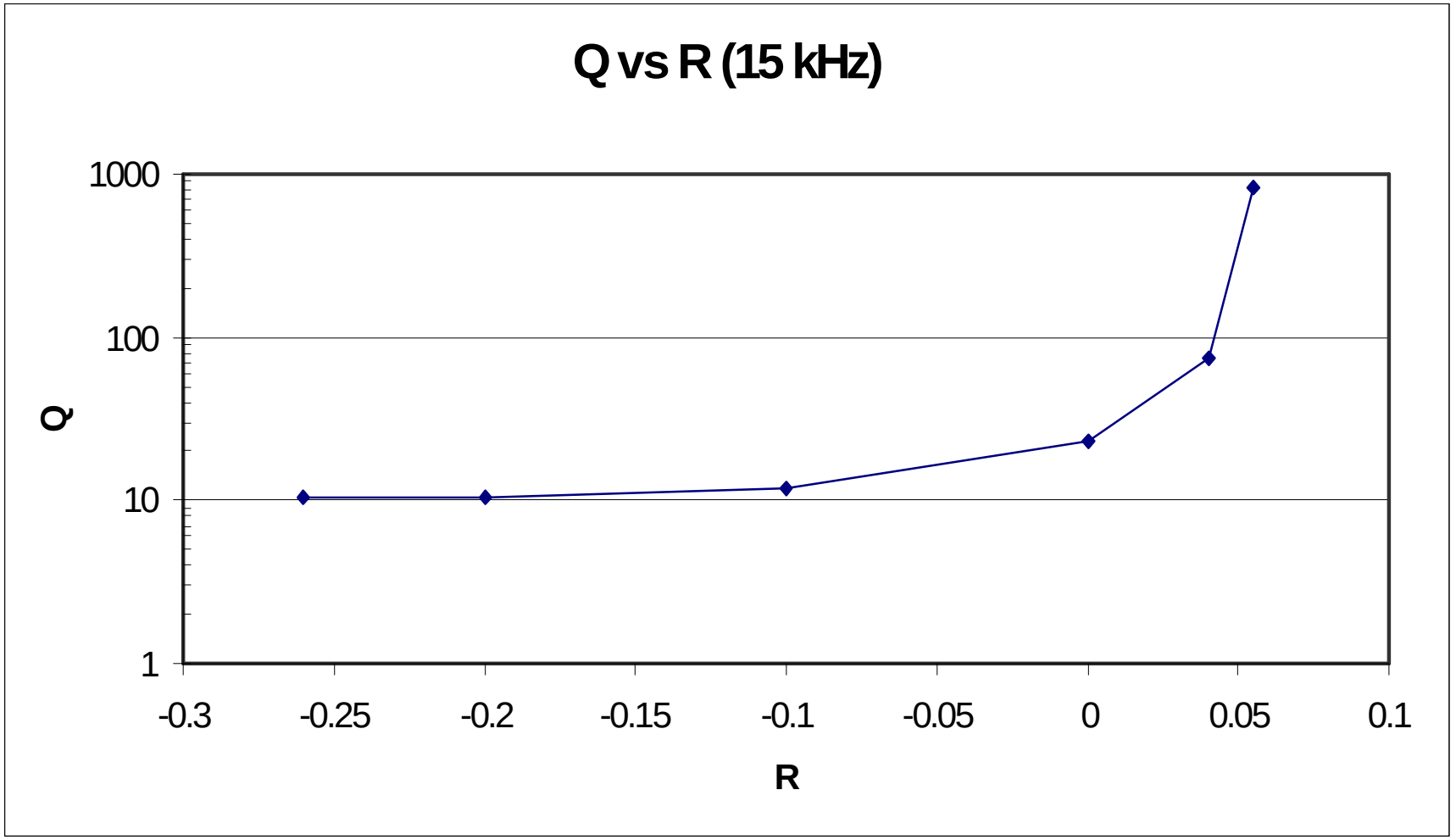

Figure 3.11. Graph of the change in Q as a function of R for the 15 kHz cantilever.

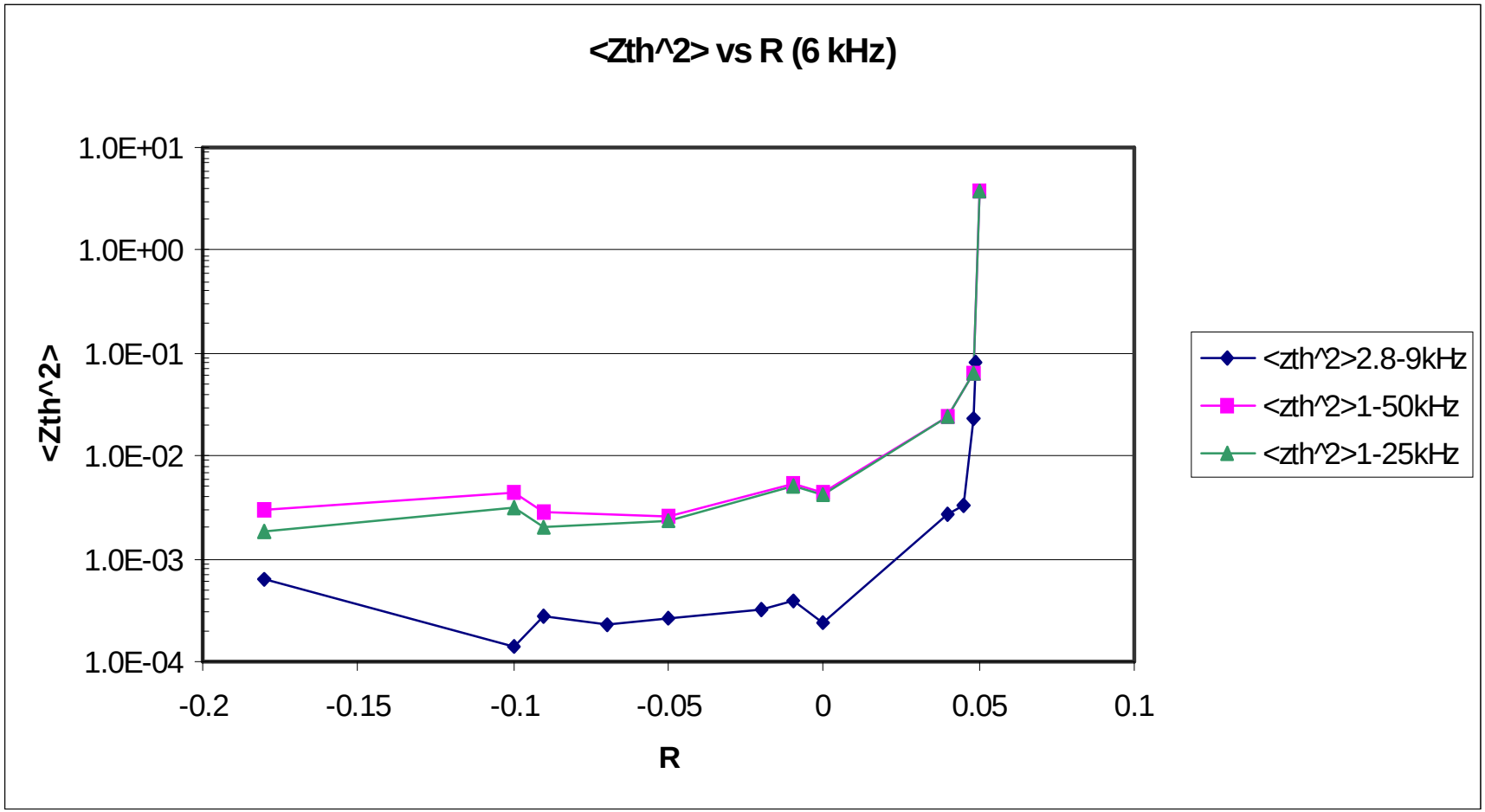

Figure 3.12. Plots of the mean squared amplitude of the end of the cantilever, $<z_{th}^2>$, vs R for the 6 kHz cantilever. The graph is a composite of calculating $<z_{th}^2>$ over the bandwidths shown.

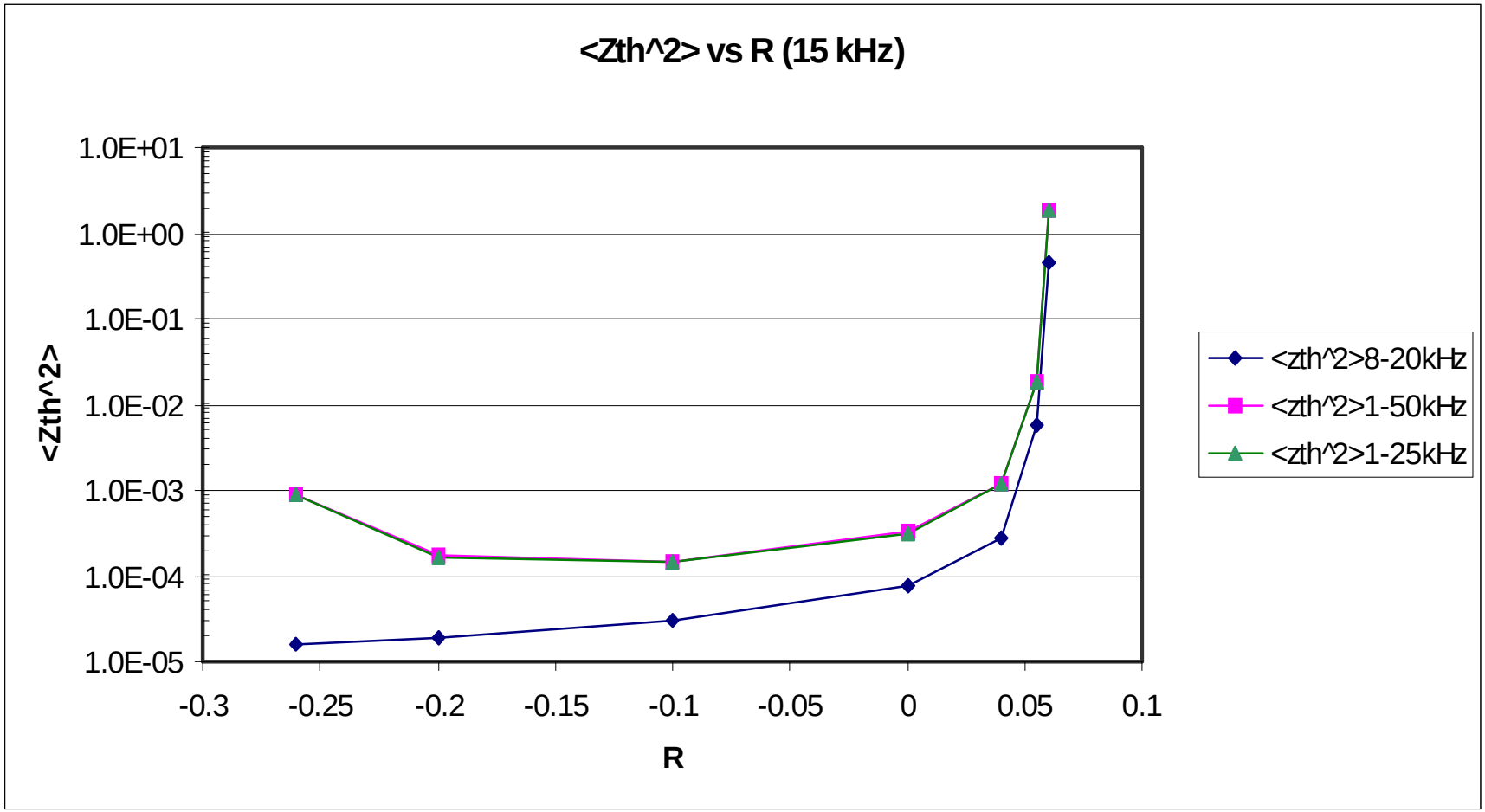

Figure 3.13. Plots of the mean squared amplitude of the end of the cantilever, $<z_{th}^2>$, vs R for the 15 kHz cantilever. The graph is a composite of calculating $<z_{th}^2>$ over the bandwidths shown.

3.5 Conclusions

The experimental results definitely show that the Q of a cantilever can be actively modified by a DSP-based feedback system expanding upon the technique of Mertz et al. [10]. It allows for both increasing and decreasing the Q over almost three orders of magnitude by just changing a coefficient in the processor's memory. This, to the knowledge of the author, is the first demonstration of changing the Q of a cantilever using a DSP based feedback system. In addition it is the first to both increase and decrease the Q with the same controller. In addition it is the first to report the effects of the technique on higher frequency harmonics which should be further investigated. If the bandwidth of the detection system is not restricted to the main resonance region these higher harmonics will contribute to the overall noise floor of the system and lower sensitivity.

The technique affords some amount of changing the effective temperature of the cantilever for the damping case which should result in an improved signal to noise ratio as well as allows for higher speed scanning. The demonstrated Q-damping should allow improvement in scan speed of a factor of 10 for a 6 kHz cantilever. Using higher speed A/D converters should enable applying the technique to higher resonant frequency cantilevers using the same speed processor if the same simple algorithm is used. For the case where increasing Q is desired for FM detection techniques, adding a look-up table for the lower power levels of the laser should enable a larger dynamic range of force on the cantilever which should allow boosting Q to better than 10,000. Higher Q improves FM detection. A higher speed A/D converter would also be beneficial. The increase in the effective temperature as shown in Figures 3.13 and 3.14 shows that the technique only improves signal to noise when a system is not thermally limited. Because the bandwidth can be controlled independently of Q the method may be able to achieve a reasonable signal to noise ratio although operate at a slower speed than was achieved by Albrecht et al. passive approach. The significance of this approach is the ability to use the same basic hardware to implement several different aspects of the control and

feedback functions of the various modulation and detection techniques for scanned force microscopes.

3.6 References

1. Binnig, G., C.F. Quate, and C. Gerber, *Atomic force microscope*. Physical Review Letters, 1986. **56**(9): p. 930-933.
2. Martin, Y., C.C. Williams, and H.K. Wickramasinghe, *Atomic force microscope-force mapping and profiling on a sub 100-Å scale.* Journal of Applied Physics, 1987. **61**(10): p. 4723-4729.
3. Albrecht, T.R., et al., *Frequency modulation detection using high-Q cantilevers for enhanced force microscope sensitivity.* Journal of Applied Physics, 1991. **69**(2): p. 668-673.
4. Paloczi, G.T., et al., *Rapid imaging of calcite crystal growth using atomic force microscopy with small cantilevers.* Applied Physics Letters, 1998. **73**(12): p. 1658-1660.
5. Viani, M.B., et al., *Fast imaging and fast force spectroscopy of single biopolymers with a new atomic force microscope designed for small cantilevers.* Review of Scientific Instruments, 1999. **70**(11): p. 4300-4303.
6. Sulchek, T., et al., *High-speed tapping mode imaging with active Q control for atomic force microscopy.* Applied Physics Letters, 2000. **76**(11): p. 1473-1475.
7. Marion, J.B., *Classical Dynamics of Particles and Systems*. 2nd ed. 1970, New York: Academic Press.
8. Butt, H.-J. and M. Jaschke, *Calculation of thermal noise in atomic force microscopy.* Nanotechnology, 1995. **6**: p. 1-7.
9. Rabe, U., K. Janser, and W. Arnold, *Vibrations of free and surface-coupled atomic force microscope cantilevers: Theory and experiment.* Review of Scientific Instruments, 1996. **67**(9): p. 3281-3293.
10. Mertz, J., O. Marti, and J. Mlynek, *Regulation of a microcantilever response by force feedback.* Applied Physics Letters, 1993. **62**(19): p. 2344-2346.
11. Marti, O., et al., *Mechanical and thermal effects of laser irradiation on force microscope cantilevers.* Ultramicroscopy, 1992. **42-44**: p. 345-350.
12. Brigham, E.O., *The Fast Fourier Transform and its Applications*. Prentice Hall Signal Processing Series, ed. A.V. Oppenheim. 1988, Englewood Cliffs: Prentice Hall.
13. Hobbs, P.C.D., *Building Electro-Optical Systems: Making It All Work*. Wiley Series in Pure and Applied Optics, ed. J.W. Goodman. 2000, New York: John Wiley & Sons, Inc.
14. Gould, S.A.C., et al., *The atomic force microscope - a tool for science and industry*. Ultramicroscopy, 1990. **33**(2): p. 93-98.

Chapter 4

Sculpting Nanoscale Potentials with Optical Tweezers and Digital Feedback

4.1 Introduction

The laser light trap, or optical tweezers, for confining small particles including atoms offers numerous possibilities for manipulating minute objects. Derived from Arthur Askin's initial discovery and demonstration of the mechanism, several significant applications have been made [1]. One of the more notable applications has been for trapping and cooling atoms [2, 3]. Manipulation of single cells and bacteria using laser traps is now common place. It is the basic tool for studying the molecular motors found in cells, RNA polymerase [4] and kinesin [5] being two significant examples.

We present here an advance on the ability to use light traps to manipulate objects on the nanometer scale. Although nanometer positioning of objects with light traps has been demonstrated using acousto-optic or electro-optic deflectors [6], they are still limited by the Brownian motion of the trapped particle. For a 1 μm diameter microsphere this is on the order of 30 nm. The technique presented here allows defining an edge with near nanometer resolution. There is a significant need for tools such as this for progress in nanoscience. In the biological community the ability to manipulate molecules on the molecular scale has proven necessary to further elucidate the critical details of interaction. The above-mentioned research on molecular motors being a dramatic example. In addition nanometer manipulations are greatly needed for progress in integrated circuit fabrication. The technique presented here can be used for writing on photoresist with nanometer resolution without the need of high vacuum for an e-beam lithography setup.

Using the Brownian motion of a particle confined to a trapping potential and the radial dependence of this motion with the intensity or power level of the trapping beam, we

have demonstrated the ability to define potentials with almost arbitrary shaped perimeters. The perimeter shape must be describable by a vector from the trap center that does not cross any of the perimeter boundaries when rotated to sketch out the entire perimeter. Because optical tweezers confine particles to nanometer scale regions, the technique offers a method to manipulate a particle with nanometer resolution without moving the beam or its optics. The technique has applications for directing chemical or physical interaction on the nanometer scale and imaging methods on the same scale.

4.2 Theoretical Background

For this application we are interested in the trapping forces that can be used to manipulate dielectric particles such as silica and polystyrene micro-spheres having dimensions *d* of 0.5μm to 10 μm in diameter. Unfortunately these particles fall between the Mie ($\lambda << d$) and Rayleigh ($\lambda >> d$) regime making an exact analysis of the optical forces on these particles problematic as discussed by Svoboda and Block [7] (λ is the wavelength of the trapping light). However the physical basis for confining a particle in a light trap seems to be similar for both regimes. One model which seems to be the most intuitive to understand is that of the impinging photons experiencing a change in momentum as they interact with the trapped particle. The change in momentum imparts a force onto the particle. The most obvious force is that from photons scattered off the surface of the particle facing the light source. This imposes a "scattering" force, which pushes the particle away from the light source. The second force is the key to being able to create a three-dimensional trap with a single beam. This is the gradient force which results from the momentum imparted by the photons which are not scattered by the particle but still experience an angular change in direction from interacting with the particle. In the case of a highly focused beam this gradient force sums to be in the opposite direction of the scattering force. Also in the case of a focused beam both the scattering and gradient forces push the particle into the center of the beam forming a local potential minimum perpendicular to the axis of the beam. This is typically defined as the x, y plane. It is only when the focused beam has a large numerical aperture (NA) can the gradient force be made large enough to be equal and opposite to that of the scattering force. Its force is greatest near the focal point of the beam. The net result is that a particle is trapped in a

position down from the focal point of the trap. This also produces a local potential minimum along the beam axis or z direction. If the particle moves towards the focusing lens, the gradient force decreases but the scattering force does not and pushes the particle towards the focal point. If the particle moves closer to the focal point, the gradient force increases pushing it back away. Taken all together, the focused light produces a three-dimensional trap for a dielectric particle.

Although not immediately obvious, a laser light source is the most convenient way to produce a diffraction limited spot of high enough intensity to capture particles. In order to trap a particle, the trapping potential must be greater than the thermal forces, which would otherwise push a particle out of the trap. For the purposes of discussion here this net force can be simply described by the equation [7]

$$F = \frac{Qn_m P}{c}, \tag{1}$$

where Q is a dimensionless coefficient describing the efficiency of the trap and accounting for all of the above combined effects, n_m is the index of refraction of the suspending medium, c is the speed of light, and P is the incident power on the trapped particle. What is important here is that the trapping force is proportional to the laser power.

The trapping force is zero at trap center and can be approximated in one dimension by a harmonic potential.

$$U(x) = \frac{1}{2}kx^2, \tag{2}$$

where x is the distance from the trap center and k is the spring constant of the trap potential. An exact theoretical description of the potential is problematic at best [7]. Ashkin has done a detailed analysis using ray optics [8] but it is still an approximation in the regime used here. Svoboda and Block cite several other analyses employing either ray-optics or electromagnetic models but they do not exactly match experimental results. Measurement is still the most functional. But we still need some basis to analyze the

data. The harmonic potential seems to match what has been measured. From the equipartition theorem [9],

$$\frac{1}{2}k\left\langle x^2\right\rangle = \frac{1}{2}k_B T$$
$$\left\langle x^2\right\rangle = \frac{k_B T}{k} \quad , \tag{3}$$

where k_B is Boltzmann's constant and T is the absolute temperature of the particle and its environment.

$$k \propto P$$
$$\left\langle x\right\rangle \propto \sqrt{\frac{k_B T}{P}} \tag{4}$$

Because the restoring spring force is proportional to the intensity of the light trap the root mean square (RMS) amplitude can be varied by changing the intensity of light. However you must vary the intensity a great deal to get a reasonable change in the RMS amplitude of the particle position (i.e., decreasing the light power by a factor of 100 increases the RMS amplitude by only a factor of 9). This is not a significant limitation.

By using this property the boundary or the potential walls can be moved by adjusting the laser power. If the position of a particle in a light trap is monitored the location of the potential wall can be adjusted depending on the particle's position. In principle you should be able to control it within a three dimensional area. However measuring the displacement of a particle in a light trap along the beam axis adds complexity we did not want to address at this time. Measuring its position in a plane perpendicular to the beam axis is straightforward. In the experimental work presented here, the x-y position in the above plane of a trapped polystyrene bead was measured and the intensity of the trapping light was varied according to a map. If the bead was within the map boundary, the laser intensity was set at its lowest power level. If the bead crossed over the map boundary, the laser intensity was increased to its maximum value thus pushing the bead back in towards the center of the light trap. Because beads with diameters of 1 to 5um in a laser trap are restricted to Brownian motion with RMS amplitudes of 10s of nanometers, the edges of a perimeter defined in the above way should be on the order of nanometers. The results of the experimental work presented here verify this.

4.3 Experimental Setup.

The apparatus used is a variation of an earlier setup used for measuring polymer and bead dynamics in a fluid [10]. Referring to Figures 4.1 and 4.2, the apparatus consists of a 500 mW Nd:YAG λ=1024 nm laser focused down with a 60x oil immersion objective into an enclosed region formed by a microscope cover glass, microscope slide and a parafilm gasket.

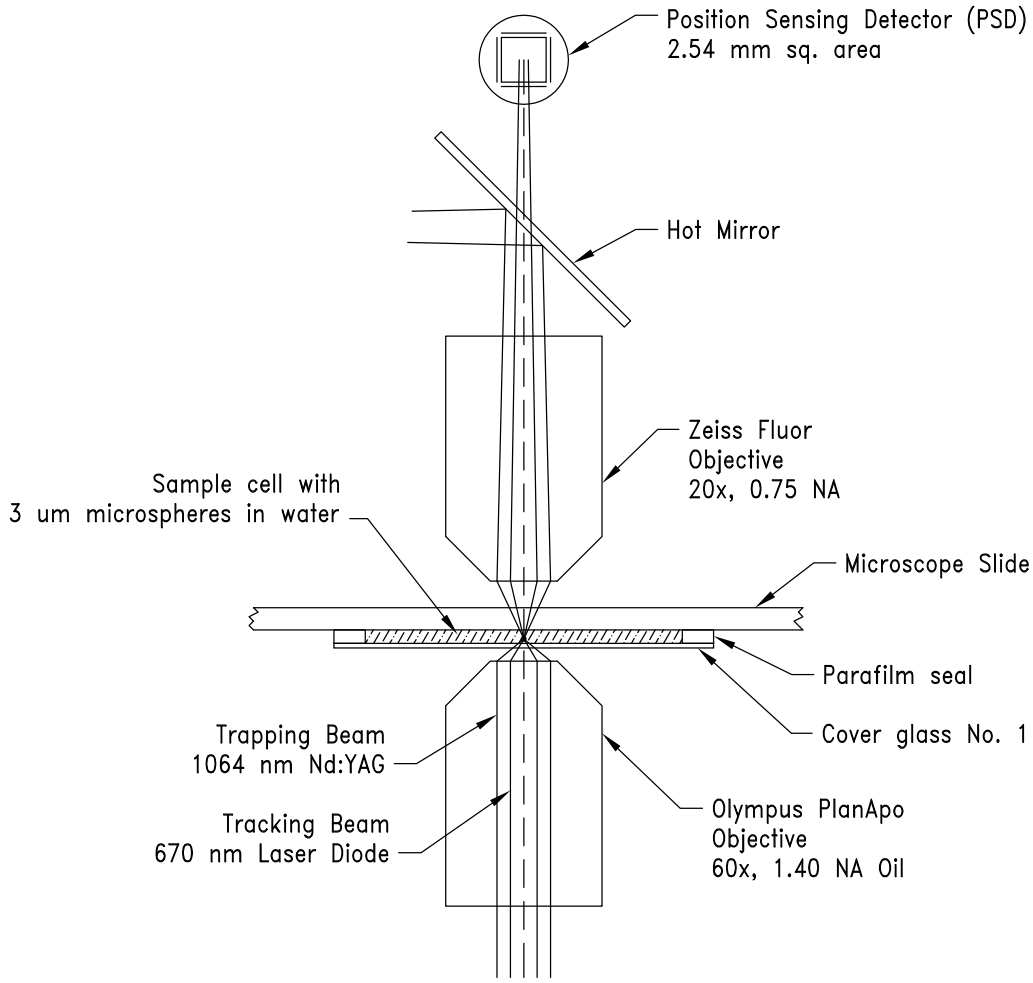

Figure 4.1 Schematic drawing of the optical tweezer and detection arrangement used for the experiment. The 60x objective focuses down the 1064nm beam to a diffraction limited spot forming the trapping potential. The back aperature of the objective is slightly overfilled to obtain optimum trapping force. The 670 nm tracking beam is similarly focused to the same spot (overfilling is not needed). The light deflected by the microsphere is projected onto the linear PSD to measure its position.

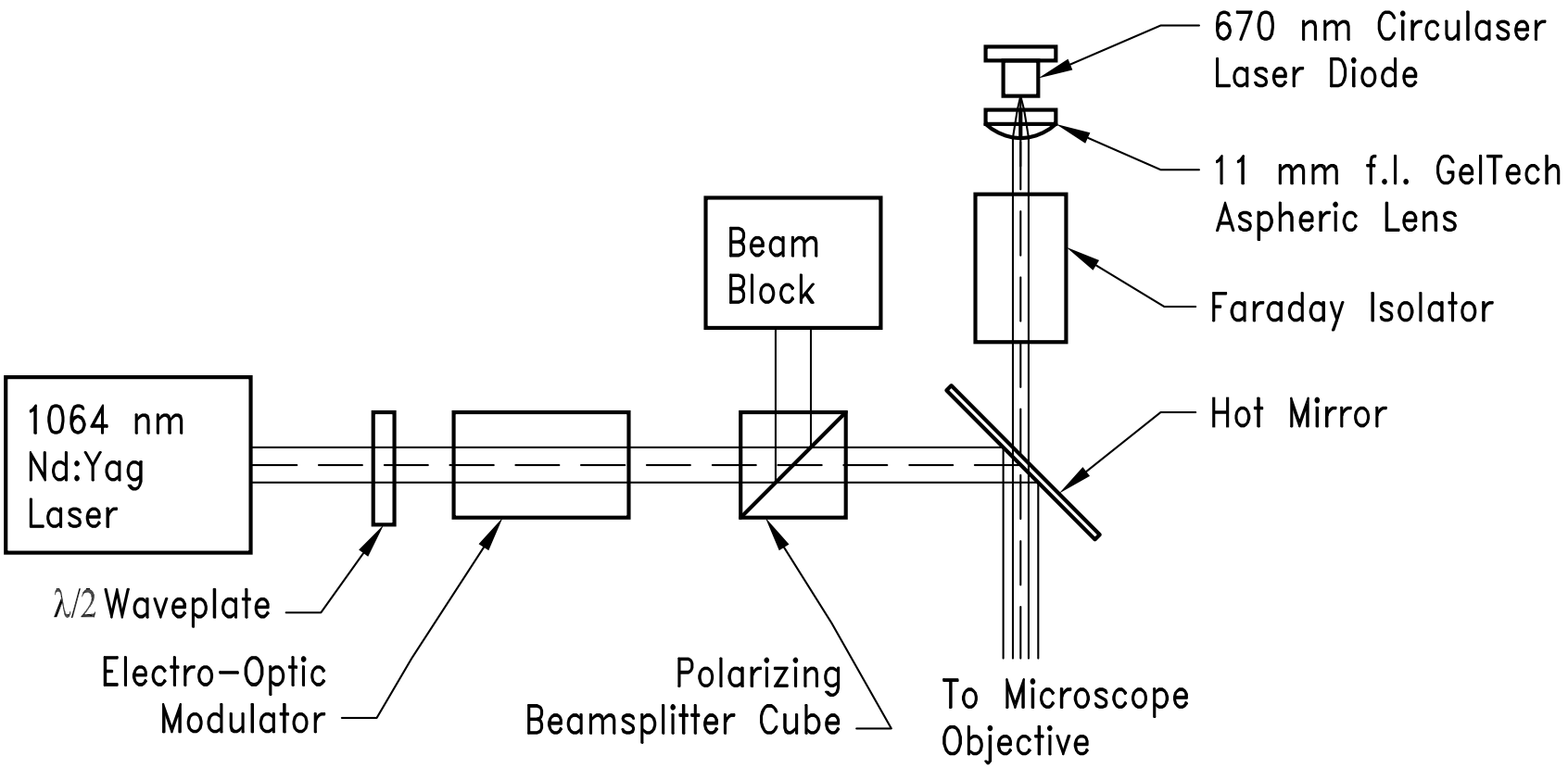

Figure 4.2 Schematic drawing of the optical arrangement used to sum the two lasers and the Electro-Optic Modulator for regulating the 1064 nm lasers power.

The sample cell is formed by cutting out a U-shaped parafilm gasket slightly bigger on the outside than the size of the cover glass and approximately 2 mm smaller on the inside than the cover glass. The microscope slide, parafilm and cover glass assembly are placed on metal surface heated by a lamp. This slightly melts the parafilm sealing the three edges of the assembly. The sample cell is filled by injecting the fluid containing the microspheres into the open end of the assembly. The open end is then sealed by two to three coats of clear acrylic nail polish. This forms a cell that is approximately 100 to 125 μm deep. If the seal is done well it lasts for several days.

The trapping depth is approximately 20 μm above the surface of the cover glass. The microscope is constructed in an inverting configuration. The cover glass faces down and is supported in a bridge type arrangement by the microscope slide, which rests on the microscope's translation stage. A second red laser diode (BlueSky Research Circulaser λ=670 nm 10 mW max.) is used to measure the position of the trapped bead. This laser diode is driven in constant power mode by a ThorLabs LD1100 laser diode driver. This is done to minimize intensity noise. Because the intensity of the trapping laser is modulated, it becomes difficult to use for monitoring the bead position. Although the intensity fluctuation can be normalized out from the position data, it does introduce a noise floor modulation. The tracking beam was easier to implement in the current setup and also enabled monitoring the experiment in real time. In addition the tracking beam can verify that the technique used to modulate the trapping beam does not also deflect the beam.

The 1024 nm laser power is modulated by an electro-optic (EO) modulator (New Focus Model 4104, San Jose, California) combined with a wave plate and a polarizing beam splitter (See Fig. 4.2). The modulator is driven by a transistor switching circuit which biases the EO with one of two voltages depending on a TTL level signal input. The two voltage levels can be independently adjusted. The above arrangement is able to modulate the laser power with better than 80:1 ratio.

The bead position is measured by the beam steering effect that a bead has on a focused beam [6]. This light is collected by an opposing 20x objective. After passing the collected light through a hot mirror to block the trapping beam laser light, the steered 670nm beam spot is directed onto a linear position sensing detector (PSD) (Part No. SC-4D, UDT Sensors Inc., Hawthorne, California). In order to increase the positional resolution of this detector, the deflected beam spot is not imaged onto this detector. Instead the collection objective is adjusted until the beam fills approximately 50% of the detection area of the linear PSD. This forms an optical lever. The linear PSD detector enables this gain in sensitivity by this optical lever technique. A quad-photodiode does not. If the total power on a quad-photodiode is constant, as the spot size is increased the translation resolution goes down. The translation resolution is roughly the spot-diameter divided by the noise floor of the photodiode and its electronics. It can be seen that when the optical lever is increased so is the spot size which counteracts the gain in sensitivity. The linear PSD by its method of detection does not have this constraint. It measures the optical center of mass of the projected spot. Linear PSD's typically have poorer noise performance than quad-photodiodes, but in this case it is not the limiting factor.

The linear PSD's four photocurrents are converted to voltages by four op-amps arranged in a transimpedance configuration. This is similar to the circuit used elsewhere for quad-photodiodes (see Appendix A, Fig. A.21). The most significant distinction is the linear PSD requires different polarity biasing than the quad-photodiode circuit. These amplifiers are then followed by four gain of two inverting amplifiers to accommodate the signal conditioning electronics for the A/D converters used to measure these signals. The resulting signals from the amplifiers are converted to digital data by four 16-bit A/D converters running at a 384KHz sample rate. These converters are clocked and their data read by a DSP56362 Digital Signal Processor (DSP) Circuit (see Chapter 2, Fig 2.1 and Appendix A). The DSP calculates the x-y position of the spot from the four photocurrents as described in the linear PSD manufacturer' s literature. Other implementations perform this calculation using additional op-amp circuits. The resulting x-y value is used to point to a map in the DSP memory. If according to the map the x-y value is within the region where it is desired to confine the particle, the DSP outputs the

appropriate TTL signal to drive the EO for lowest laser power. If the x-y value points outside of this region, the DSP outputs the signal to drive the EO for maximum laser power. For the experimental results presented in the discussion that follows 3 μm polystyrene beads in 18 meg ohm purity water with 0.02% Tween 20 were used in the sample cell. The DSP also outputs the x-y positions at a 96KHz rate via an optical link for recording by a personal computer.

4.4 Results and Discussion.

Figures 4.3, 4.4, and 4.5 present a nice demonstration of the technique. We call this the "T" potential. Figures 4.3 and 4.4 are histogram images of the x-y location of a bead in the modulated beam trap described above. This is for data taken for a 5½ minute period. Figure 4.3 displays the histogram using a linear scale. Figure 4.4 uses a logarithmic scale. Figure 4.5 is the image of the map loaded into the DSP's memory. The intensity scale for Figures 4.3 and 4.4 goes from white, indicating the microsphere was never in that location to black representing the most frequent locations where the particle was found. The figure captions contain the number of hits that black represents for a particular histogram. The solid bar represents 50nm length for these histograms and the others that follow. From this it can be seen that the technique affords defining an arbitrarily shaped trapping potential with near nanometer resolved edges.

Figure 4.3. Linear histogram image of the x-y location of a bead in the "T" potential. The black bar represents 50 nm. The intensity scale here goes from light representing 0 times the particle was found at that location to dark representing 3976, meaning the particle was found in that x-y location bin 3976 times.

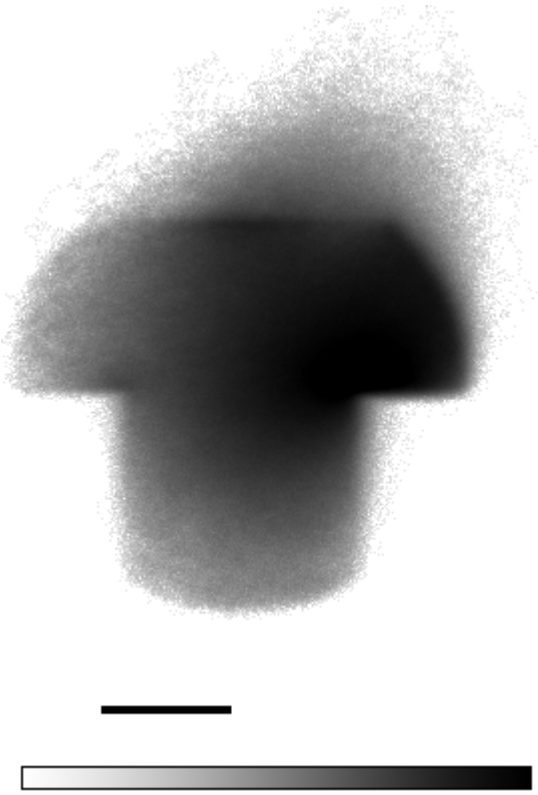

Figure 4.4. Logarithmic histogram image of the x-y data shown in Figure 4.3. The black bar shows a distance of 50 nm. The intensity scale here goes from light representing $\log_{10}(1)$ times the particle was found in that location to black representing $\log_{10}(3976)$

Figure 4.5. "T" Potential shape programmed into the DSP for Figures 4.3 and 4.4

To determine the above-mentioned scale of the trap, the following technique and analysis were used. The trapping shape modulator was turned off. The trap potential was adjusted for maximum laser power and the bead x-y location was measured and recorded for 2 to 3 minutes. Using either Smoluchowski's equation

$$\frac{\partial c}{\partial t} = \frac{\partial}{\partial x}\frac{1}{\zeta}\left(k_B T \frac{\partial c}{\partial x} + c\frac{\partial U}{\partial x} \right) \tag{5}$$

or Langevin's equation

$$\zeta \frac{dx}{dt} = -\frac{\partial U}{\partial x} + f(t) \tag{6}$$

(where c is the concentration of particles at x at time t, U is an external potential, ζ is the friction or dampening constant for a particle in a fluid and $f(t)$ is the random force from thermal fluctuations) we can derive the relation of the autocorrelation of a particles motion in a one-dimensional harmonic potential.

$$\langle x(t)x(0)\rangle = \frac{k_B T}{k} e^{-t/\tau} \tag{7}$$

τ is the time constant of the potential that is related to the spring and dampening constants.

$$\tau = \zeta / k \tag{8}$$

For a sphere of radius a in a fluid of viscosity η_s the dampening constant can be derived from hydrodynamic calculations [11].

$$\zeta = 6\pi\eta_s a \tag{9}$$

If the particle is within a particle's radius to a surface, the dampening constant needs to be corrected for surface fluid interactions [7].

$$\beta = \frac{6\pi\eta a}{\left[1 - \frac{9}{16}(a/h) + \frac{1}{8}(a/h)^3 - \frac{45}{256}(a/h)^4 - \frac{1}{16}(a/h)^5\right]}, \tag{10}$$

where h is the distance of the particle's center to the surface. For our experiment this is not needed since $a/h << 1$.

By taking the numerical autocorrelation of the recorded x-y locations of the bead in the trap at a fixed laser power level, the time constant τ can be determined by least-square

fitting to the exponential function given by equation (7) where the temperature and spring coefficients are lumped into one constant. Then by using equations (8) and (9) the spring constant for the trap can be calculated. Knowing the spring constant the scale of the data can be determined from equation (7). Before the autocorrelation is calculated on the recorded data, the x and y mean values of the data set is subtracted from all values in their respective channels to remove DC offsets.

Figures 4.6 and 4.7 are the linear and logarithmic position histograms for the bead in the laser trap with the laser set at maximum power into the microscope optics. They were generated by analyzing every other x-y data point for almost the entire recorded data set. For programming convenience the last 64k or less points were not included in the histograms. This applies to these histograms and the ones that follow. The data for the histograms and autocorrelation calculations were recorded for 2 to 3 minutes. This means that the histograms represent from 5 to 8 million data points.

Figures 4.8 and 4.9 show graphs of the numerical autocorrelation and the best fit line to the initial 800 data points of the autocorrelation result for the x and y axis. Only 1 million data points from the x and y data were used for the autocorrelation calculation. This is approximately 10 seconds of data. From the fits to these lines, the time constant was 3.6ms in x and 3.7ms in y and the spring constant of the trap was 7.8 pN/μm in x and 7.6 pN/μm in y. This is within reasonable agreement of data taken on earlier configurations of the trapping apparatus when the difference in the bead diameter is taken into account [12].

Figures 4.10 and 4.11 are the linear and logarithmic position histograms for the bead with laser power set as low as possible and still have the bead confined in the trap. Please note that while the cloud sizes look similar in size to the earlier figures the scale of these figures is nearly twice that of the previous figures (the 50 nm scale bars are shorter). Figures 4.12 and 4.13 show graphs of the numerical autocorrelation and the best fit line. As can be seen from these graphs, the exponential fit is not as good as for the data at maximum power. This suggests the likelihood of additional interactions. One possible

source is the tracking laser. At the lower power levels of the trapping laser, the tracking beams effect should be more significant. However, this measurement was done to confirm that the RMS motion was changed by the modulation in laser power which it does show. From the fits to this data set the time constant was determined to be 23ms in x and 20ms in y and the spring constant was 1.2 pN/μm in x and 1.4 pN/μm in y.

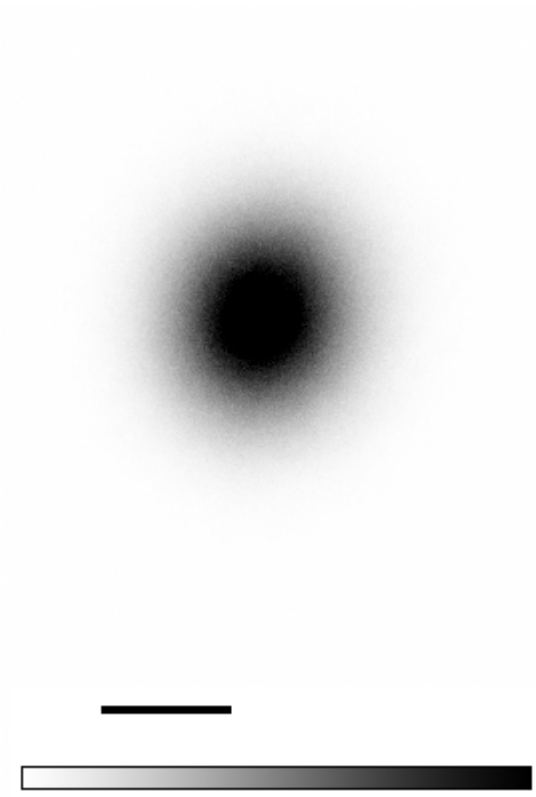

Figure 4.6. Linear position histogram for bead in trap with laser set at maximum power for autocorrelation measurements. Black bar represents 50 nm distance. Intensity scale goes from 0 to 1402.

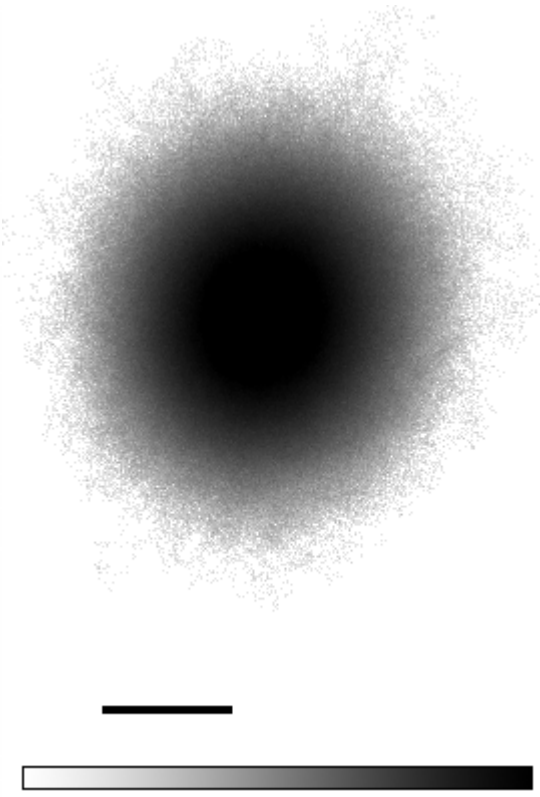

Figure 4.7. Logarithmic position histogram of the data represented by Figure 4.6. Distance scale is the same. Intensity scale goes from $Log_{10}(1)$ to $Log_{10}(1402)$.

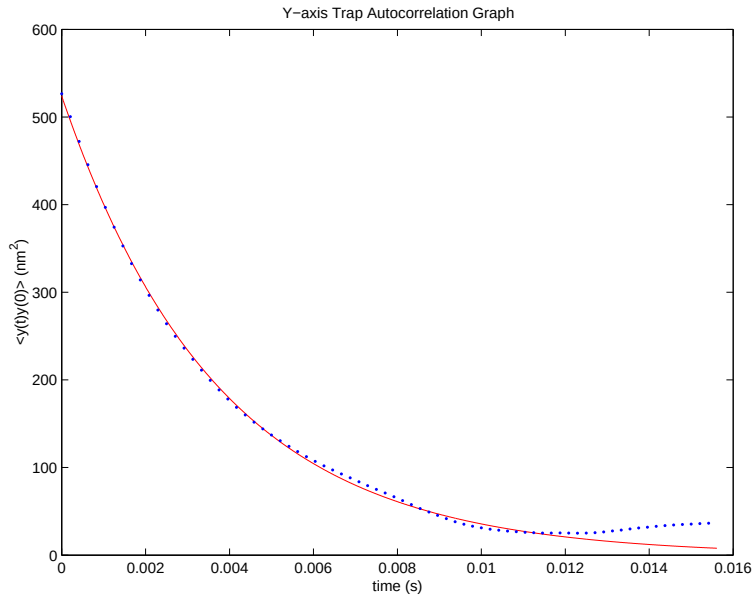

Figure 4.8. Autocorrelation result of the x position data represented in Fig. 4.6. For clarity only Every 20th data point is plotted. These are represented by a dot. The solid line is the least squares fit to equation (7).

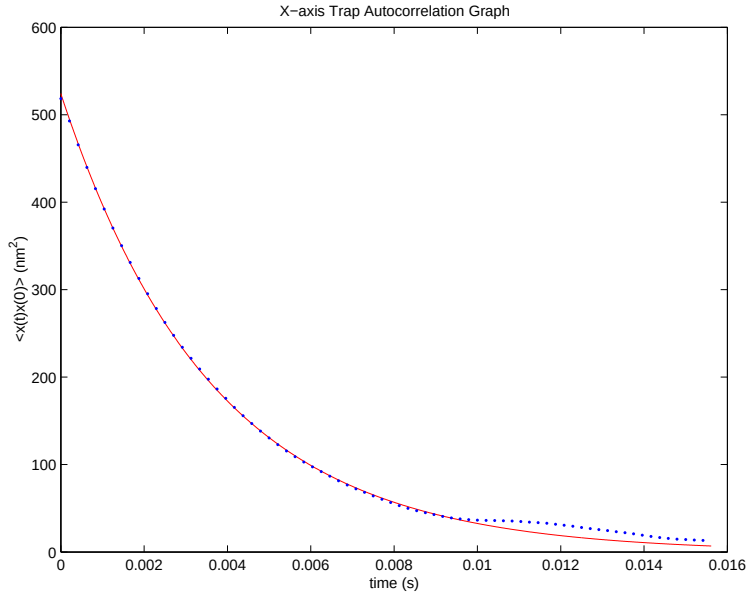

Figure 4.9. Autocorrelation result of the y position data represented in Fig. 4.6. For clarity only Every 20th data point is plotted. These are represented by a dot. The solid line is the least squares fit to equation (7).

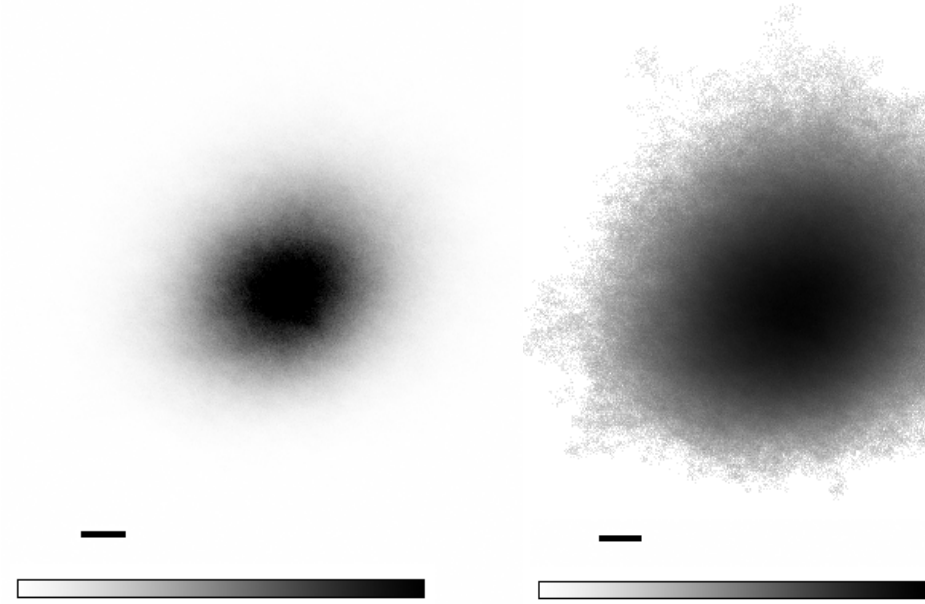

Figure 4.10. Linear position histogram for the bead with the trap set at the lowest laser power level. The black bar represents 50 nm. The intensity scale goes from zero to 1402 .

Figure 4.11. Logarithmic position histogram for the data in Figure 4.10. Distance scale is the same. The intensity scale goes from $Log_{10}(1)$ to $Log_{10}(1402)$.

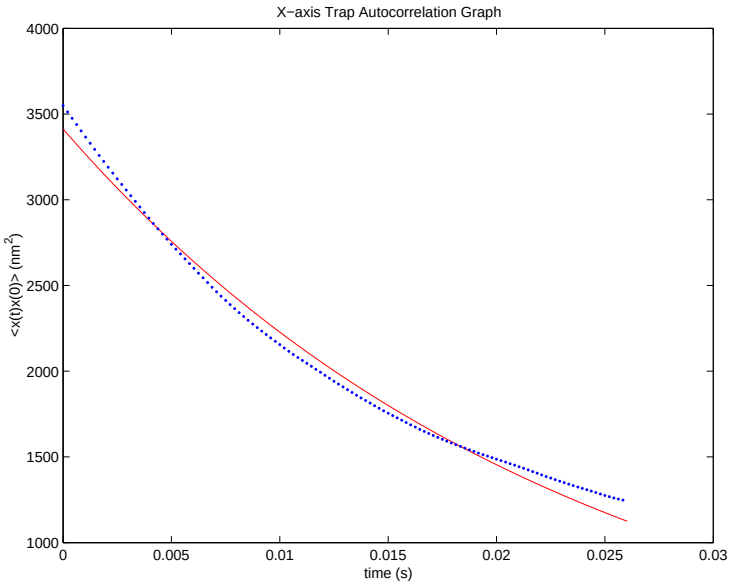

Figure 4.12. Autocorrelation result of the x position data represented in Fig. 4.10. For clarity only every 20th data point is plotted. These are represented by a dot. The solid line is the least squares fit of this data to equation (7).

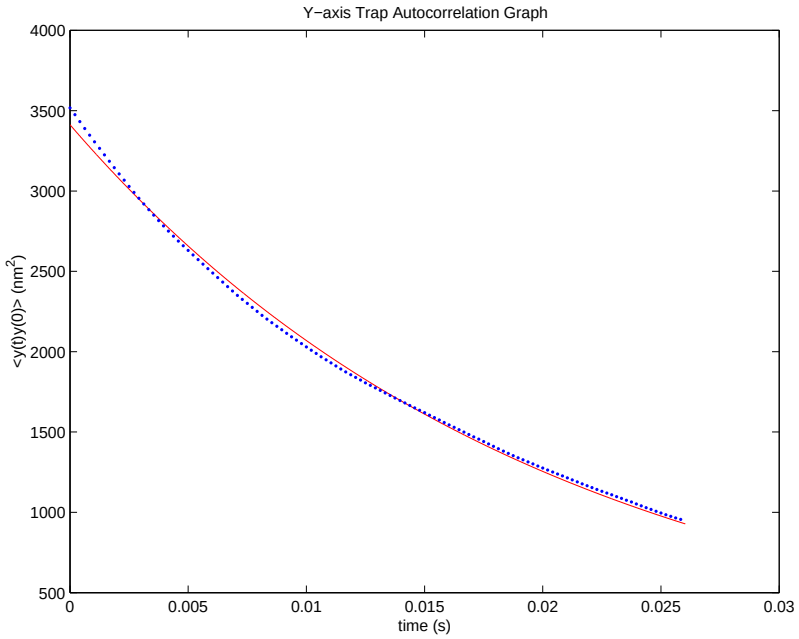

Figure 4.13. Autocorrelation result of the y position data represented in Fig. 4.10. For clarity only every 20th data point is plotted. These are represented by a dot. The solid line is the least squares fit of this data to equation (7).

Figure 4.14. "Pacman" potential loaded into the DSP. The resulting histograms are showed in Figures 4.15 and 4.16.

To confirm and demonstrate (on some level) that other potentials can be made the map shown in Figure 4.14 was loaded into the DSP. This is a cut pie shape or for those gamers amongst us the "Pacman" potential. Figures 4.15 and 4.16 show the measured linear and logarithmic histogram images. This was actually the first potential tried because of its simplicity. However, it was tried before some critical alignment issues and possible optical distortion issues were realized. These will be discussed later. Figures 4.17 through 4.20 show the autocorrelation histogram images and curve fit graphs. There is an elevated baseline in the autocorrelation data that is probably the result of alignment issues. A constant was added to equation (7) for the curve fits to account for this effect. The spring and time constant derived from curve fitting to these data still agree reasonably with the values for the "T" potential : 2.2 ms in x and 4.1 ms in y, 13 pN/μm in x and 6.8 pN/μm in y.

Figure 4.15. Linear histogram image of the "Pacman" potential data. The intensity scale goes from zero to 4015 hits in a given x-y location.

Figure 4.16. Logarithmic histogram image of the "Pacman" potential data. Intensity scale is the $\log_{10}$ of the scale in Figure 4.15.

Figure 4.17. Linear position histogram for the autocorrelation data taken to calibrate the trap for the "Pacman" potential. Black bar represents 36 nm distance. Intensity scale goes from 0 to 962.

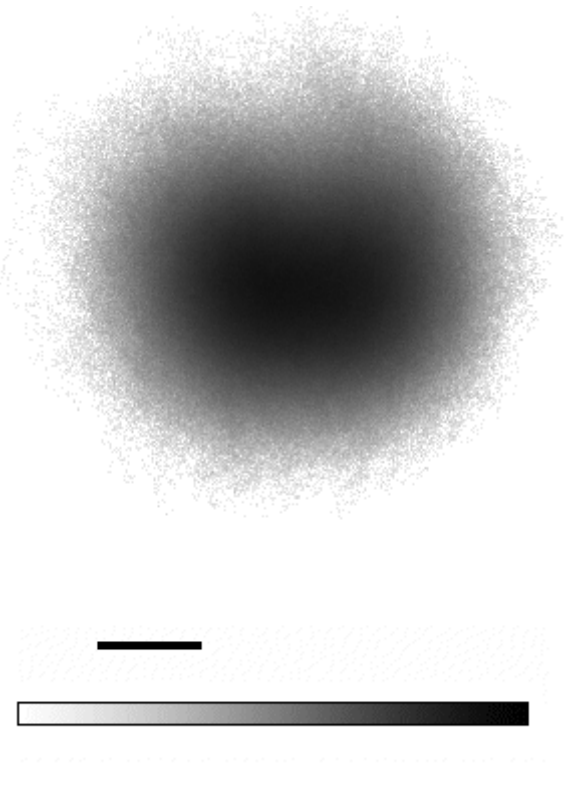

Figure 4.18. Logarithmic position histogram of the data represented by Figure 4.17. Distance scale is the same. Intensity scale goes from $Log_{10}(1)$ to $Log_{10}(962)$.

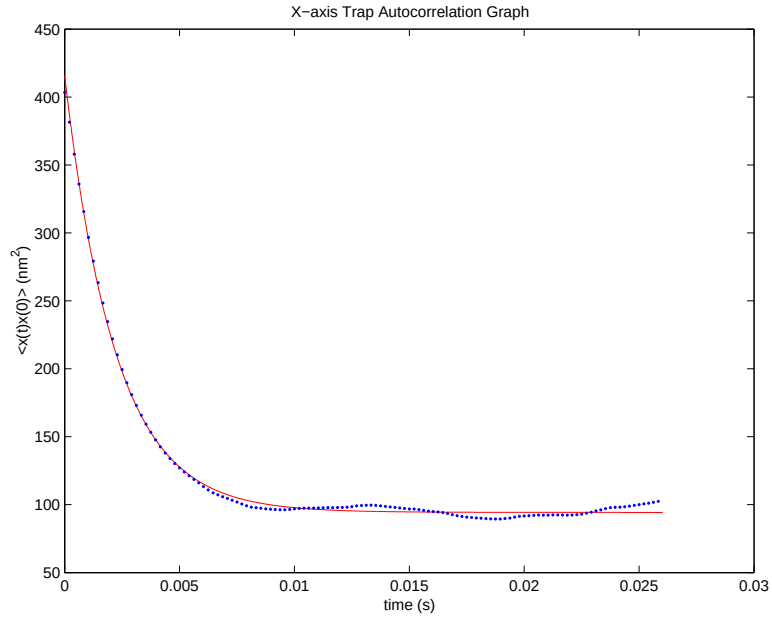

Figure 4.19. Autocorrelation result of the x position data represented in Fig. 4.17. For clarity only every 20th data point is plotted. These are represented by a dot. The solid line is the least squares fit of this data to equation (7) plus a constant.

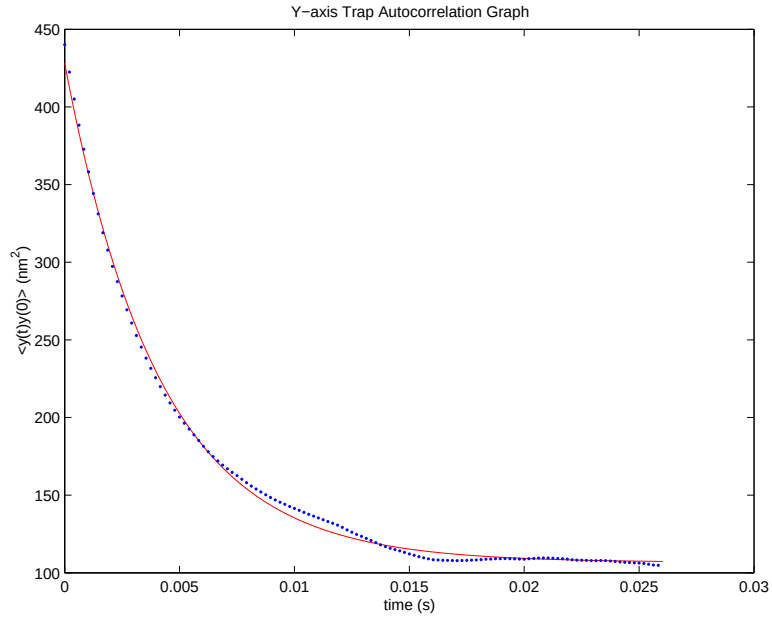

Figure 4.20. Autocorrelation result of the y position data represented in Fig. 4.17. For clarity only every 20th data point is plotted. These are represented by a dot. The solid line is the least squares fit of this data to equation (7) plus a constant.

Initial attempts to demonstrate this technique were problematic at best. As can be imagined thermal and vibrational motions of the optical setup have a significant chance of completely defeating the ability to see any effect even if it was actually occurring; especially when you are trying to observe motions on a nanometer scale. One typical solution is to employ techniques that make these noise sources common mode to what you are trying to measure. The other solution of course is to minimize the noise sources. The optical lever technique with the PSD is an example of the former. It does provide a gain in the positional signal that does not incorporate changes in the position of the tracking beam relative to the beam optics and mechanics or the PSD. However it does not eliminate the apparent critical alignment of the trapping beam, the tracking beam, and the collection optics. The latter was what proved to be the last adjustment to get the images shown in Figures 4.3 and 4.4.

Figures 4.21 and 4.22 show the first attempt to produce the "T" shaped potential. After adjusting the x and y location of the collection ojective 5 μm at a time, the flaring at the left corner of the "T" was minimized. Eliminating the beret hat of the "T" did not appear possible with this technique. It is suspected that a more critical alignment of the tracking and trapping beam lasers will be needed. There is also the annoying problem of the hot spot not being in the center of the "T" shape. This is also probably an alignment issue. In this experimental configuration attempts to move it only resulted in destabilizing the shaped potential and the microsphere escaping. An alternative technique would be to use the trapping beam alone after building additional electronics to normalize the signal for intensity fluctuations. The normalization can be done by the DSP at the above sample rate if the calculation of the x-y position is done by external electronics. This would be a division performed on the 16-bit data by the DSP. This is not possible with readily available analog signal dividers with 16-bit resolution.

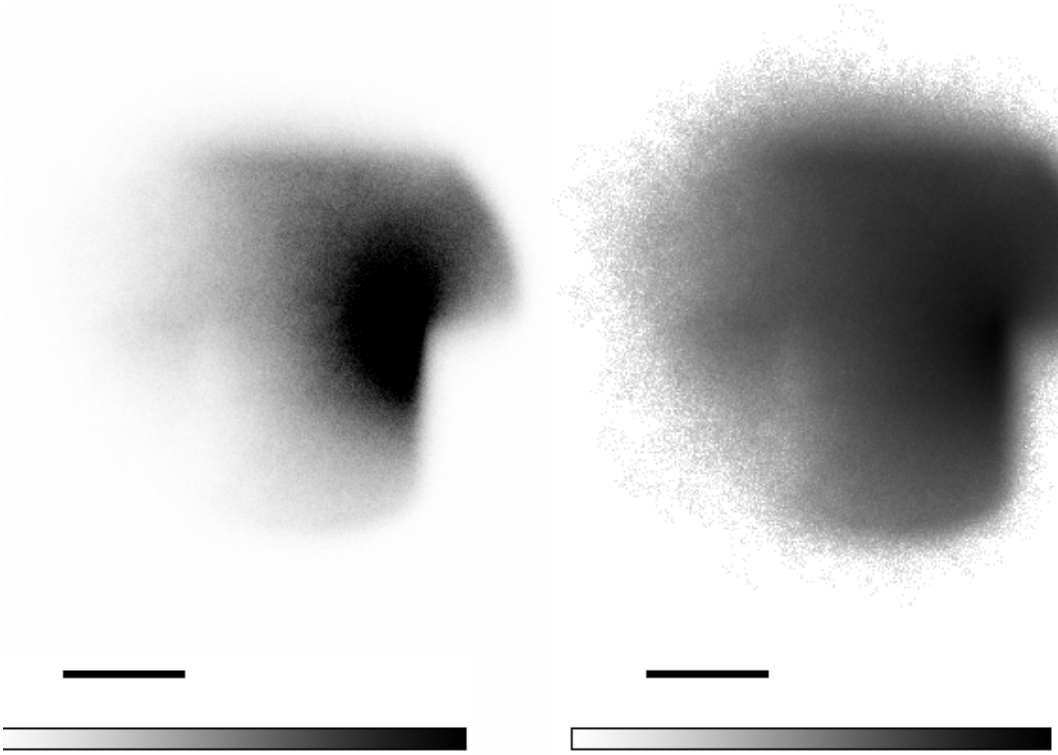

Figure 4.21. Linear histogram image of the data taken for the first attempt to produce the "T" potential. The black bar represents 50 nm. The intensity scale goes from zero to 1003.

Figure 4.22. Logarithmic histogram image of the data in Figure 4.21. Distance scale is the same. Intensity scale is the Log_{10} of that in Figure 4.21.

4.5 Conclusions and Additional Discussion

One significant interpretation of the above results is around the logarithmic histogram images. From the statistics of a particle in a time invariant potential the probability *P(x)* of a particle being at a position *x* is given by

$$P(\mathbf{x}) = \frac{e^{-U(\mathbf{x})/k_B T}}{\int_{-\omega}^{\omega} e^{-U(\mathbf{x})/k_B T} d\mathbf{x}} \tag{11}$$

If you make *N* measurements or there are N particles, you would multiply the probability by N. Taking the logarithm of both sides,

$$\log(P(\mathbf{x}) \cdot N) = -\frac{U(\mathbf{x})}{k_B T} - \log\left(\int e^{-U(\mathbf{x})/k_B T} dx\right) + \log N\,, \tag{12}$$

where the last two terms are constant and can be combined under one variable. The *N* on the left-hand side can be treated in the same fashion. Rewriting the equation

$$\log(P(\mathbf{x})) = -\frac{U(\mathbf{x})}{k_B T} + C \tag{13}$$

It can be argued from the above equation that the logarithm histograms presented here represent the time independent potential of the potential well that has been created by this technique. While it was hoped that they would appear flatter than what has been shown here, a significant result is the steepness of the edges of the potentials. This has been enhanced when compared to the fixed laser power images used to measure the spring constant of the potentials.

The above interpretation is reasonable, provided the feedback of the control system is high enough otherwise the potential created by this technique has a time dependence. The 3 μm bead used in this case moves slowly enough such that the control system has adequate bandwidth. Besides alignment issues this is another contributing reasons for the edges not being sharper. A 1 μm bead was used for initial experiments but only modest effects were achieved. Additional straightforward improvements can be made to the control electronics to increase the bandwidth. This should enable manipulating smaller microspheres which would allow for higher resolution than what was achieved here. Because the distribution of the particles velocity is Lorentzian, the bandwidth requirements would appear to be more demanding than for other typical feedback control type applications.

The technique offers a significant additional tool to nanoscience. To the author a very useful immediate application would be for photolithography. Using acousto-optic or electro-optic deflection to move the trapping beam on a larger scale, the microlensing effect of microspheres combined with this manipulation technique would allow writing on the nanometer scale in photoresist. The apparatus would still have the speed limitations similar to e-beam lithography, but the apparatus would seem to be less expensive and could be operated under ambient conditions, a significant advantage. Other applications would be directed molecular interactions where the microsphere is coated with a compound to interact with a surface. Nanometer scale reactive edged areas could be defined using this technique.

An extension of this technique, which may be more applicable for chemical interactions, would be measuring the particle velocity and using a velocity map to control its profile. Although not focused on, a significant issue is the ability to do this at all. It is difficult to conceive of a way to implement these shaped potentials without the availability of high speed digital signal processors and high speed high resolution A/D converters.

4.6 References

1. Ashkin, A., *Acceleration and trapping of particles by radiation pressure*. Physical Review Letters, 1970. **24**(4): p. 156-159.
2. Ashkin, A., et al., *Observation of a single-beam gradient force optical trap for dielectric particles.* Optics Letters, 1986. **11**(5): p. 288-290.
3. Chu, S., *Laser manipulation of atoms and particles.* Science, 1991. **253**(5022): p. 861-866.
4. Wang, M.D., et al., *Force and velocity measured for single molecules of RNA polymerase.* Science, 1998. **282**(5390): p. 902-907.
5. Visscher, K., M.J. Schnitzer, and S.M. Block, *Kinesin motors studied with an optical force clamp.* Biophysical Journal, 1998. **74**(2): p. A49-A49.
6. Visscher, K., S.P. Gross, and S.M. Block, *Construction of multiple-beam optical traps with nanometer-resolution position sensing.* IEEE Journal of Selected Topics in Quantum Electronics, 1996. **2**(4): p. 1066-1076.
7. Svoboda, K. and S.M. Block, *Biological applications of optical forces.* Annual Review of Biophysics and Biomolecular Structure, 1994. **23**: p. 247-285.
8. Ashkin, A., *Forces of a single-beam gradient laser trap on a dielectric sphere in the ray optics Regime.* Biophysical Journal, 1992. **61**(2): p. 569-582.
9. Heer, C.V., *Statistical mechanics, kinetic theory, and stochastic processes*. 1972, New York: Academic Press.
10. Meiners, J.C. and S.R. Quake, *Direct measurement of hydrodynamic cross correlations between two particles in an external potential.* Physical Review Letters, 1999. **82**(10): p. 2211-2214.
11. Doi, M. and S.F. Edwards, *The Theory of Polymer Dynamics*. The International Series of Monographs on Physics, ed. J. Birman, et al. 1988, Oxford: Oxford Universiy Press.
12. Meiners, J.C. and S.R. Quake, *Femtonewton force spectroscopy of single extended DNA molecules.* Physical Review Letters, 2000. **84**(21): p. 5014-5017.

Part II

Microfluidic Manipulations

II.1 Introduction

The following work was done in collaboration with other members in our group, specifically Anne Fu and Hou-Pu Chou, under the direction of our advisors, Professors . Stephen Quake, Axel Scherer and Francis Arnold. The work in Chapter 5 was published in Nature Biotechnology. The work in Chapter 6 was published in the Proceedings of the National Academy of Sciences USA.

Chapter 5

A Microfabricated Fluorescence-Activated Cell Sorter

Anne Y. Fu, Charles Spence, Axel Scherer, Frances H. Arnold, and Stephen R. Quake

5.1 Introduction

Conventional fluorescence-activated cell sorters (FACSs) are widely used to study eukaryotic cell populations. Although they provide impressively efficient sorting, they are costly ($250,000), mechanically complex, and require trained personnel for operation and maintenance. Inexpensive devices that rapidly sort live cells, particles, and even single molecules would greatly facilitate screening of combinatorial chemistry libraries or cell populations during in vitro molecular evolution. Moreover, such devices would have wide applications in clinical medicine and basic biological and materials research.

All modern conventional flow cell sorters are designed to have a flow chamber with a nozzle and are based on the principle of hydrodynamic focusing with the sheath flow [1–5]. In addition, most sorting instruments combine the technology of ink-jet printing and electrostatic deflection to achieve droplet generation and high sorting rates [6,7]. However, this mechanism is delicate and many failures of the instrument can result from problems in the flow chamber. For example, clogging of the orifice and particle adsorption and contamination in the tubing can cause turbulent flow in the jet stream, inducing variation in illumination and detection. Sample carryover can occur during consecutive runs when remnants of previous samples backflush into the new sample stream, and sterilizing the system between runs is time-consuming and results in machine downtime. Furthermore, cells passing through the orifice may perturb droplet formation: Larger cells can change the droplet size, nonspherical cells tend to align with the long axis parallel to the flow axis, and deformable cells may elongate in the direction of the flow [1,2]. Such perturbations in droplet formation can introduce variation in the time from the analysis to the actual sorting event. Finally, a number of technical problems

make it difficult to generate identically charged droplets, in turn increasing the deflection error.

Replacing the conventional flow chamber in FACS with microfabricated devices potentially can allow more sensitive optical detection, easier mechanical setup, and innovative sorting schemes. Other groups have demonstrated that cells, particles, and reagents can be manipulated in microfluidic devices by pressure, dielectrophoresis, and electro-osmosis [8–11]. In previous work, we described a microfabricated flow cytometer capable of detecting single DNA molecules [12]. We now have constructed a complete microfabricated fluorescence-activated cell sorting μFACS) device and demonstrated its effectiveness for sorting micron-sized latex beads and bacterial cells.

This disposable sorting device is fabricated using a micromachining technology called "soft lithography," [13] which enables the design of inexpensive and flexible miniaturized fluidic devices. Microfabrication permits integration of cell sorting with other tech-niques such as PCR [14], microfabricated total analysis systems [15], and DNA chip hybridization [16] , and allows novel sorting algorithms that are not possible in conventional cell sorters. Another advantage is that multiple cell sorters can be fabricated in parallel on a single chip, allowing increased throughput or successive enrichments of a sample.

5.2 Results and discussion

The μFACS device is a silicone elastomer chip with three channels joined at a T-shaped junction (Fig. 5.1). The channels are sealed with a glass coverslip. A buffer solution is introduced at the input channel and fills the device by capillary action. The pressure is equalized by adding buffer to the two output ports and then adding a sample containing the cells to the input port. The cells are manipulated with electro-osmotic flow, which is controlled by three platinum electrodes at the input and output wells. The chip is mounted on an inverted optical microscope, and fluorescence is excited near the T-shaped junction with a focused laser beam. The fluorescent emission is collected by the

microscope and measured with a photomultiplier tube (PMT). A computer digitizes the PMT signal and controls the flow by the electro-osmotic potentials (Fig. 5.2).

The standard "forward" sorting algorithm consists of running the cells from the input channel to the waste channel until a cell's fluorescence is above a preset threshold, at which point the voltages are temporarily changed to divert the cell to the collection channel (Fig. 5.3). Extending the system to include detection of multiple-color fluorescence and light scattering, as are used in conventional FACS machines, is straightforward. An advantage of μFACS is the small detection volume, typically approximately 250 femtoliters, which greatly reduces background fluorescence from cell suspension and chamber material.

Different algorithms for sorting in the microfluidic device can be implemented by computer. As an example, consider a pressure-switched scheme instead of electro-osmotic flow. With the latter, switching is virtually instantaneous and throughput is limited by the highest voltage that can be applied to the sorter (which also affects the run time through ion depletion effects). A pressure-switched scheme does not require high voltages and is more robust for longer runs.

Mechanical compliance in the system is likely to cause the fluid switching speed to become rate limiting with the forward sorting program. Because the fluid is at low Reynolds number and is completely reversible, it is possible when trying to separate rare cells to implement a sorting algorithm that is not limited by the intrinsic switching speed of the device. The cells flow at the highest possible static (non-switching) speed from the input to the waste. When an interesting cell is detected, the flow is stopped. By the time the flow stops, the cell is past the junction and part way down the waste channel. The system is then run backward at a slow (switchable) speed from waste to input, and the cell is switched to the collection channel when it passes through the detection region. At that point the cell is saved, and the device can be run at high speed in the forward direction again (Fig. 5.3). This reversible sorting method is not possible with standard

FACS machines and should be particularly useful for identifying rare cells or making multiple measurements of a single cell.

The use of μFACS for forward and reverse sorting with electro-osmotic flow was demonstrated with fluorescent beads of different emission wavelengths in different ratios and up to 33,000 beads per hour throughput (Table 5.1). Extra reservoir wells were incorporated on the outer side of the three wells in order to avoid ion depletion, and platinum electrodes (with the ground electrode in the input well) were inserted into the reservoir wells. The collection wells were filled with buffer, and a mixture of red and blue fluorescent beads was injected into the input well in aliquots of 10–30 ml. The optical filter in front of the PMT passed only red fluorescence, allowing selective sorting of red beads. Sorting can be performed for as long as 3 hours with occasional readjustment of the voltage settings. The coefficient of variation in bead intensity was measured to be 1–3%, depending on the depth of the channel and the surface treatment of the elastomer.

A single pass through the μFACS in the forward mode produced a highly enriched sample of red beads (Table 5.1). Whereas the initial concentration of red beads was 10%, the output well held 84% red beads, whereas the waste had <1%. Similar results were obtained when running in reverse sorting mode when the initial concentration of red beads was lowered to 1%. Run times varied from 10 minutes to 3 hours. With both forward and reverse sorting, enrichments of 80-fold to 96-fold were obtained in single runs, in which the enrichment is defined by the increase in the fractional concentration of red beads.

We have also demonstrated that the device can sort living *Escherichia coli* cells, and that the cells are viable after sorting. Different ratios of wild type to green fluorescent protein (GFP)-expressing *E. coli* cells were introduced into the input well (volume ranges from 10 to 30 ml of sample); the collection wells were filled with 10–30 ml of buffer with 10 - 5 M SDS. After the three platinum electrodes were inserted into the wells (with the ground electrode in the input well), the voltages were set for forward sorting. After 2

hours of sorting, cells were collected through with a pipette and streaked onto Luria–Bertani (LB) agar plates and incubated overnight at 37°C for colony counting. We achieved enrichments of 30-fold with yields of 20%, where the yield is defined by the number of colonies on the plate divided by the number of positive fluorescence events detected in the device. Recovery of viable cells was relatively constant at 20% in electric fields up to about 100 V/cm, corresponding to velocities of about 1–3 mm/s (Table 5.1).

Table 5.1. Results of sorting red from blue fluorescent beads (forward mode and reverse mode) and of sorting GFP-expressing HB101 *E. coli* from wild-type HB101 *E. coli* (forward mode)[a]

	Input well		**Collection well**		**Waste well**	
Bead color	Blue	Red	Blue	Red	Blue	Red
Forward-mode bead sorting	0.925	0.074	0.160	0.840	0.998	0.002
Reverse-mode bead sorting	0.988	0.012	0.043	0.957	0.999	0.001
	Wt	GFP	Wt	GFP	Wt	GFP
HB101 *E. coli* cell sorting	0.992	0.008	0.693	0.307	0.992	0.008

[a]For the forward mode, after running for 22 min the collection channel had a sample of red beads that had been enriched by 8.4 times from an initial blue:red bead ratio of 10:1. For the reverse mode, after 6 min of sorting, red beads in the collection channel had been enriched 80 times from an initial blue:red bead ratio of 100:1. The throughput was ~10 beads/s. The initial ratio of wild type-(Wt) to green fluorescent protein (GFP)-expressing HB101 *E. coli* cells was 100:1. After 2 hours of sorting, cells recovered from the collection well were enriched 30 times (approximately 120,000 cells sorted). Numbers in the table represent the fraction of different beads or cells in each well.

Our μFACS system offers several advantages over traditional sheath flow methods. Because the channels in the device can be made with micron dimensions, the volume of the interaction region can be precisely controlled, and there is no need for hydrodynamic focusing. The planar geometry of the devices allows the use of high numerical aperture (NA) optics, increasing the sensitivity of the detection system. We previously showed that microfluidic analytical systems with a similar geometry are sensitive enough to identify a single 2 kbp molecule of DNA [12]. As fluid flows continuously through the system, there is no need for droplet formation and a host of challenging technical issues can be sidestepped. Furthermore, no aerosol is formed because the system is entirely self-contained, allowing relatively safe sorting of biohazardous material. The

disposability of the sorting devices obviates the need for cleaning and sterilizing the instrument and prevents cross-contamination between samples.

The throughput of 20 cells/s is considerably slower than conventional FACS machines, but there is reason to believe the throughput can be augmented by increasing the electric field by up to a factor of six [10]. Throughput also can be improved in future systems either through parallel device fabrication or with a pressure-driven switching scheme. It should also be possible to sort eukaryotic cells with μFACS, given that others have shown that eukaryotic cells can be manipulated electro-osmotically in microfabricated devices [10] and are compatible with the elastomeric surface chemistry [11] (Robert H. Austin, personal communication).

A working μFACS system can be assembled for approximately $15,000. Most of this amount represents the cost of the external optics and detectors used to read out the chip, since the cost of the chip itself is negligible. Considerable cost savings can potentially be realized by fabricating the detectors and optical filters directly on the chip. We believe that this will be an important component of future integrated biomedical chip-based systems.

5.3 Experimental protocol

Microfabrication. The chip was fabricated as described [12]. Briefly, standard micromachining techniques were used to create a negative master mold out of a silicon wafer. The silicone elastomer was poured on the wafer and allowed to cure for 2 hours at 80°C. The resulting device could be peeled off of the wafer and bonded hermetically to glass. It was rendered hydrophilic by boiling in HCl (pH 2.7, 0.01% in water) at 60°C for 40 minutes. The master wafer can be reused indefinitely.

System setup. The cell-sorting device is mounted on an inverted microscope (Zeiss Axiovert 35; Carl Zeiss Inc., Thornwood, NY) with an oil immersion objective (Plan Apo Chromat ~6′, 1.4 NA; Olympus America Inc., Melville, NY). Epifluorescent excitation

was provided by an argon ion laser (Innova 70, Coherent Inc., Santa Clara, CA) for cells and a 100 W mercury lamp for beads. Fluorescence was collected with the same objective and projected onto the cathode of a Hamamatsu R928 (Hamamatsu, Bridgewater, NJ) PMT with custom current-to-voltage amplifier. Part of the light can be directed onto a charge-coupled device (CCD) camera for imaging. The detection region is approximately 5–10 μm below the T-shaped junction and has a window of about 15 x 5 μm in dimension. The window is implemented with a Zeiss adjustable slit. Cells or particles can be directed to either side of the T channels depending on the voltage-potential settings. The voltages on the electrodes are provided by a pair of Apex PA42 HV operational amplifiers (Apex Microtechnology, Tuscon, AZ) powered by 150 V Acopian power supplies. The third electrode is ground. The PMT signal is digitized by the personal computer, which also controls the high voltage settings via a National Instruments (Austin, TX) Lab PC1200 card.

Preparation of beads. Red and blue fluorescent beads (1 μm diameter, Interfacial Dynamics Corporation, Portland, OR) were suspended in PBS (137 mM NaCl, 2.7 mM KCl, 4.3 mM $Na_2HPO_4 \times 7H_2O$, 1.4 mM KH_2PO_4) with 10% BSA (1 g/L) and 0.5% Tween 20 in a 10:1 blue:red ratio and overall concentration of 1.5%. Fluorescence of the beads was excited by 100 W mercury lamp with 488DF20 optical filter. A 630DF30 optical filter (Chroma Technology Corp., Brattleboro, VT) was used to select the red fluorescent emission. The μFACS device had 3 x 4 μm channels. A 100:1 blue:red ratio was used for reverse sorting. Preparation of *E. coli* cells for sorting. The *E. coli* cells (HB101) expressing GFP were grown at 30°C for 12 hours in LB liquid medium containing ampicillin (one colony inoculated into 3 ml medium containing 50 mg/ml of ampicillin). Wild-type *E. coli* HB101 cells were incubated for 12 hours in LB-only medium. After incubation, HB101 and GFP-expressing HB101 *E. coli* cells were resuspended into PBS (ionic strength = 0.021) three times and stored at 4°C for sorting. Immediately before sorting, the cells were resuspended again into phosphate buffer (4.3 mM $Na_2HPO_4 \times 7H_2O$, 1.4 mM KH_2PO_4) containing 10^{-5} M SDS and diluted to a concentration of 10 9 cells/ml. The cells were filtered through a 5 mm syringe filter (Millipore Bioscience Inc., Bedford, MA) for elimination of any elongated cells. A

μFACS device with 10 x 4 μm channels was used. Fluorescence was excited by the 488 nm line of an argon ion laser (6 mW into the objective), Coherent Innova 70 (Laser Innovations), and the emitted fluorescence was filtered with a 535DF20 filter (Chroma).

5.4 References

1. Shapiro, H.M., *Practical flow cytometry*. 1995, New York: Wiley-Liss.
2. Melamed, M.R., Lindmo, T. and Mendelsohn, M.L., *Flow cytometry and sorting*. 1990, New York: Wiley-Liss.
3. Crosland-Taylor, P.J., *A device for counting small particles suspended in a fluid through a tube.* Nature, 1953. **17**1: p. 37–38.
4. Coulter, W., *Means for counting particles suspended in a fluid.* US 2,656,508 (1949).
5. Kamentsky, L.A., Melamed, M.R. and Derman, H. *Spectrometer: new instrument for ultrarapid cell analysis.* Science, 1965. **150**: p. 630–631.
6. Sweet, R.G., *High frequency recording with electrostatically deflected ink jets.* Rev. Sci. Instrum., 1965. 36:p. 131–133.
7. Fulwyer, M.J., *Electronic separation of biological cells by volume.* Science, 1965. **150**: p. 910–911.
8. Brody, J.P. *Valveless liquid microswitch.* US 656,155 (1998).
9. Fiedler, S., Shirley, S.G., Schnelle, T. and Fuhr, G., *Dielectrophoretic sorting of particles and cells in a microsystem.* Anal. Chem., 1998. **70**: p. 1909–1915.
10. Li, P.H. and Harrison, D.J., *Transport, manipulation, and reaction of biological cells on-chip usingelectrokinetic effect.* Anal. Chem., 1997. **69**: p. 1564–1568.
11. Carlson, R.H. et al., *Self-sorting of white blood cells in a lattice.* Physical Review Letters, 1997. **79**: p. 2149–2152.
12. Chou, H.P., Spence, C., Scherer, A. and Quake, S.R., *A microfabricated device for sizing and sorting DNA.* Proc. Natl. Acad. Sci. USA, 1999. **96**: p. 11–13.
13. Whitesides, G. and Xia, Y., *Soft lithography*. Angew. Chem. Int. Edn Engl., 1998. **37**: p. 550–575.
14. Kopp, M.U., De Mello, A. and Manz, J.A., *Chemical amplification: continuous-flow PCR on a chip.* Science, 1998. **280**: p. 1046–1048.
15. Harrison, D.J. et al., *Micromachining a miniaturized capillary electrophoresis-based chemical analysis system on a chip.* Science, 1993. **261**: p. 895–897
16. Fodor, S.P.A. et al., *Light-directed, spatially addressable parallel chemical synthesis.* Science, 1991. **251**: p. 767–773.

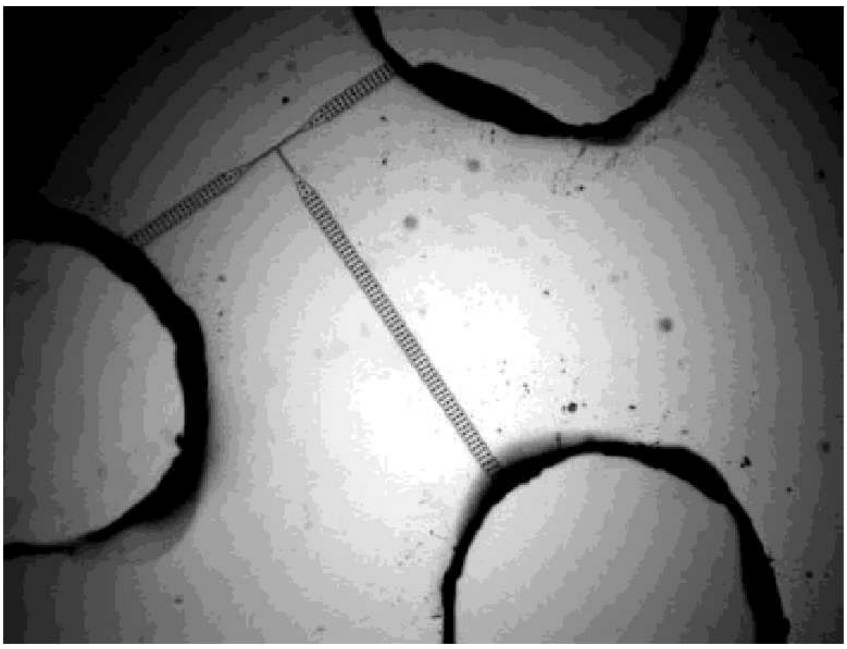

Figure 5.1. Optical micrograph of the μFACS device. The device shown has channels that are 100 mm wide at the wells, narrowing to 3 mm at the sorting junction. The channel depth is 4 mm, and the wells are 2 mm in diameter.

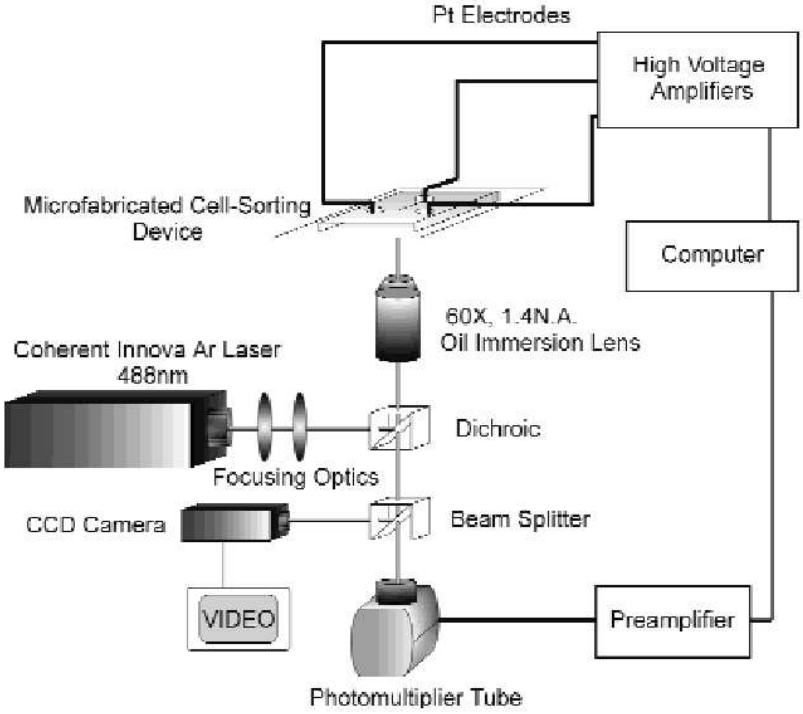

Figure 5.2. Schematic diagram of the cell sorting apparatus. See Experimental Protocol for details.

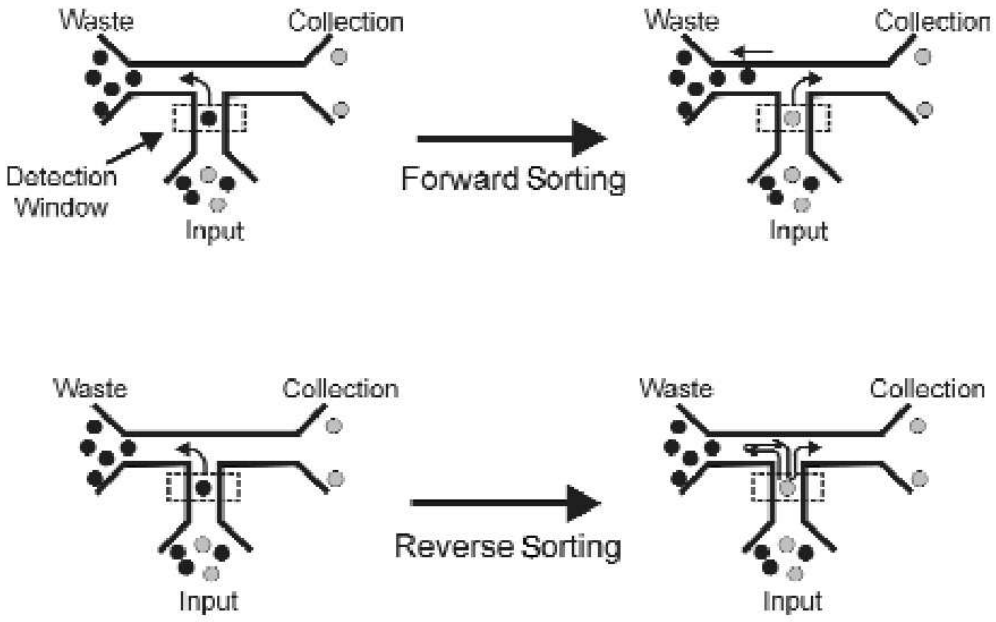

Figure 5.3. A sketch of the algorithms for the forward sorting and reverse sorting is shown with the schematic of the T-shaped junction. Top: With the forward-sorting algorithm, the fluid flow is switched as fluorescence is detected so that red beads are sent directly to the collection channel. Bottom: The reverse-sorting algorithm allows rare-event capture at a rate independent of the switching speed of the device. Fluid flow is established at a high rate from the input well to the waste channel. After event detection, the fluid flow is halted and reversed until the bead is detected a second time. It is then directed at a slower speed to the collection channel.

Chapter 6

A Microfabricated Device for Sizing and Sorting DNA Molecules

Hou-Pu Chou, Charles Spence, Axel Scherer, and Stephen Quake

6.1 Introduction

Many assays in biology require measurement of the length distribution of DNA molecules in a heterogeneous solution. This measurement is commonly done with gel electrophoresis; the molecules are separated by mobility, from which the lengths are inferred. This method is powerful, yet has some drawbacks. For medium to large DNA molecules the resolution is limited to approximately 10%. Gel electrophoresis is time consuming. It generally takes at least an hour to run the gel, not including the setup time to cast the gel. Furthermore, for large molecules the procedure fails. This problem has been alleviated to some extent by the development of pulsed-field gel electrophoresis [1], but running times can be days.

With the development of high affinity intercalating DNA stains [2], it has become possible to directly measure the length of single molecules by quantitating fluorescence. The amount of intercalated dye is proportional to the length of the molecule, so measuring the total fluorescent intensity from a single molecule gives a direct measurement of its length. This method in principle allows the measurement of extremely long DNA molecules because the signal increases with the length of the molecule. This technique has been used with traditional methods of flow cytometry to measure length distributions of DNA molecules [3, 4]. Other groups have imaged restriction enzymes digesting extended single DNA molecules for ‘‘optical mapping’’ [5, 6].

We have developed microfabricated devices to size and sort microscopic objects based on measurement of fluorescent properties. The devices have a network of microfluidic channels and are fabricated from a silicone elastomer by using a replica technique [7].

Master molds are made from silicon wafers by using standard micromachining techniques. Because the molds can be reused indefinitely, this method of fabrication allows economical mass production of the devices. The devices were patterned as shown in Fig. 6.1. This fabrication technique is one of a new set of technologies known as soft lithography. Previous work has demonstrated that elastomers can replicate gratings and other test patterns with high (' 50 nm) resolution and fidelity [8, 9]. Although some groups have made large (' 30 mm) elastomer structures for capillary electrophoresis [10], there is only one other example of a micron scale fluidic network with the elastomer [11].

6.2 Materials and Methods

Device Fabrication. Negative master devices were fabricated in silicon and used as molds for the silicone elastomer. Contact photolithography was used to pattern the oxide surface of a silicon wafer, which then was etched by reactive ion etch (RIE) with a C_2F_6yCHF_3 gas mixture. A 3 minute O_2 RIE was used to remove fluorocarbon polymer residue on the silicon surface. The oxide then was used as a mask for the silicon underneath, which was etched with KOH. The silicone elastomer (General Electric RTV 615) components were mixed together and pumped in an evacuated chamber for 30 min to remove air bubbles. The liquid elastomer then was poured on the mold and cured in an oven at 90°C for 2 hours. After this procedure, the devices could be peeled from the silicon master and would bond hermetically to glass. Number 1 coverslips were used to seal the devices.

The elastomer is naturally hydrophobic, preventing aqueous solution from entering the channels. The surfaces of the devices were modified by soaking in dilute HCl (pH 2.7, 0.01% in water) for 40 min at 43°C. After this treatment, the devices were hydrophilic, and aqueous solution would enter easily by capillary action. The devices could be cleaned and reused several times if desired. All of the data for this paper were taken with the same device. We have found that the geometry of the device does not affect reproducibility of the results; data taken from a device with slightly different channel dimensions were comparable. Results from run to run and day to day are highly

reproducible; the histograms can be overlaid without adjusting any parameters and there is no need to recalibrate the apparatus.

Sample wells were created during the fabrication process by gluing small aluminum cylinders to the silicon wafer molds. The final elastomer devices were attached to a coverslip in such a way that the sample wells were only partially covered, which allowed access with a pipette tip for introduction of the sample and also provided convenient electrode insertion. The flow rate was determined by a balance between capillary action within the channels and electro-osmotic flow.

Experimental Apparatus. A 10 mW air-cooled argon ion laser (Uniphase, San Jose, CA) emitting at 488 nm was used for fluorescent excitation. The laser was focused through a 603 1.4 NA oil immersion objective, which also was used to collect the emitted fluorescence, on an upright microscope (Olympus BH-2, New Hyde Park, NY). Auxiliary lenses were used to adjust the focused spot to a full width half maximum of 30 mm. The large spot size was chosen to give uniform excitation across the width of the channel. The quality and uniformity of the spot was evaluated by imaging a thin layer of fluorescein in solution with a charge-coupled device camera. The image was digitized and evaluated for symmetry and Gaussian shape. Dielectric filters were used to filter laser tube fluorescence (CVI 488-nm line filter, CVI Laser, Albuquer-que,NM) and to reduce background and scattered light from the emitted fluorescence (Chroma D535y50M, Chroma Technology, Brattleboro, VT). A dichroic filter was used to intro-duce the laser light into the optical train (Chroma 500 DCLP).

Fluorescence was imaged onto a 5 mm avalanche photodiode detector (Advanced Photonix, Camarillo, CA). The detector was cooled to 240° with a two-stage thermoelectric cooler (ITI 6320y157y040C, Chelmsford, MA), which reduced the dark current of the detector from 50 nA to 90 pA. The detector was reverse-biased at 2,450 V, giving a gain of 500. A transimpedance amplifier (Burr Brown OP128, Tucson, AZ) converted the photocurrent to a voltage at a gain of 100 mVynA. A second stage amplifier provided additional voltage gain of 10. The signal was low-pass filtered at 1.6

kHz and digitized at 5 kHz by a National Instruments (Austin, TX) Lab PC1200 board on a personal computer running LABVIEW.

The depth of focus of the microscope was checked by centering a 1 mm fluorescent bead in the laser beam. The detector output as a function of focal distance shows that the signal is essentially flat over a depth of 5 mm. The depth of the device channels was chosen to be 3 mm so that the DNA molecules always remained in the plane of focus of the microscope.

Sample Preparation. Lambda phage DNA (GIBCO) was either digested with *Hi*ndIII (GIBCO) or ligated with T4 ligase (New England Biolabs), then was diluted in buffer (Tris-EDTA, pH 6.8 with 5 mM NaCl) and stained with the intercalating dye YOYO-1 (Molecular Probes) at a stoichiometry of one dye molecule per 4 bp. Single molecules of DNA gave measurable pulses whose height corresponded to the length of the molecule. Pulses were collected in large batches and then analyzed offline with custom software written for peak detection. One of the advantages of this device is the simplicity of the data processing: no fitting is needed. The analog signal from the avalanche photodiode is digitally low-pass filtered (cutoff ' 300 Hz), and peak heights are extracted with a thresholding algorithm. The analysis is extremely efficient to implement in real time and can be done for DNA sorting applications, as described below.

6.3 Results

To test the utility of these devices for screening restriction digests, we analyzed a *Hi*ndIII digest of λDNA. A solution containing the stained digest was introduced to the device, and fluorescence was collected with a microscope and monitored with an avalanche photodiode. Figure 6.2 shows a histogram of the observed peak heights. After collection of data for 10 minutes, the major fragments are clearly resolved. The 2 and 2.3 kbp pieces are not resolved from each other, but are well above the noise floor of the device. For larger fragments, the resolution is on the order of 5% and improves with the length of the molecule (Fig. 6.3). Anotable feature of this method is that it requires very small amounts of sample: 28 femtograms of DNA were analyzed, about 3,000 molecules.

The detection volume for the single-molecule DNA sizing (SMS) devices is 375 femtoliters, more than an order of magnitude smaller than what has been achieved so far with flow cytometry. This small detection volume reduces the background signal proportionately. Furthermore, the geometry of the microfabricated devices allows the use of a high numerical aperture objective for efficient collection of the fluorescent light. DNA fragments of size 2 kbp, containing ' 500 fluorophores, were easily measured. The noise floor of the histogram for the *Hin*dIII digest indicates that the current sensitivity of the device is approximately 1 kbp. To determine the upper length limits of analysis in the device, we analyzed l DNA ladders in the devices and have been able to detect molecules of up to 200 kbp (Figure 6.4). That limit is determined solely by the geometry of the optical setup and does not represent an inherent limitation of the technology. As with the *Hin*dIII digest, about 3,000 molecules were analyzed in 10 minutes.

The microfabricated devices have several advantages over macroscopic systems, including design flexibility, size, cost, and sensitivity. An important example of this flexibility is that one can actively sort molecules in the microfabricated devices. By inserting electrodes in the sample wells and manipulating the DNA with electric fields, we have shown that molecules can be sent down one channel or the other at will. Speeds of 125 mm/sec were attained with an electric field of 20 V/cm. The response time of the DNA to a rapidly switching potential was faster than 30 msec, the video data acquisition rate. Thus, after detection, if the molecule passes a given criterion, a computer or circuit can be used to control the destiny of the molecule. The T channels can be cascaded to give an arbitrary number of bins in which the molecules can be collected. In contrast, the hydrodynamic focusing methods used in flow cytometry do not permit easy manipulation of the sample after detection.

6.4 Discussion

We have shown that the SMS devices can be used for rapid, efficient sizing of DNA molecules ranging from 2 to 200 kbp. The operating time of 10 min is independent of the size of the DNA molecules being sorted and represents a significant improvement over gel electrophoresis. Furthermore, the devices require only tens of femtograms of DNA to

operate, making it possible to envision future applications in which SMS devices obviate the need for PCR.

By directly measuring length via fluorescent dye intercalation, SMS devices allow an absolute measurement of length which eliminates the need for sizing standard in each run. Finally, for gel electrophoresis the resolution decreases as the molecules being analyzed become longer. SMS has the opposite property: the longer the molecules, the better the signal to noise, and the fewer fluctuations because of the statistics of dye binding (Fig. 6.3). For the longest molecules in the lambda ladder (Fig. 6.4), the SMS resolution begins to degrade as a result of the optical setup: the molecules become bigger (or longer) than the region illuminated by the laser beam used to excite fluorescence. This problem can be easily remedied in the future, as applications require. The ultimate sizing limit probably will be determined by the ability of DNA molecules to survive fluid shear forces in the device.

There are several possible direct applications for SMS DNA sizing. Restriction fragment length polymorphism analysis and genetic mapping are amenable to analysis in these devices. Another important application is in the Human Genome Project. There has been a proposal to use bacterial artificial chromosome (BAC) libraries for human genome sequencing (12). This proposal requires restriction digest fingerprinting of 600,000 BAC clones, a slow and expensive task with current technology. SMS devices are capable of rapid, cheap restriction fingerprinting and mapping of BAC clones, which have a typical size of 200 kbp.

Because the devices are microfabricated, additional features could be added directly to the chip. It is easy to construct many devices in parallel on a chip, allowing rapid multiplex analysis of samples. One can envision future SMS devices with cascaded T channels capable of sorting fragments according to size and then recutting the individual fragments with different enzymes for ordered mapping, something that is not possible with electrophoretic or optical mapping techniques. Furthermore, because the detection system is all solid state and does not in principle require imaging optics, it should be

possible to build an integrated SMS device with semiconductor laser excitation and detection on a single chip.

6.5 References

1. Burmeister, M. and Ulanovsky, L., eds. (1992) *Pulsed-Field Gel Electrophoresis: Protocols, Methods, and Theories* (Humana, To-towa, NJ).
2. Haugland, R. P. (1996) *Handbook of Fluorescent Probes and Research Chemicals* (Molecular Probes, Eugene, OR).
3. Castro, A., Fairfield, F. R. and Schera, E. B. (1993) *Anal. Chem.* **65,** 849–852.
4. Huang, Z., Petty, J. T., Quinn, O. B., Longmire, J. L., Brown, N. C., Jett, J. H. and Keller, R. A. (1996) *Nucleic Acids Res.* **24,** 4202–4209.
5. Guo, X. H., Huff, E. J. andSchwartz, D. C. (1992) *Nature (London)* **359,** 783–784.
6. Cai, W. W., Jing, J. P., Irvin, B., Ohler, L., Rose, E., Shizuya, H., Kim, U. J., Simon, M., Anantharaman, T., Mishra, B. and Schwartz, D. C. (1998) *Proc. Natl. Acad. Sci. USA* **95,** 3390–3395.
7. Carlson, R. H., Gabel, C. V., Chan, S. S., Austin, R. H., Brody, J. P. & Winkelman, J. W. (1997) *Phys. Rev. Lett.* **79,** 2149–2152.
8. Jackman, R. J., Wilbur, J. L. and Whitesides, G. M. (1995) *Science* **269,** 664–666.
9. Xia, Y. & Whitesides, G. M. (1998) *Angew. Chem. Int. Ed. Engl.* **37,** 550–575.
10. Effenhauser, C. S., Bruin, G. J. M., Paulus, A. &Ehrat, M. (1997) *Anal. Chem.* **69,** 3451–3457.
11. Delamarche, E., Bernard, A., Schmid, H., Michel, B. and Biebuyck, H. (1997) *Science* **276,** 779–781.
12. Venter, J. C., Smith, H. O. & Hood, L. (1996) *Nature (London)* **381,** 364–366.

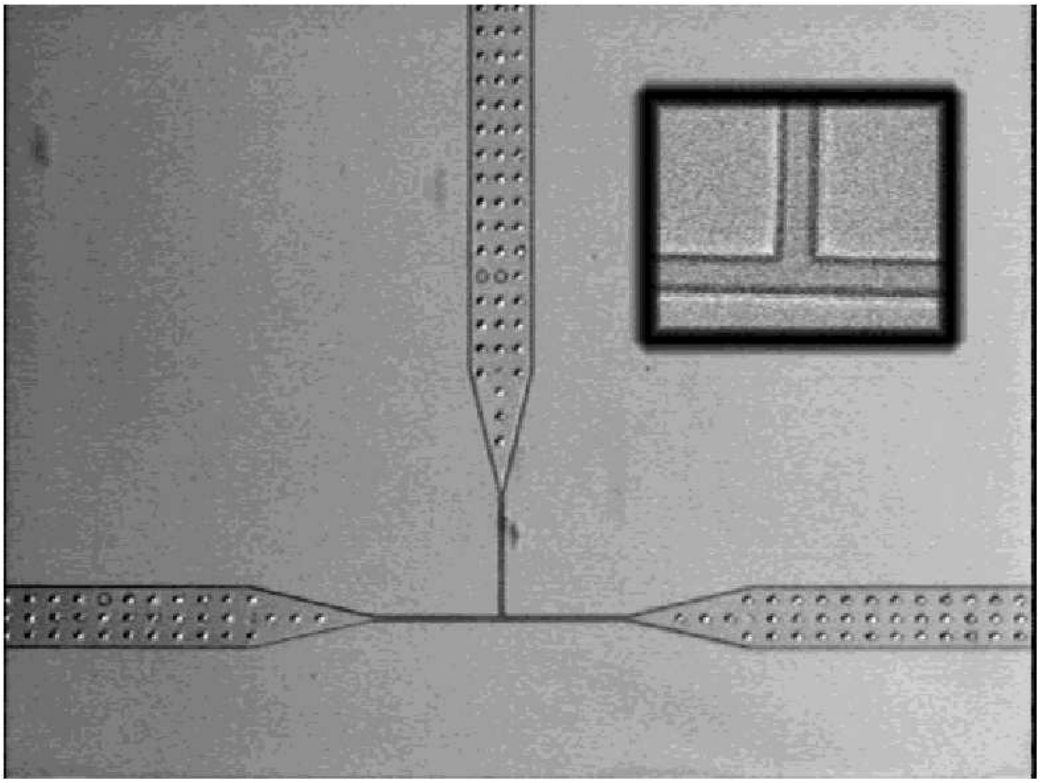

Figure. 6.1. Optical micrograph of T-channel device. The large channels have lateral dimensions of 100 mm, which narrow down to 5 mm at the T junction. The depth of the channels is 3 mm. In early prototypes, we found that because of the large aspect ratio (100 mm in width by 3 mm in depth), some of the elastomer channels would bow and pinch off by sealing directly to the glass. This problem was remedied in later versions by adding support pillars to the mask that would prop up the large channels and prevent bowing. *(Inse*t) Magnified view of T junction. The channels are 5 mm wide at this point. Note the high fidelity of the elastomer replica.

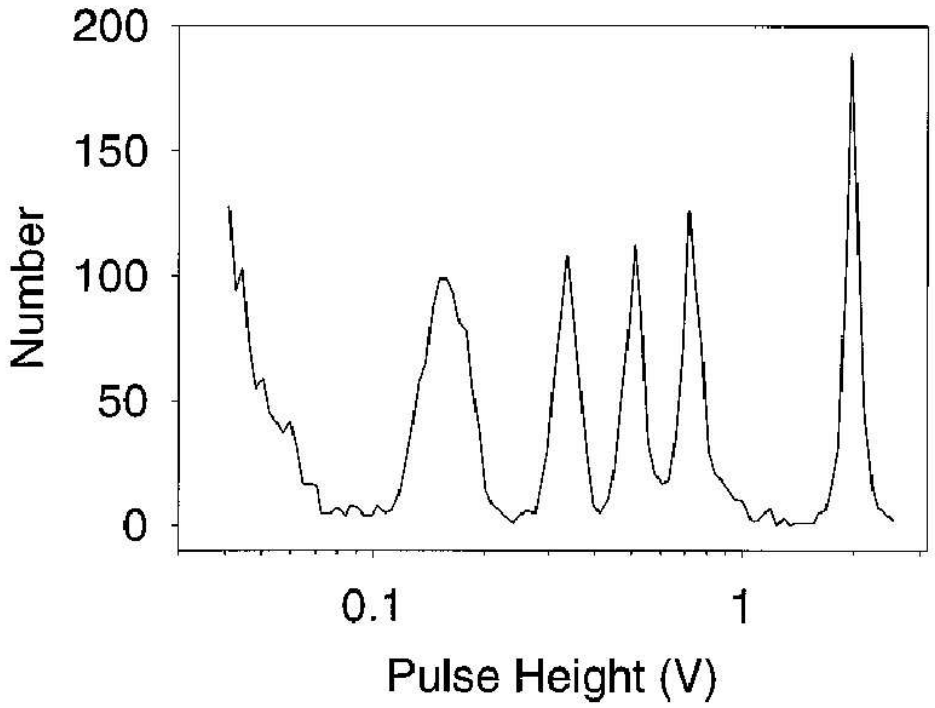

Figure. 6.2. Histogram of *Hi*ndIII digest of λ DNA. The peaks represent (from right to left) fragments of length 23 kbp, 9 kbp, 6 kbp, 4 kbp, and an unresolved combination of 2 kbp and 2.3 kbp.

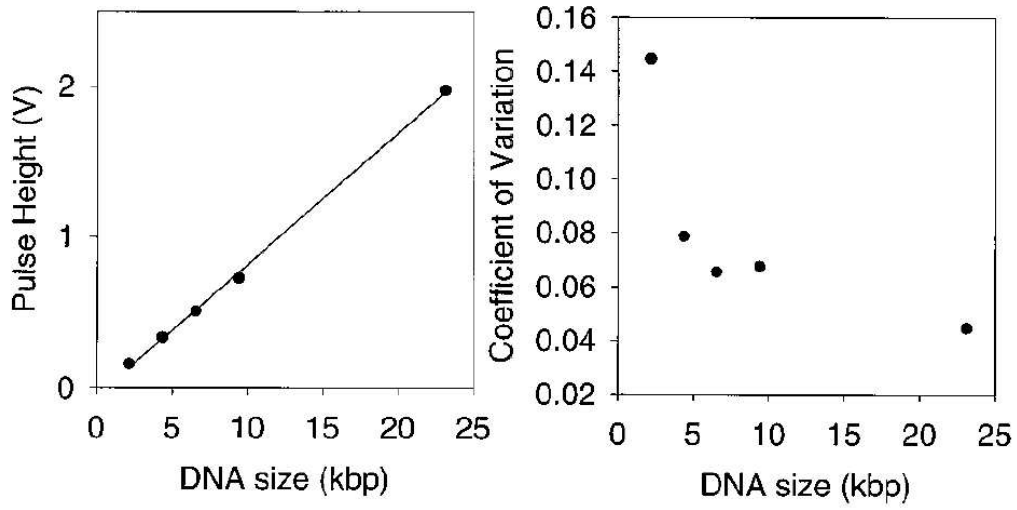

Figure 6.3. Precision and resolution of *Hi*ndIII digest. The histogram of Fig. 6.2 was fit with 5 Gaussians to estimate the precision and resolution of the measurement. *(Left*) The known sizes of the restriction fragments are compared with the fitted peak locations. The measurements are linear with a precision of a few percent. *(Right*) The widths of the peaks determine the resolution of the measurement. The coefficient of variation is the peak's SD divided by its height, and is an indication of the fractional resolution. Resolution improves with longer molecules. In both graphs, the error bars are smaller than the size of the data point symbols.

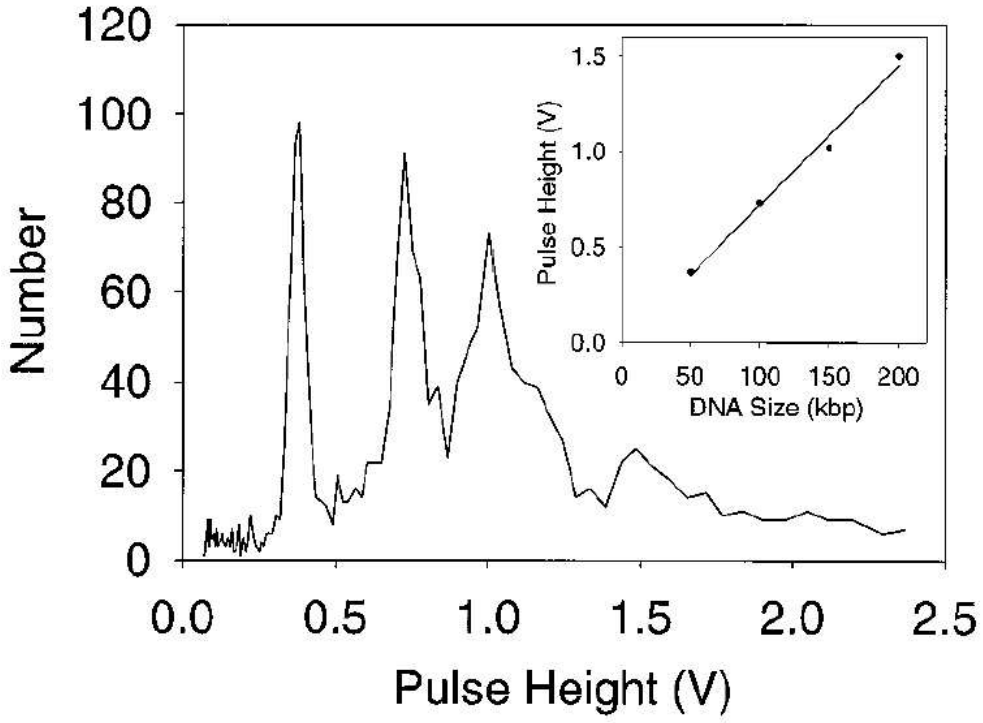

Figure. 6.4. Analysis of λ ladder. To test the upper length limit of the device, a l ladder was analyzed. Peaks corresponding to 50, 100, 150, and 200 kbp can clearly be resolved. *(Inset*) The peak height measurement is linear even out to 200 kbp.

Appendix A

The following pages contain the schematics, board layouts, and parts placement drawings for the DSP Feedback Controller. They are meant as a guide for those who would like to build such a thing. The board layout images are all viewed as if looking through the board from the top or component surface. Most of these layouts were printed at a scale of one to one (except where noted) from the original artwork for the printed circuit boards. Please be advised that depending on the reproduction process used to make copies of this manuscript these drawings will probably not be scaled correctly. Also included are parts lists for each board. Please be advised that although these parts lists have been done with care there are probably errors. The pricing was included for estimating but should be quickly outdated. Please also note that only one of the AC transformer based dual output power supplies is included in the schematics. It is representative of the layout for the others. Also because of time constraints the parts list for the linear power supplies and the regulator boards is a combined list for a combination printed circuit board which contained all of these boards. The parts numbers do not match the boards but were included to provide an idea of what parts were used. The power supplies are classic designs so hopefully the confusion will be minimal.

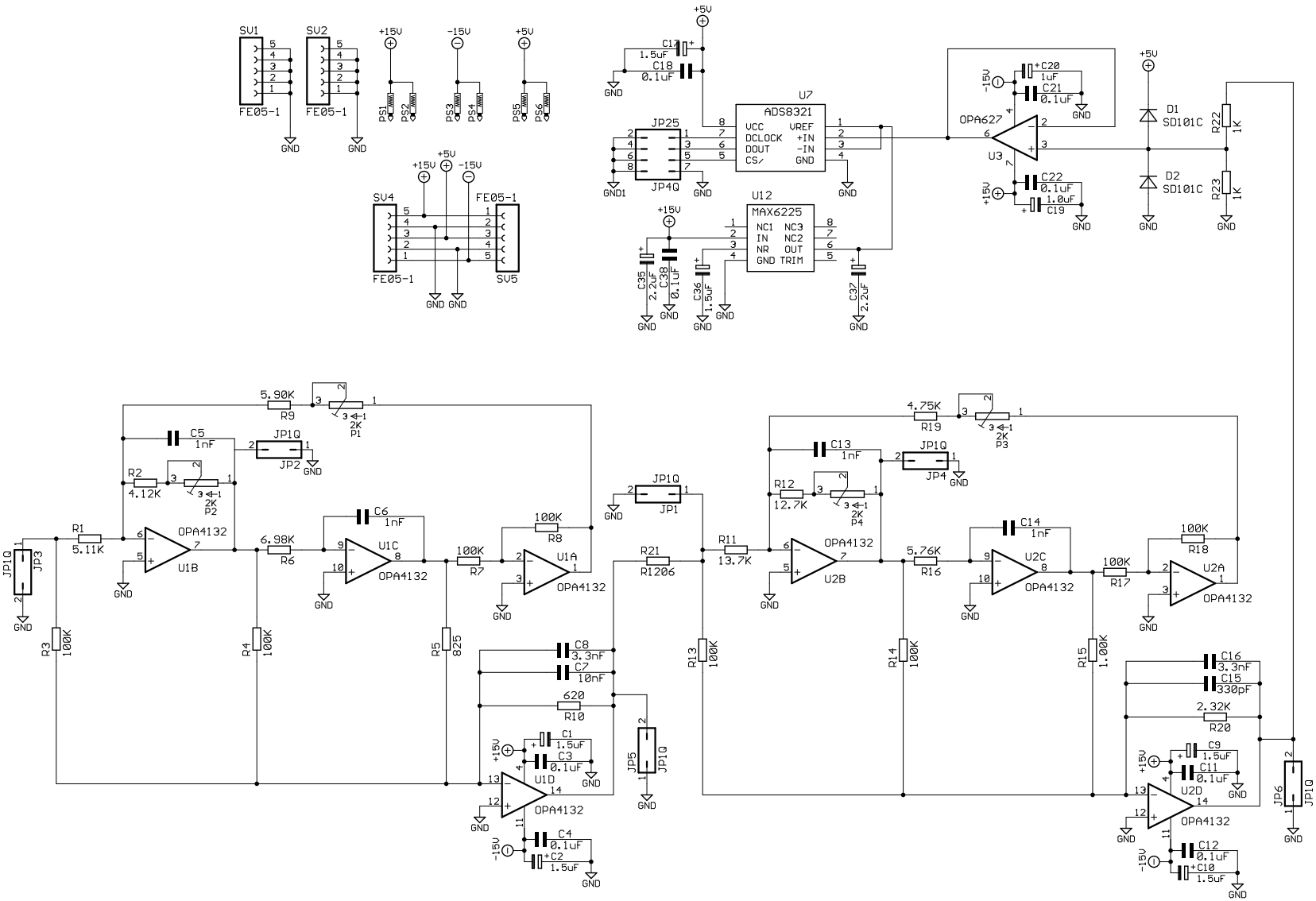

Figure A.1. 100 kHz 16-bit quad A/D converter board schematic. This schematic shows one of four identical circuits except for the power supply connections.

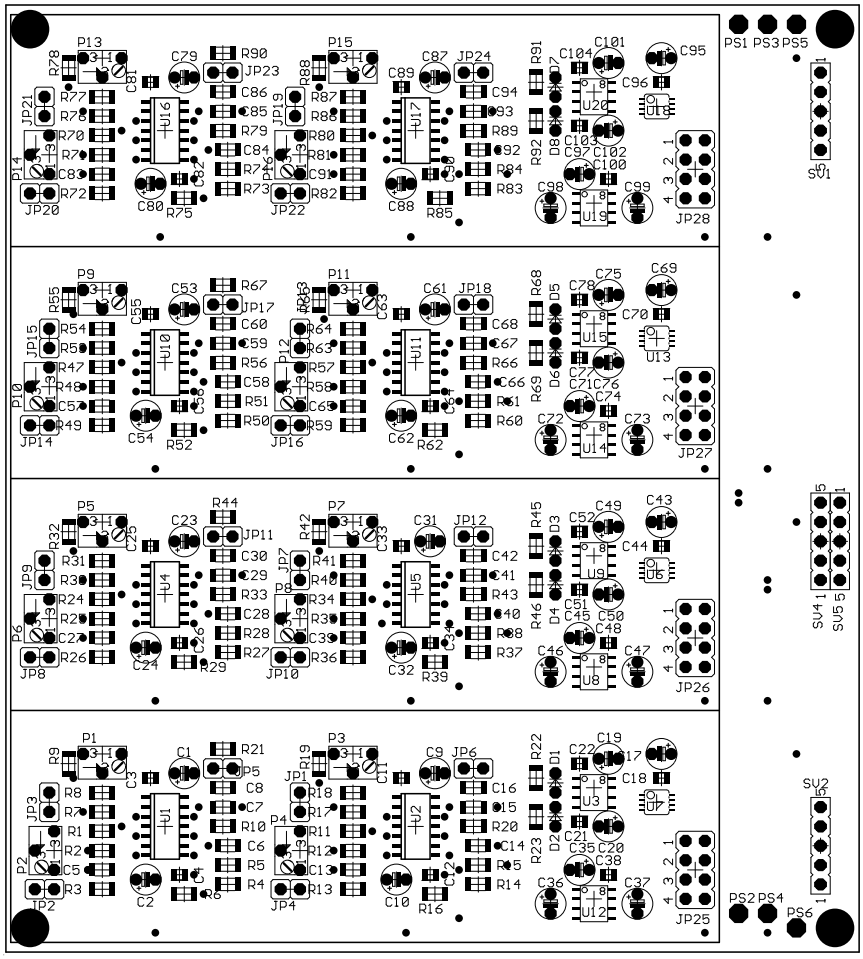

Figure A.2. 100 kHz 16-bit quad A/D board top silk-screen (approx. 1:1 scale).

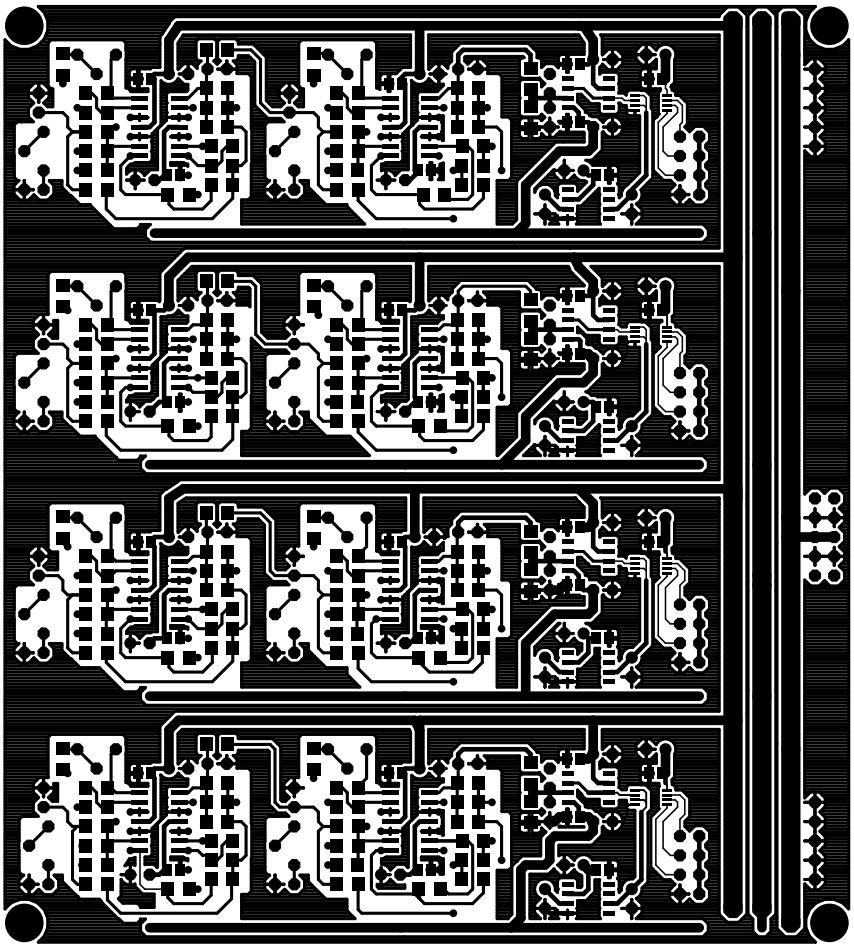

Figure A.3. 100 kHz 16-bit quad A/D board top metallization (approx. 1:1 scale).

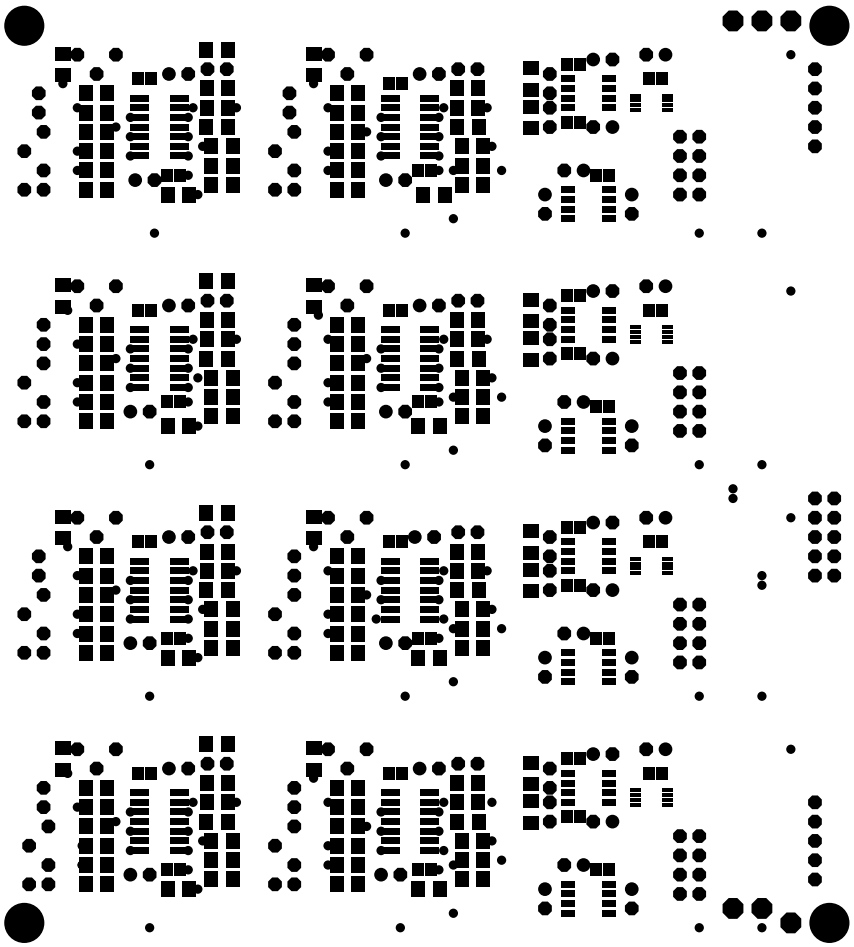

Figure A.4. 100 kHz 16-bit quad A/D board top solder mask (approx. 1:1 scale).

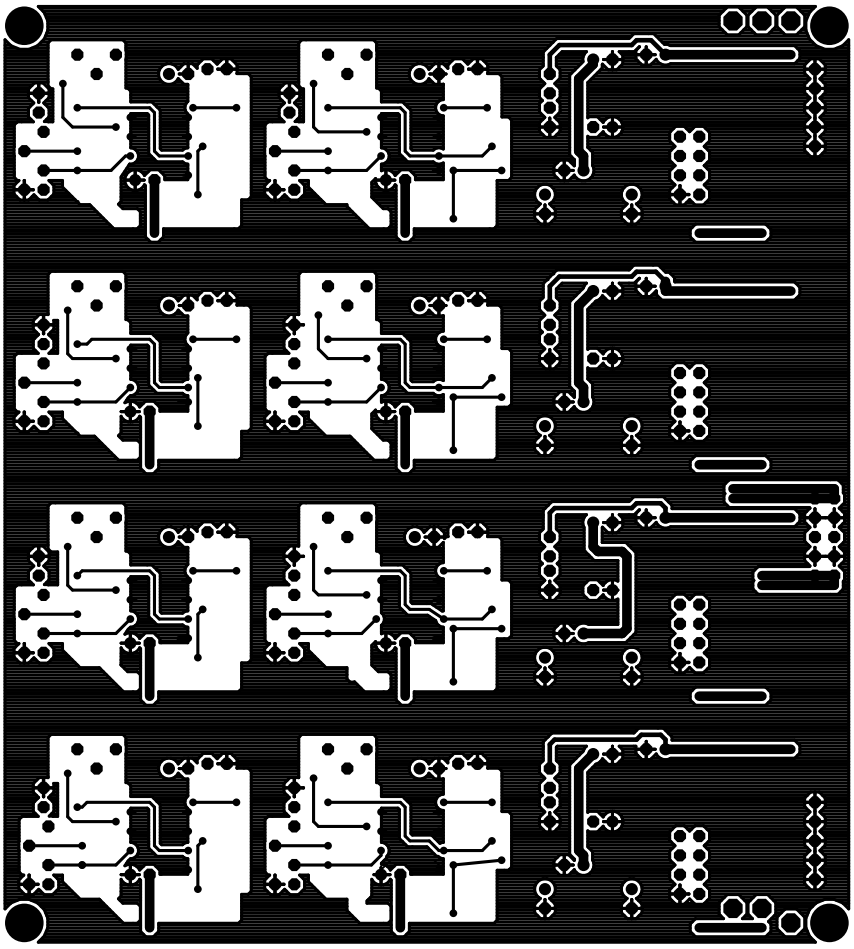

Figure A.5. 100 kHz 16-bit quad A/D board bottom metallization (approx. 1:1 scale).

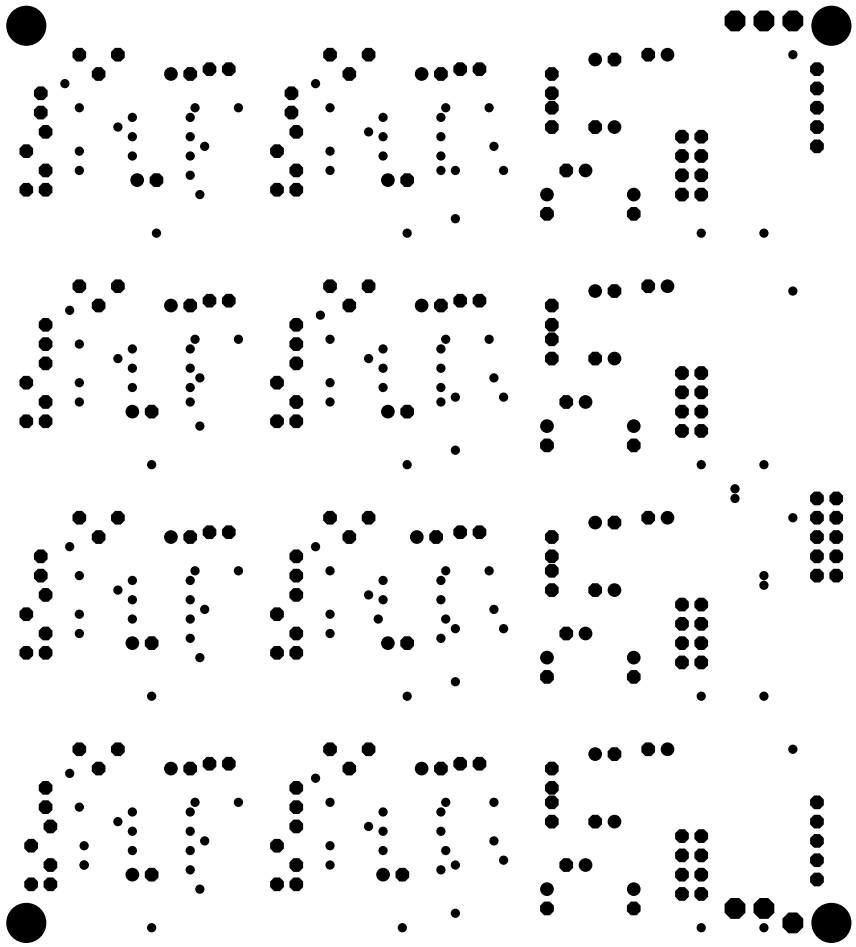

Figure A.6. 100 kHz 16-bit quad A/D board bottom solder mask (approx. 1:1 scale).

Table A.1. 100 kHz 16-bit quad A/D board parts list

Item	Qty	Value	Parts	Description	Catalog No.	Price	Subtotal
1	24	1.5uF	C1, C2, C9, C10, C17, C23, C24, C31,C32, C36, C43, C46, C53, C54, C61, C62,C69, C72, C79, C80, C87, C88, C95, C98	1.5uF@25V EF Series Tantalum Cap.	P2044-ND	0.291	6.984
2	4	1.0uF	C19, C49, C75, C101	1.0uF@35V EF Series Tantalum Cap.	P2059-ND	0.336	1.344
3	4	1uF	C20, C50, C76, C102	1.0uF@35V EF Series Tantalum Cap.	P2059-ND	0.336	1.344
4	32	0.1uF	C3, C4, C11, C12, C18, C21, C22, C25,C26, C33, C34, C38, C44, C48, C51, C52,C55, C56, C63, C64, C70, C74, C77, C78,C81, C82, C89, C90, C96, C100, C103,C104	0.1uF @50V X7R Ceramic 0805 Cap.	PCC1840CT-ND	0.11	3.52
5	8	2.2uF	C35, C37, C45, C47, C71, C73, C97, C99	2.2uF@25V EF Series Tantalum Cap.	P2045-nd	0.324	2.592
6	16	1nF	C5, C6, C13, C14, C27, C28, C39, C40,C57, C58, C65, C66, C83, C84, C91, C92	1000pF@50V NPO Ceramic 1206 Cap.	PCC102CCT-ND	0.2	3.2
7	4	330nF	C15, C41, C67, C93	330pF@50V NPO Ceramic cap. 1206 pkg.(see alt below)		0.22	0.88
8	4	3.3nF	C16, C42, C68, C94	3.3nF@50V NPO Ceramic cap. 1206 pkg.(see alt below)		0.49	1.96
9	8	SD101C	D1, D2, D3, D4, D5, D6, D7, D8	1N914 possibly stock rm. Mouser has			0
10	24	JP1Q	JP1, JP2, JP3, JP4, JP5, JP6, JP7, JP8,JP9, JP10, JP11, JP12, JP13, JP14, JP15,JP16, JP17, JP18, JP19, JP20, JP21,JP22, JP23, JP24	Cut from 72 pin Dual Row header if needed. Mainly test points.	S2011-36-ND	2.37	56.88
11	4	JP4Q	JP25, JP26, JP27, JP28	Cut from 72 pin Dual Row header if needed. Solder coax direct.	S2011-36-ND	2.37	9.48
12	16	2K	P1, P2, P3, P4, P5, P6, P7, P8, P9, P10,P11, P12, P13, P14, P15, P16	2k 1/4" Sq. Multiturn Pot 3266 Series Bourns	3266W-202-ND	3.25	52
13	6	P1-17	PS1, PS2, PS3, PS4, PS5, PS6				0
14	4	5.11K	R1, R24, R47, R70	1/8Watt 1% 1206 pkg Thick Film resistor	P5.11KFCT-ND	0.098	0.392

15	4	620	R10, R33, R56, R79	1/8Watt 1% 1206 pkg Thick Film resistor	P620FCT-ND	0.098	0.392
16	4	13.7K	R11, R34, R57, R80	1/8Watt 1% 1206 pkg Thick Film resistor	P13.7KFCT-ND	0.098	0.392
17	4	12.7K	R12, R35, R58, R81	1/8Watt 1% 1206 pkg Thick Film resistor	P12.7KFCT-ND	0.098	0.392
18	4	1.00K	R15, R38, R61,R84	1/8Watt 1% 1206 pkg Thick Film resistor	P1.00KFCT-ND	0.098	0.392
19	4	5.76K	R16, R39, R62, R85	1/8Watt 1% 1206 pkg Thick Film resistor	P5.76KFCT-ND	0.098	0.392
20	4	4.75K	R19, R42, R65, R88	1/8Watt 1% 1206 pkg Thick Film resistor	P4.75KFCT-ND	0.098	0.392
21	4	4.12K	R2, R25, R48, R71	1/8Watt 1% 1206 pkg Thick Film resistor	P4.12KFCT-ND	0.098	0.392
22	4	2.32K	R20, R43, R66, R89	1/8Watt 1% 1206 pkg Thick Film resistor	P2.32KFCT-ND	0.098	0.392
23	4	R1206	R21, R44, R67, R90	Zero ohm jumper 1206 or 0805 pkg.		0.1208	0.4832
24	8	1K	R22, R23, R45, R46, R68, R69, R91, R92	1/8Watt 1% 1206 pkg Thick Film resistor	P1.00KFCT-ND	0.098	0.784
25	32	100K	R3, R4, R7, R8, R13, R14, R17, R18, R26,R27, R30, R31, R36, R37, R40, R41, R49,R50, R53, R54, R59, R60, R63, R64, R72,R73, R76, R77, R82, R83, R86, R87	1/8Watt 1% 1206 pkg Thick Film resistor	P100KFCT-ND	0.098	3.136
26	4	825	R5, R28, R51, R74	1/8Watt 1% 1206 pkg Thick Film resistor	P825FCT-ND	0.098	0.392
27	4	6.98K	R6, R29, R52, R75	1/8Watt 1% 1206 pkg Thick Film resistor	P6.98KFCT-ND	0.098	0.392
28	4	5.90K	R9, R32, R55, R78	1/8Watt 1% 1206 pkg Thick Film resistor	P5.90KFCT-ND	0.098	0.392
29	2	FE05-1	SV1, SV2, SV4, SV5	Cut from 36 pin Single Row header	S1011-36-ND	1.28	2.56
	1	FE05-1	SV4, SV5	Cut from 72 pin Dual Row header goes in both	S2011-36-ND	2.37	2.37
30	2	OPA4132	U1, U2	OPA4132UA Quad FET Op-amp SO-14pkg	OPA4132UA-ND	8.7252	17.4504
31	1	MAX6225	U12	MAX6225AESA 2.5V prec. Ref SO-8 pkg	MAX6225AESA-ND	9.48	9.48
32	1	OPA627	U3	OPA627AU Prec Op-amp SO-8 pkg	OPA627AU-ND	12.01	12.01
33	6	OPA4132	U4, U5, U10, U11, U16, U17	OPA4132UA Quad FET Op-amp SO-14pkg	OPA4132UA-ND	8.7252	52.3512
34	4	ADS8321	U6, U7, U13, U18	ADS8321ECT 16-bit A/D MSOP-8 pkg	ADS8321ECT-ND	17.22	68.88
35	3	MAX6225	U8, U14, U19	MAX6225AESA 2.5V prec. Ref SO-8 pkg	MAX6225AESA-ND	9.48	28.44
36	3	OPA627	U9, U15, U20	OPA627AU Prec Op-amp SO-8 pkg	OPA627AU-ND	12.01	36.03
							378.8628
	4	5.62K		1/8Watt 1% 1206 pkg Thick Film resistor	P5.62KFCT-ND	0.098	0.392
	4	10.0K		1/8Watt 1% 1206 pkg Thick Film resistor	P10.0KFCT-ND	0.098	0.392
	4	13.0K		1/8Watt 1% 1206 pkg Thick Film resistor	P13.0KFCT-ND	0.098	0.392

	10	5K pot		5k 1/4" Sq. Multiturn Pot 3266 Series Bourns	3266W-502-ND	3.25	32.5
	4	3.92K		1/8Watt 1% 1206 pkg Thick Film resistor	P3.92KFCT-ND	0.098	0.392
	2	FE05-1	SV1, SV2	Digikey precut version	S1011-05-ND	0.76	1.52
	1	FE05-1	SV4,SV5	Digikey precut version	S2011-05-ND	1.32	1.32
7&8	8	6.8nF	C7, C29, C59, C85, C8, C30, C60, C86	6.8nF@50V NPO Ceramic cap. 1210 pkg.		0.27	2.16
The above non number items may be needed for alternative							
configurations of the low pass filters.							
Most catalog numbers are from Digi-key, Theif River Falls, MN							
100 k sample/sec 16-bit Quad A/D converter parts list							

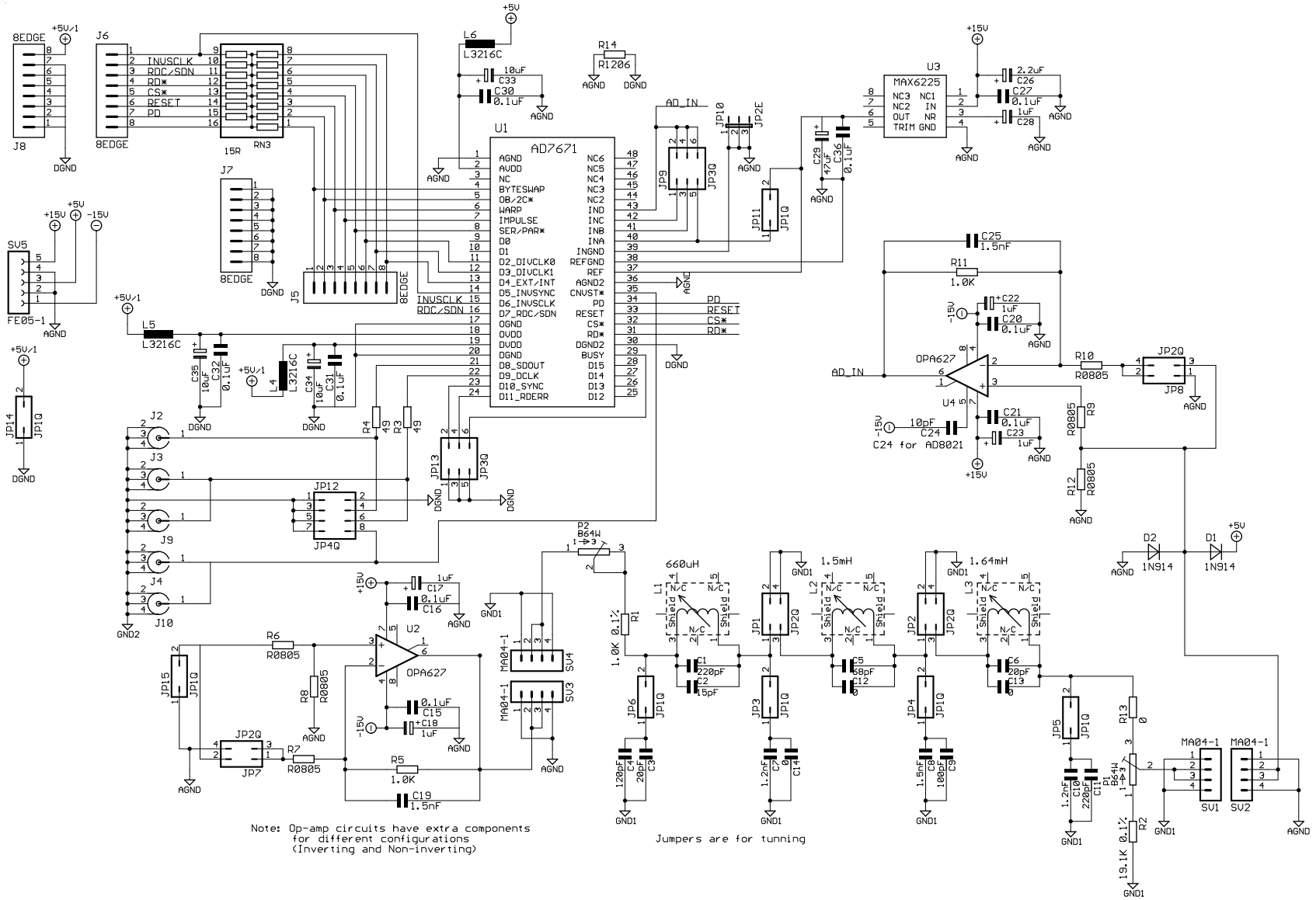

Figure A.7. 1 MHz 16-bit quad A/D converter board schematic. This schematic, except for the power connections, shows one of four identical sections.

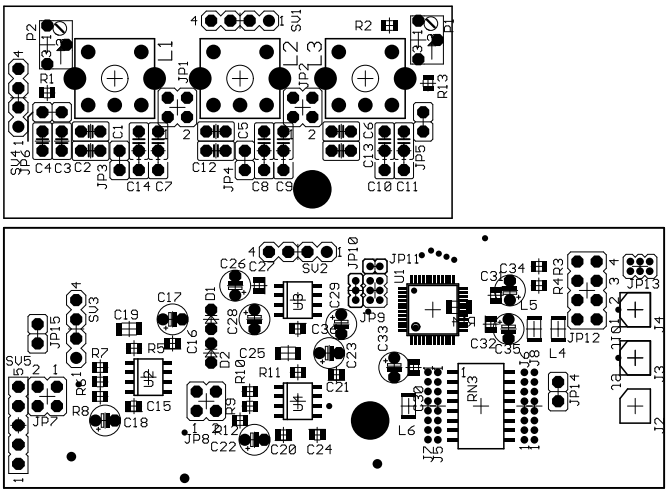

Figure A.8. 1 MHz 16-bit quad A/D board top silk-screen (approx. 1:1 scale). Note this is one of four similar section pairs on the finished circuit board. Top section plugs into lower section via connectors SV1 through SV4. Part numbers match schematic in Fig. A.7. but do not match part numbers in part list.

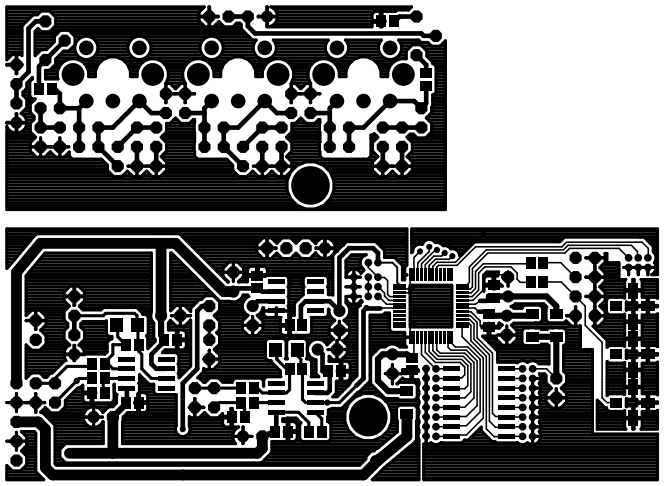

Figure A.9. 1 MHz 16-bit A/D board top metallization.

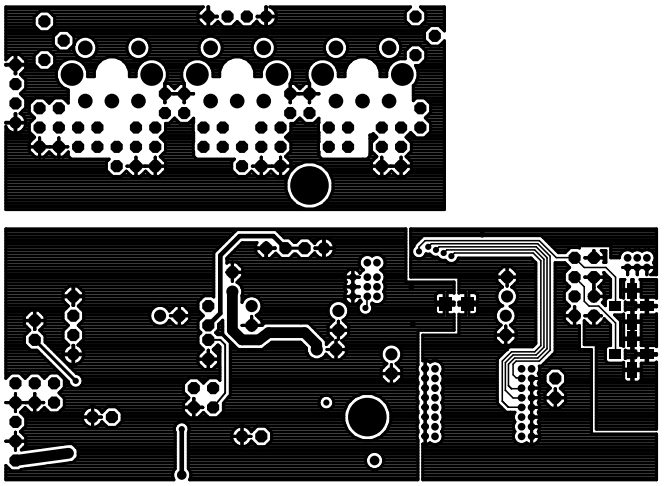

Figure A.10. 1 MHz 16-bit A/D board bottom metallization.

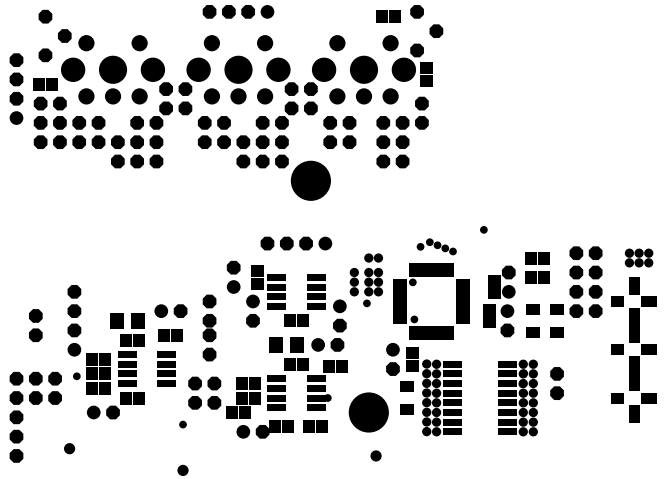

Figure A.11. 1 MHz 16-bit A/D board top solder mask.

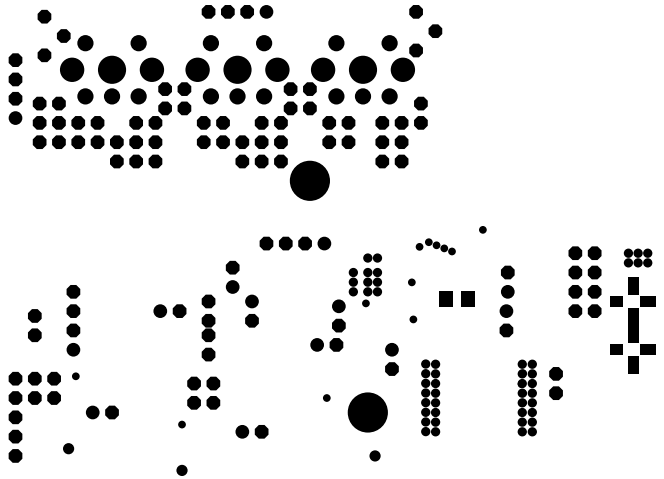

Figure A.12. 1 MHz 16-bit A/D board bottom solder mask.

Table A.2. 1 MHz 16-bit quad A/D board parts list

Item	Qty	Value	Parts	Description	Catalog No.	Price	Subtotal
1	36	0.1uF	C1, C2, C6, C7, C13, C15, C16, C20, C21,C27, C30, C31, C32, C36, C38, C39, C40,C44, C45, C46, C50, C51, C57, C60, C61,C62, C66, C67, C68, C72, C73, C79, C82,C83, C84, C88	0.1uF@50V X7R 0805 Ceramic Chip Capacitor	PCC1840CT-ND	0.109	3.906
2	4	10pF	C10, C24, C54, C76				0
3	8	0	C100, C101, C114, C115, C128, C129,C142, C143	None installed			0
4	4	0	C102, C116, C130, C144	None installed			0
5	4	2.2uF	C12, C26, C56, C78	2.2uF@25V tant EF-Series Cap.	P2045-ND	0.462	1.848
6	4	47uF	C29, C37, C59, C81	47uF@10V tant EF-Series Cap.	P2030-ND	1.578	6.312
7	20	1uF	C3, C4, C8, C9, C14, C17, C18, C22, C23,C28, C47, C48, C52, C53, C58, C69, C70,C74, C75, C80	1.0uF@25V tant. EF-Series Cap.	P2059-ND	0.483	9.66
8	12	10uF	C33, C34, C35, C41, C42, C43, C63, C64,C65, C85, C86, C87	10uF@16V tant. EF-Series Cap.	P2038-ND	0.846	10.152
9	8	1.5nF	C5, C11, C19, C25, C49, C55, C71, C77	1500pF@100V 1206 NPO Ceramic Chip Cap. Or 1500pF@50V 0805 pkg.	PCC2004CT-ND	0.57	4.56
10	4	220pF	C89, C103, C117, C131	220pF@100V COG Ceramic Leaded Cap.	BC1058CT-ND	0.146	0.584
11	4	15pF	C90, C104, C118, C132	15pF@50V COG Ceramic Leaded Cap.	BC1032CT-ND	0.108	0.432
12	8	20pF	C91, C94, C105, C108, C119, C122, C133,C136	10pF@100V COG Ceramic Leaded Cap.	BC1054CT-ND	0.108	0.864
13	4	120pF	C92, C106, C120, C134	120pF@50V COG Ceramic Leaded Cap.	BC1014CT-ND	0.124	0.496
14	4	68pF	C93, C107, C121, C135	68pF@50V COG Ceramic Leaded Cap.	BC1011CT-ND	0.113	0.452
15	8	1.2nF	C95, C98, C109, C112, C123, C126, C137,C140	1.2nF @ 50V Polypropylene Cap. P-Series	P3122-ND	0.39	3.12
16	4	1.5nF	C96, C110, C124, C138	1.5nF@50V Polypropylene Cap. P-Series	P3152-ND	0.39	1.56
17	4	100pF	C97, C111, C125, C139	100pF@100V COG Ceramic Leaded Cap.	BC1057CT-ND	0.113	0.452

18	4	220pF	C99, C113, C127, C141	See item 10 above			0
19	8	1N914	D1, D2, D3, D4, D5, D6, D7, D8				0
20	2		E$1, E$2	Cut from SIP Breakaway Header 5-pin	S1011-36-ND	1.28	2.56
21	1		E$11				0
22	4		E$3, E$4, E$5, E$6	Cut from SIP Breakaway Header 2-pin	S1011-36-ND	1.28	5.12
23	4		E$7, E$8, E$9, E$10	Zero Ohm shorting resistor 1206 pkg.	P0.0ECT-ND	0.1	0.4
24	20		J1, J2, J3, J4, J9, J10, J11, J12, J17,J18, J19, J20, J21, J26, J27, J28, J29,J30, J35, J36	H.FL Series Coax Connector w/ Cap	H9148-ND	1.65	33
25	16	8EDGE	J5, J6, J7, J8, J13, J14, J15, J16, J22,J23, J24, J25, J31, J32, J33, J34	0.050" Jumper blocks cut from header & use ED8450-ND as jumpers	ED8250-ND	7.1	113.6
26	16	JP2Q	JP1, JP2, JP7, JP8, JP19, JP20, JP28,JP29, JP37, JP38, JP43, JP44, JP49,JP50, JP55, JP56	Cut from DIP Breakaway Header 4-Pin	S2011-36-ND	2.37	37.92
27	24	JP1Q	JP14, JP15, JP17, JP18, JP26, JP27,JP35, JP36, JP39, JP40, JP41, JP42,JP45, JP46, JP47, JP48, JP51, JP52,JP53, JP54, JP57, JP58, JP59, JP60	Cut from SIP Breakaway Header 2-pin	S1011-36-ND		0
28	8	JP3Q	JP3, JP9, JP13, JP16, JP21, JP25, JP30,JP34	Uninstalled			0
29	4	JP2E	JP4, JP10, JP22, JP31	Uninstalled			0
30	4	JP1Q	JP5, JP11, JP23, JP32	Uninstalled			0
31	4	JP4Q	JP6, JP12, JP24, JP33	Uninstalled			0
32	12	L3216C	L1, L2, L3, L4, L5, L6, L7, L8, L9, L10,L11, L12	Steward EMI Chip 1206 100 ohms	240-1008-1-ND		0
33	4	660uH	L13, L16, L19, L22	680uH 10%adj. Qmin=100 variable inductor Toko 10EZ	TK1229-ND	3.46	13.84
34	4	1.5mH	L14, L17, L20, L23	1.5mH 10% adj. Qmin=80 variable inductor Toko 10PA	TK1705-ND	3.36	13.44
35	4	1.64mH	L15, L18, L21, L24	Same as item 34	TK1705-ND	3.36	13.44
36	8	B64W	P1, P2, P3, P4, P5, P6, P7, P8	Ordered 50 and 1K			0

37	8	1.0K	R1, R5, R11, R18, R23, R29, R34, R40	1.00K 1% 0805 Thick Film Resistor 1/10W	P1.00KCCT-ND	0.09	0.72
38	4	R1206	R14, R22, R33, R44	Zero Ohm shorting resistor 1206 pkg.	P0.0ECT-ND	0.094	0.376
39	24	R0805	R2, R6, R7, R8, R9, R10, R12, R13, R15,R16, R17, R19, R24, R25, R26, R27, R28,R30, R35, R36, R37, R38, R39, R41	Uninstalled			0
40	8	49	R3, R4, R20, R21, R31, R32, R42, R43	49.9ohm 1% 0805 Thick Film Resistor 1/10W	P49.9CCT-ND	0.09	0.72
41	4	1.0K 0.1%	R45, R48, R51, R54	1.00K 0.1% 0805 Metal Film Resistor 1/10W	P1.00ZCT-ND	0.684	2.736
42	4	19.1K 0.1%	R46, R49, R52, R55	19.1K 0.1% 0805 Metal Film Resistor			0
43	4	0	R47, R50, R53, R56	Zero Ohm shorting resistor 0805 pkg	P0.0ACT-ND	0.08	0.32
44	4	10K	RN1, RN2, RN3, RN4	10K ohm 16 pin bussed res. Network SOIC16	768-161-R10K-ND	0.75	3
45	16	MA04-1	SV1, SV2, SV3, SV4, SV7, SV8, SV10,SV11, SV13, SV14, SV15, SV16, SV17,SV18, SV19, SV20	Should be split into 4-pin header and socket. Need height to work with standard spacers. Try Mill-Max ED2984-ND w/ ED15050-ND	ED2864-ND	9.04	144.64
46	4	FE05-1	SV5, SV6, SV9, SV12	Uninstalled			0
47	4	AD7671	U1, U6, U10, U14	AD7671AST 16-Bit, 1MSP ADC		42	168
48	8	OPA627	U2, U4, U5, U8, U9, U12, U13, U16	OPA627 Precision High Speed Op-amp 8-SOIC	OPA627AU-ND	15.83	126.64
49	4	MAX6225	U3, U7, U11, U15	MAX6225BESA precision 2.5V Ref. 5ppm?	MAX6225BESA-ND	6.31	25.24
50	6			H.FL. Coax cables 6"	229-1004-ND	9.96	59.76
51	3			H.FL. Coax cables 12"	229-1005-ND	11.22	33.66
Most catalog numbers are from Digi-key, Theif River Falls, MN							
Quad 1 Mhz A/D converter board parts list							

The part numbers in the above parts lists do not match the numbers in the schematic. This list was generated from the board which has four A/D circuits plus connections for powering each converter. The list is included for providing a basic order list and to determine cost.

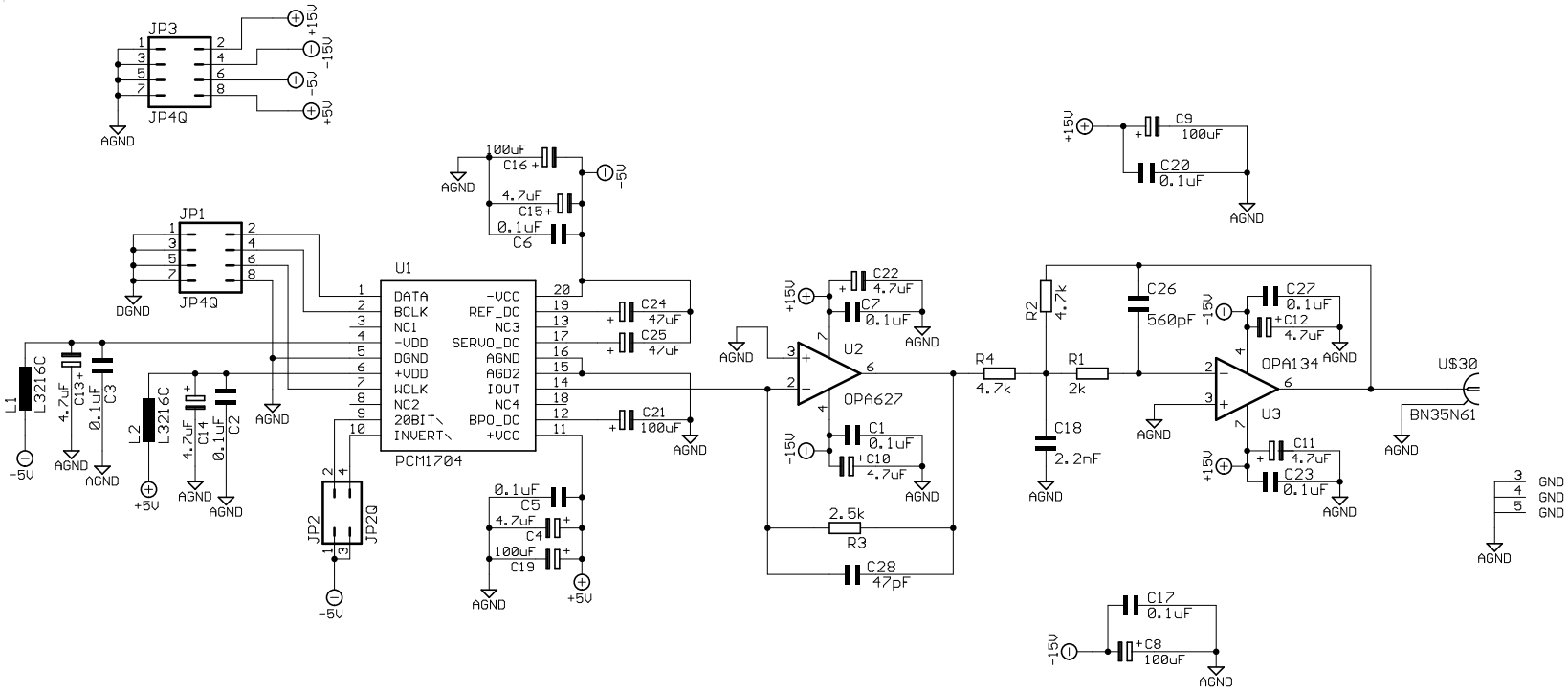

Figure A.13. 1 MHz 24-bit D/A converter schematic.

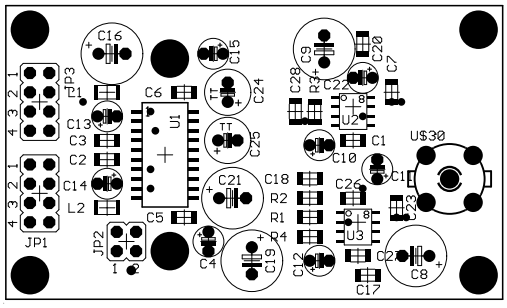

Figure A.14. 1 MHz 24-bit D/A converter top silk-screen (approx. 1:1 scale).

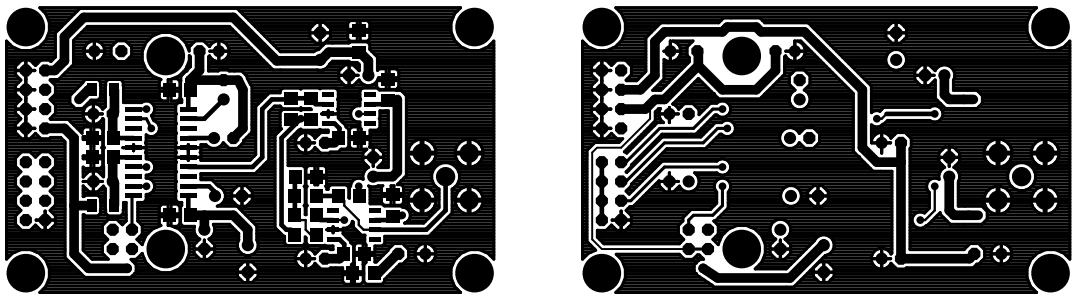

Figure A.15. 1 MHz 24-bit D/A converter top and bottom metallization. Left image is top metallization .

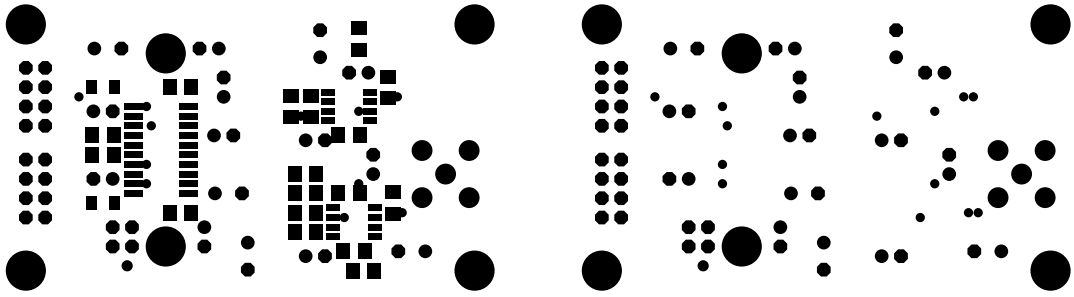

Figure A.16. 1 MHz 24-bit D/A converter top and bottom solder mask. Left image is top solder mask.

Table A.3. 1 MHz 24-bit D/A converter parts list

Item	Qty	Value	Parts	Description	Digikey No.	Price	Subtotal
1	10	0.1uF	C1, C2, C3, C5, C6, C7, C17, C20, C23,C27	0.1uF@50V X7R Ceramic cap 0805 pkg.		0.22	2.2
2	1	2.2nF	C18	2.2nF@50V NPO Ceramic Cap 1206 pkg. Garrett has stock		0.41	0.41
3	2	47uF	C24, C25	47uF@16V EF Series Tantalum Cap.	P2042-ND	1.99	3.98
4	1	560pF	C26	0.1uF @50V X7R Ceramic 0805 Cap.	PCC561CGCT-ND	0.147	0.147
5	1	47pF	C28	47pF@50V NPO Ceramic Cap 0805 pkg.	PCC470CGCT-ND	0.078	0.078
6	8	4.7uF	C4, C10, C11, C12, C13, C14, C15, C22	4.7uF@25V EF Series Tantalum Cap.	P2047-ND	0.495	3.96
7	5	100uF	C8, C9, C16, C19, C21	100uF@35V FC Series Elec.Cap.		0.63	3.15
8	2	JP4Q	JP1, JP3	Cut from 72 pin Dual Row header if needed		2.37	4.74
9	1	JP2Q	JP2	Cut from 72 pin Dual Row header if needed	S2011-36-ND	2.37	2.37
10	2	L3216C	L1, L2	Steward EMI chip 1206 pkg 100ohms	240-1008-1-ND	0.274	0.548
11	1	2k	R1	1/8Watt 1% 1206 pkg Thick Film resistor	P2.00KFCT-ND	0.98	0.98
12	2	4.7k	R2, R4	1/8Watt 1% 1206 pkg Thick Film resistor	P4.75KFCT-ND	0.98	1.96
13	1	2.5k	R3	1/8Watt 1% 1206 pkg Thick Film resistor	P2.49KFCT-ND	0.98	0.98
14	1	BN35N61	U$30	Cambridge formerly Johnson CP-BNCPC-002			0
15	1	PCM1704	U1	24 bit DAC Burr Brown 20-SOIC	PCM1704U-ND	18.56	18.56
16	1	OPA627	U2	Prec. High Speed Op Amp BB 8-SIOC	OPA627AU-ND	12.01	12.01
17	1	OPA134	U3	Audio Op Amp BB 8-SOIC	OPA134UA-ND	2.13	2.13
							58.203
	2	L3216	L1,L2	Steward EMI chip 1206 pkg 600ohms	240-1019-1-ND	0.254	
	2	JP4Q	JP1, JP3	DigiKey precut versions	S2011-04-ND	1.28	2.56
	1	JP2Q	JP2	Cut from 72 pin Dual Row header if needed	S2011-02-ND	1.2	1.2
The above non number items may be needed for alternative configurations							
Most catalog numbers are from Digi-key, Theif River Falls, MN							
24-bit D/A converter board parts list							

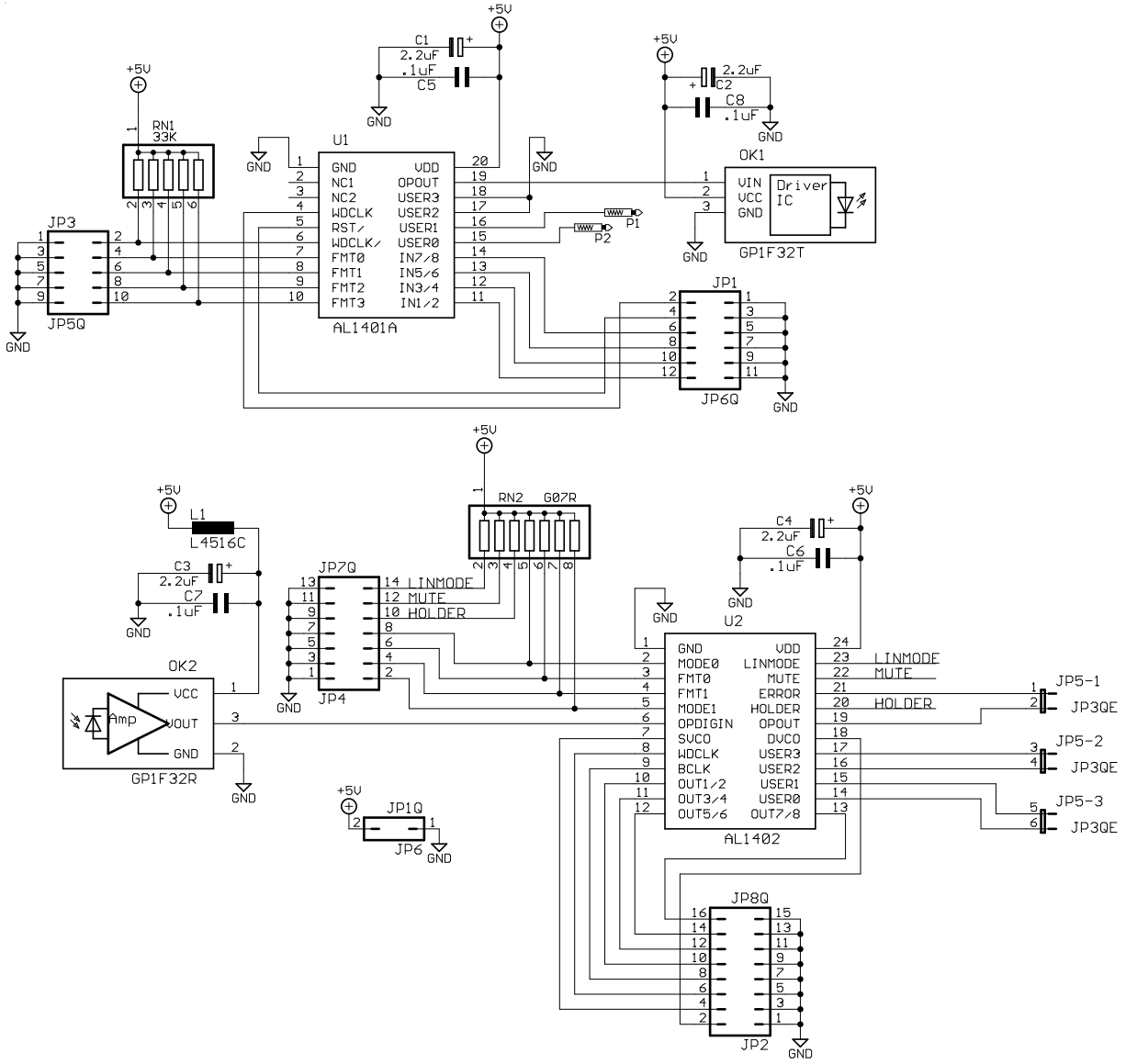

Figure A.17. ADAT optical interface schematic

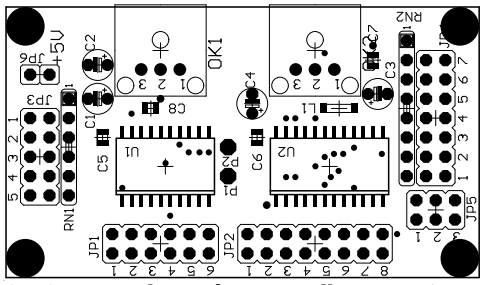

Figure A.18. ADAT optical interface top silk-screen (approx. 1:1 scale).

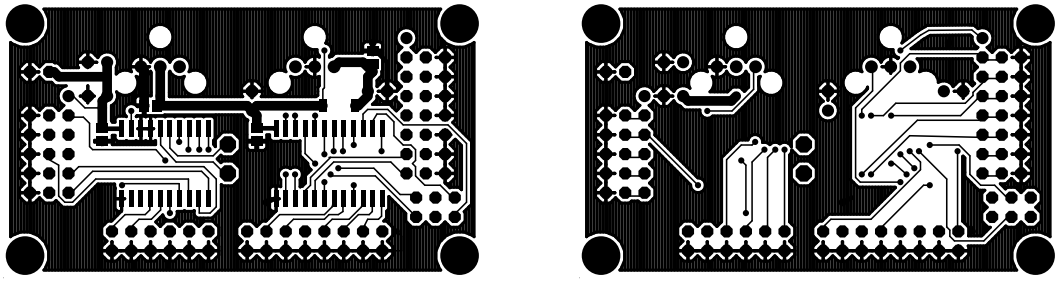

Figure A.19. ADAT optical interface top and bottom metallization. Left image is top metallization.

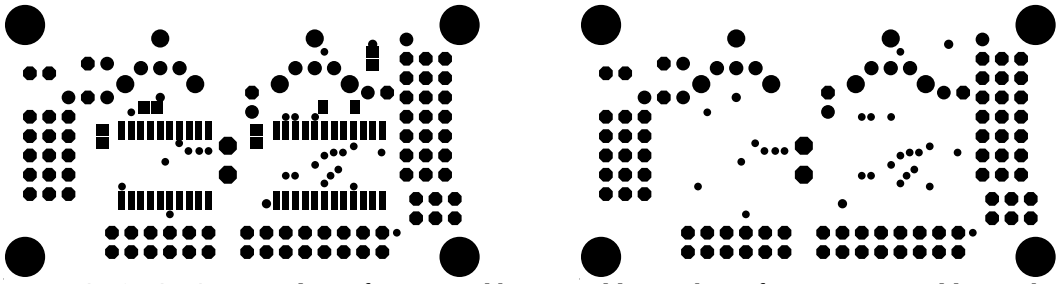

Figure A.20. ADAT optical interface top and bottom solder mask. Left image is top solder mask.

Table A.4. ADAT optical interface parts list

Item	Qty	Value	Parts	Description	Catalog No.	Price	Subtotal
1	4	2.2uF	C1, C2, C3, C4	2.2uF@25V EF Series Tantalum Cap.	P2045-nd	0.324	1.296
2	4	.1uF	C5, C6, C7, C8	0.1uF @50V X7R Ceramic 0805 Cap. (Should have plenty on hand)	PCC1840CT-ND	0.11	0.44
3	1	JP6Q	JP1	Cut from 72 pin Dual Row header if needed	S2011-36-ND	2.37	2.37
4	1	JP8Q	JP2	0.1uF @50V X7R Ceramic 0805 Cap.	S2011-36-ND	2.37	2.37
5	1	JP5Q	JP3	Cut from 72 pin Dual Row header	S2011-36-ND	2.37	2.37
6	1	JP7Q	JP4	Cut from 72 pin Dual Row header	S2011-36-ND	2.37	2.37
7	1	JP3QE	JP5	Cut from 72 pin Dual Row header if needed		2.37	2.37
8	1	JP1Q	JP6	Cut from 72 pin Dual Row header		2.37	2.37
9	1	L4516C	L1	Steward EMI chip 1806 pkg 100ohms	240-1031-1-ND	0.313	0.313
10	1	GP1F32T	OK1	Sharp Toslink transmitter module GP1F32T	GP1F32T		0
11	1	GP1F32R	OK2	Sharp Toslink receiver module GP1F32R	GP1F32R		0
12	2	P1-13	P1, P2				0
13	1	33K	RN1	2% Thick film SIP Resistor network 5 elements	Q5333-ND	0.25	0.25
14	1	33K	RN2	2% Thick film SIP Resistor network 7 elements	Q7333-ND	0.33	0.33
15	1	AL1401A	U1	Alesis ADAT interface transmitter OptoGen	AL1401A		0
16	1	AL1402	U2	Alesis ADAT interface receiver OptoRec	AL1402		0
	1	6.8K	RN1	2% Thick film SIP Resistor network 5 elements	770-61-R6.8k	0.21	0.21
	1	6.8K	RN2	2% Thick film SIP Resistor network 7 elements	770-81-R6.8k	0.29	0.29
	1	JP5Q	JP3	Digikey precut version	S2011-05-ND	1.32	1.32
	1	JP7Q	JP4	Digikey precut version	S2011-07-ND	1.4	1.4
	1	JP1Q	JP6	Digikey precut version		1.16	1.16
	20			Shorting jumpers	SSC02SYAN	0.131	2.62
The above non number items may be needed for alternative configurations							
Most catalog numbers are from Digi-key, Theif River Falls, MN							
ADAT optical interface board parts lists							

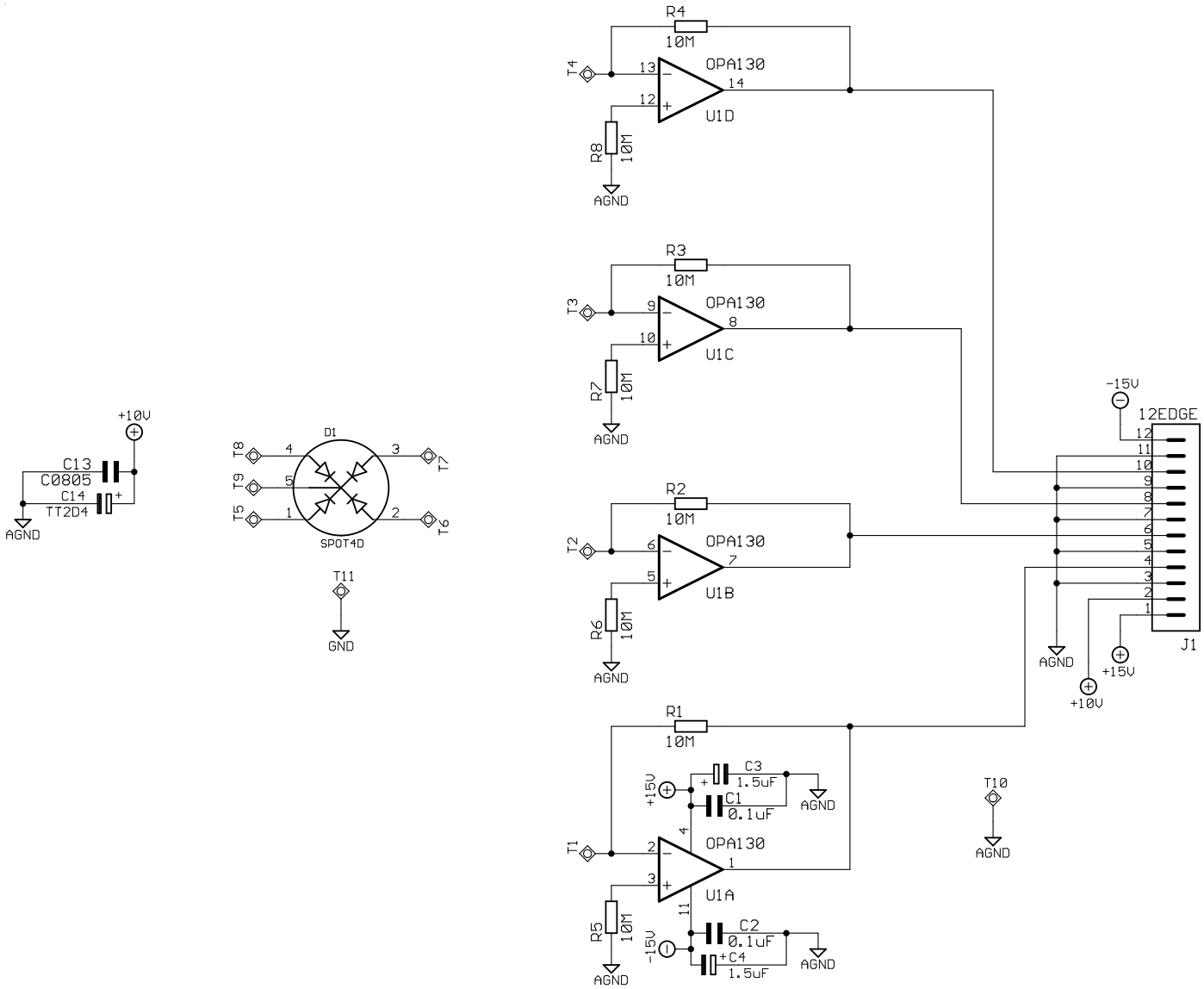

Figure A.21. Quad photodiode transimpedance amplifier schematic.

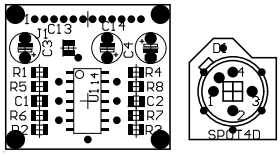

Figure A.22. Quad photodiode transimpedance amplifier top silk-screen (approx. 1:1 scale).

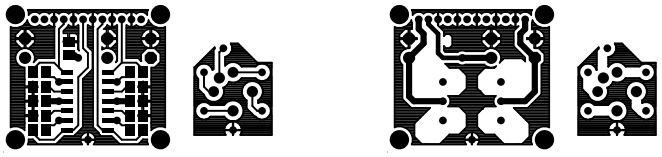
Figure A.23. Quad photodiode transimpedance amplifier top and bottom metallization. Left image is top metallization.

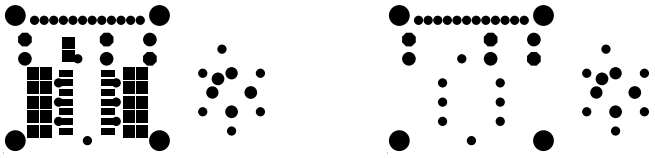
Figure A.24. Quad photodiode transimpedance amplifier top and bottom solder mask. Left image is top solder mask.

Table A.5. Quad photodiode transimpedance amplifier parts list

Item	Qty	Value	Parts	Description	Catalog No.	Price	Subtotal
1	3	0.1uF	C1, C2, C13	0.1uF @50V X7R Ceramic 0805 Cap. (Should have plenty on hand)	PCC1840CT-ND	0.11	0.33
2	3	1.5uF	C3, C4, C14	1.5uF@25V EF Series Tantalum Cap.	P2044-ND	0.291	0.873
3	1	SPOT4D	D1	Quad Diodes SPOT-4DMI, or SD 085-23-21-021 or SD 197-23-21-041 or SPOT-4D			0
4	1	12EDGE	J1	0.1uF @50V X7R Ceramic 0805 Cap.			0
5	8	10M	R1, R2, R3, R4, R5, R6, R7, R8	1/8W 1% 0805 pkg resistor thick film		0.14	1.12
6	11	SMPAD	T1, T2, T3, T4, T5, T6, T7, T8, T9, T10,T11	Solder points for Quad Diode mount			0
7	1	OPA4130	U1	Quad FET input op-amp SOIC 14 pkg		7.74	7.74
	8	20M	R1, R2, R3, R4, R5, R6, R7, R8	1/8W 5% 0805 pkg resistor thick film		0.14	1.12
The above non number items may be needed for alternative configurations							
Most catalog numbers are from Digi-key, Theif River Falls, MN							
Quad photodiode transimpedance amplifier parts list							

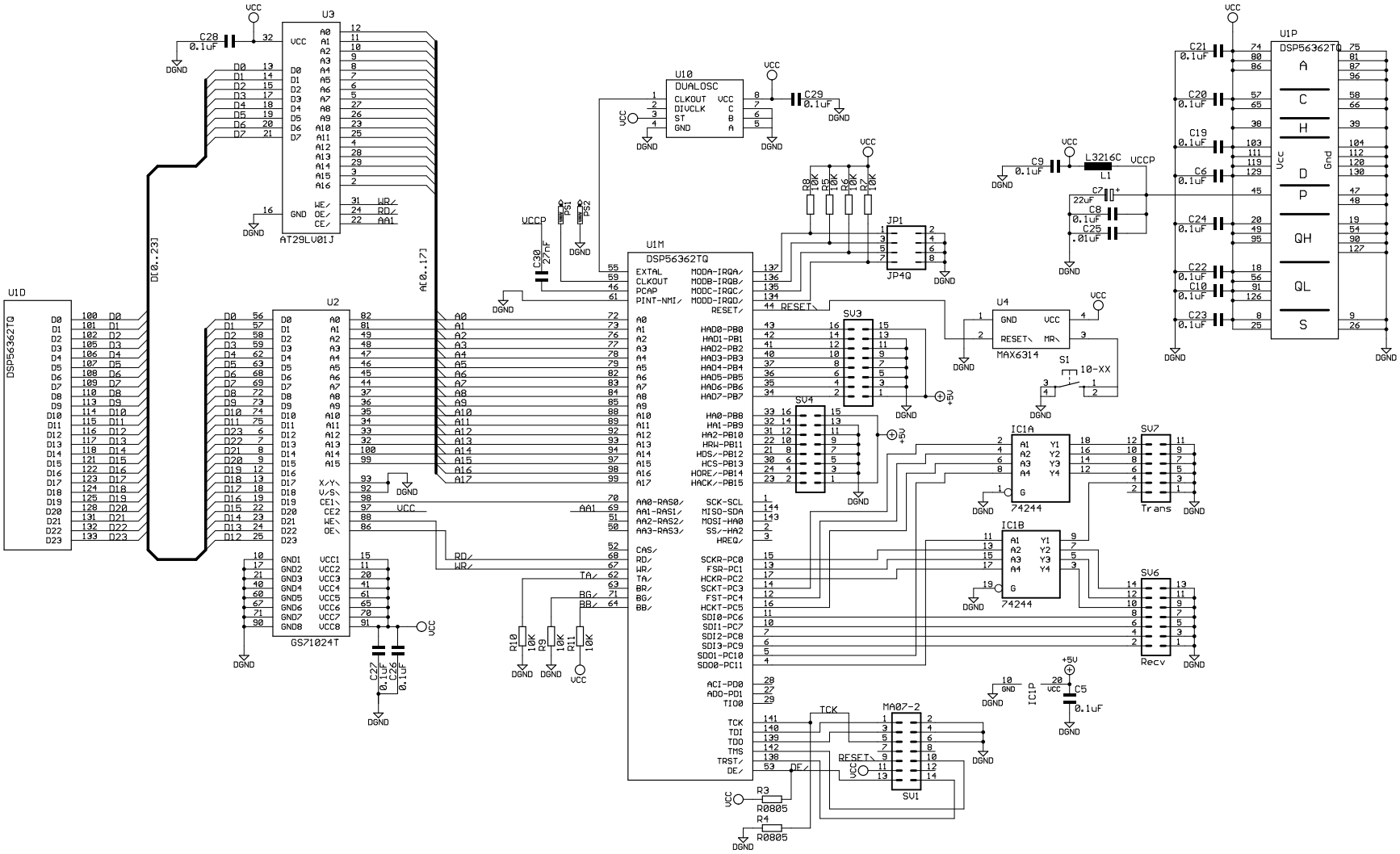

Figure A.25. DSP56362 board main logic schematic

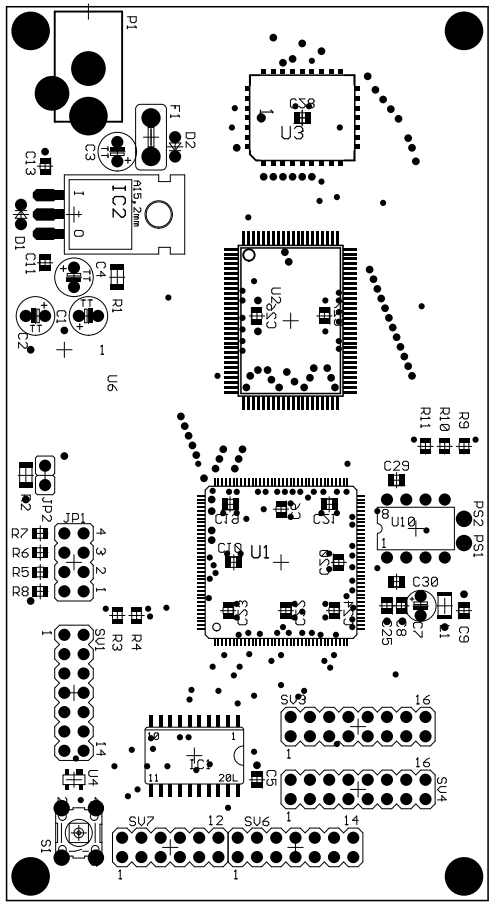

Figure A.27. DSP56362 board top silk-screen (approx. 1:1 scale).

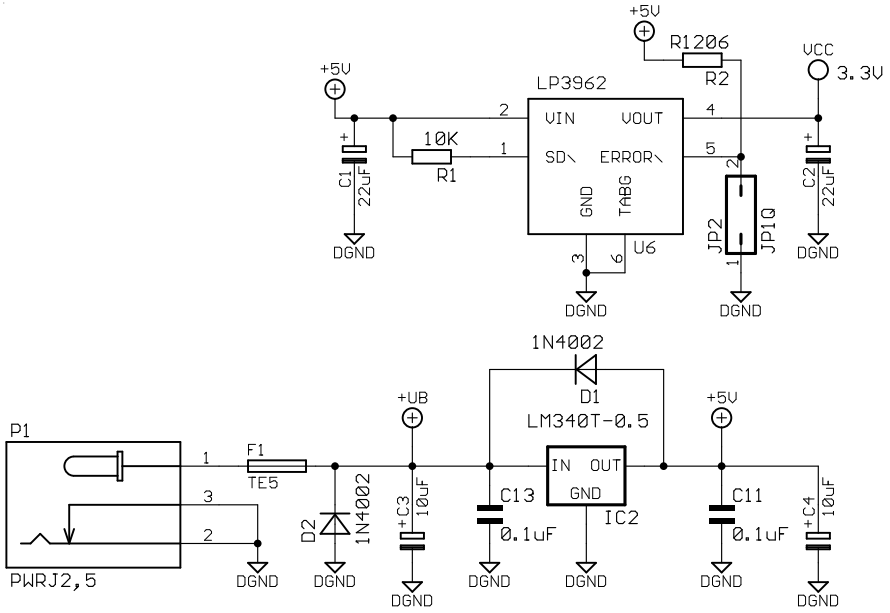

Figure A.26. DSP56362 main board power regulator section schematic.

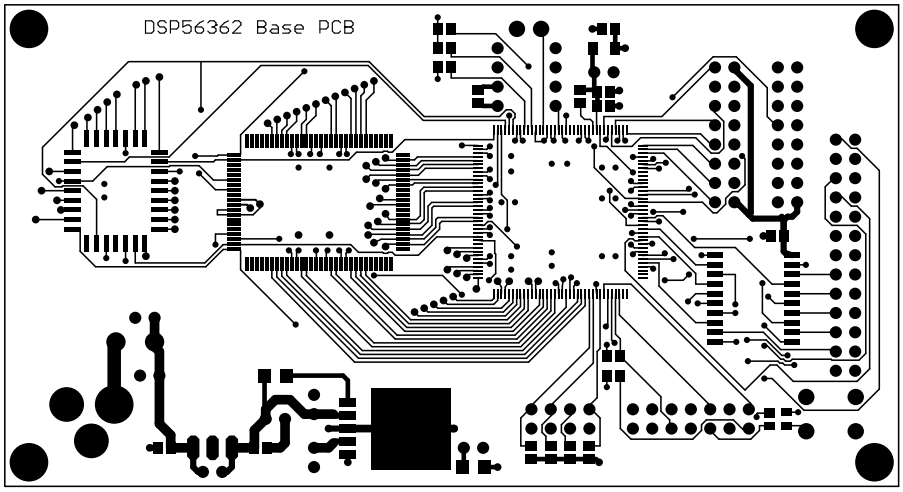

Figure A.28. DSP56362 board top metallization.

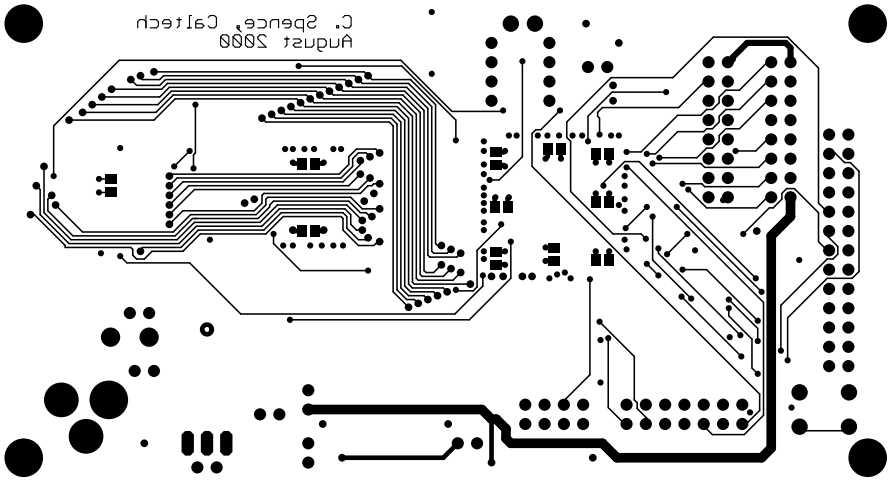

Figure A.29. DSP56362 board bottom metallization.

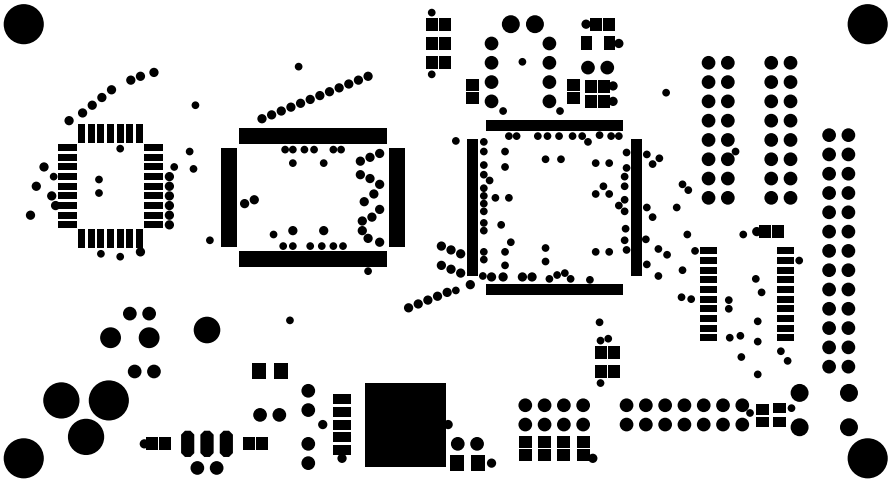

Figure A.30. DSP56362 board top solder mask.

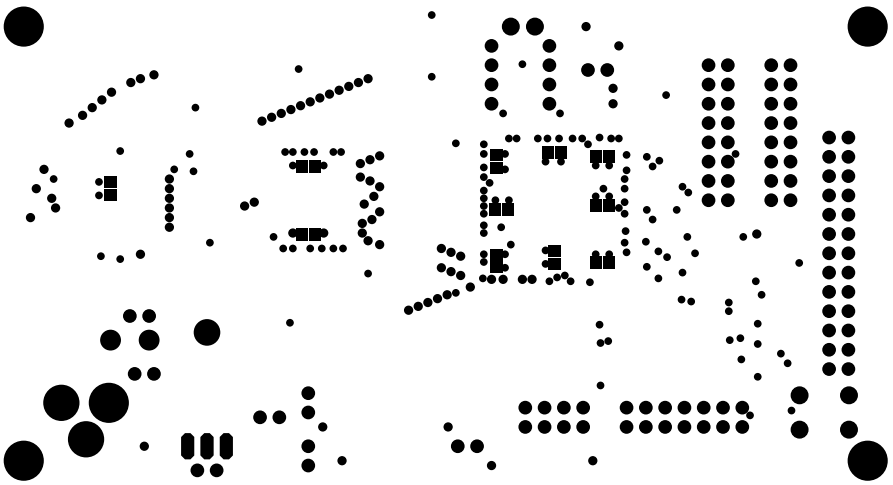

Figure A.31. DSP56362 board bottom solder mask.

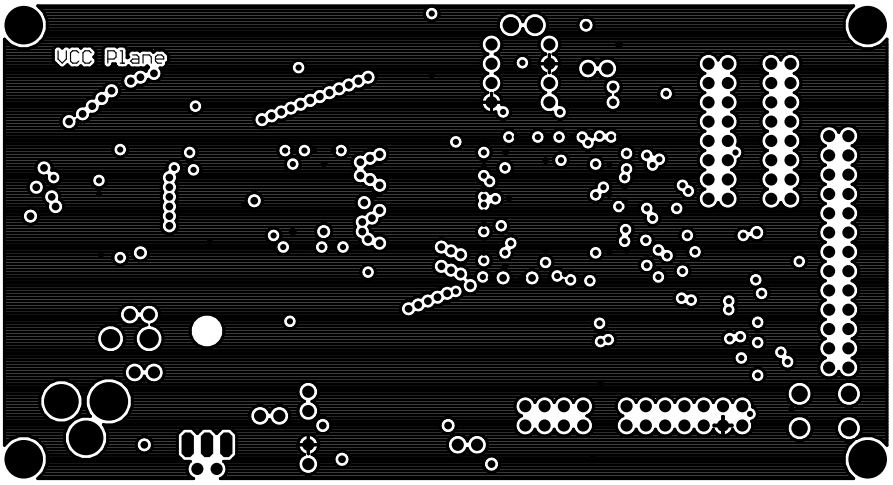

Figure A.32. DSP56362 board power plane.

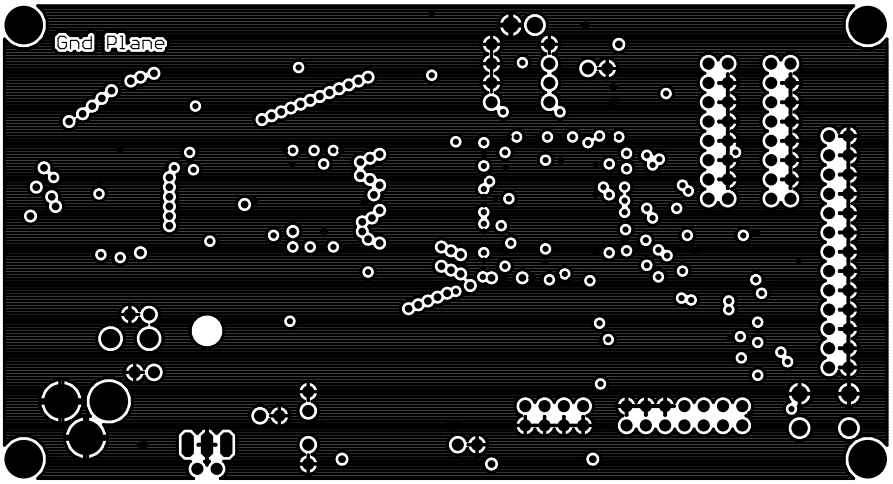

Figure A.33. DSP56362 board ground plane.

Table A.6. DSP56362 board parts list

DSP56362 Evaluation PCB Bill of Materials							
Created 9/2/00 from bom.ulp from Eagle PCB layout CFS							
Partlist exported from C:\Program Files\EAGLE\projects\DSP362st2.brd at 8/31/2000 03:23:54p							
Item	Qty	Value	Parts	Catalog No.	Description	Cost/Units	Subtotal
1							
2	2	22uF	C1, C2	P2028-ND	22uF@10V Tant. Cap. EF Series leaded	0.71	1.42
3	1	.01uF	C25	PCC103BNCT-ND	0.01uF@50V X7R Ceramic Chip Cap. 0805	0.08	0.08
4	2	10uF	C3, C4	P2049-ND	10uF@25V Tant. Cap. EF Series leaded	1.06	2.12
5	1	27nF	C30	PCC1833CT-ND	27nF@50V X7R Ceramic Chip Cap. 0805pkg	0.13	0.13
6	17	0.1uF	C5, C6, C8, C9, C10, C11, C13, C19, C20,C21, C22, C23, C24, C26, C27, C28, C29	PCC1840CT-ND	0.1uF@50V X7R Ceramic Chip Cap. 0805pkg.	0.12	2.04
7	1	22uF	C7	P2028-ND	22uF@10V Tant. Cap. EF Series leaded	0.71	0.71
8	2	1N4002	D1, D2	1N4004DICT-ND	100PIV@1A Diode Rectifier	0.043	0.086
9	1	TE5	F1	RUE110-ND	1.1Amp Polyswitch	0.62	0.62
10	1	74HCT244	IC1	MM74HCT244WM-ND	Tri-State Octal Buffer SO-20 pkg.	0.8	0.8
11	1	LM340T-5.0	IC2	LM340T-5.0-ND	5.0V 1A Positive Voltage Reg. TO-220	0.7	0.7
12	1	JP4Q	JP1	S2011-36-ND	Cut from Dual Row Straight 72 pin Header	2.37	2.37
13	1	JP1Q	JP2		wire jumper as needed		0
14	1	L3216C	L1	TKS1025CT-ND	1.0uH SMD type 32CS inductor	1.5	1.5
15	1	PWRJ2,5	P1	CP-002A-ND	2.0mm Male pwr jack closed	0.38	0.38
16	2	P1-13	PS1, PS2				0
17	1	10.2K	R1	MCR10F1022	10.2K 1/8W 1% Thick Film 0805 SMT res.	0.069	0.069
18	1	10.2K	R2	MCR10F1022	10.2K 1/8W 1% Thick Film 0805 SMT res.	0.069	0.069
19	2	10.2K	R3, R4	MCR10F1022	10.2K 1/8W 1% Thick Film 0805 SMT res.	0.069	0.138
20	7	10.2K	R5, R6, R7, R8, R9, R10, R11	MCR10F1022	10.2K 1/8W 1% Thick Film 0805 SMT res.	0.069	0.483

21	1	10-XX	S1	SW400-ND	Keyswitch 6mm mom 100gf Omron	0.24	0.24
22	1	MA07-2	SV1	S2011-36-ND	Cut from Dual Row Straight 72 pin Header. Cut one of the center pins.	2.37	2.37
23	2		SV3, SV4	S2011-36-ND	Cut from Dual Row Straight 72 pin Header	2.37	4.74
24	1	Recv	SV6	S2011-36-ND	Cut from Dual Row Straight 72 pin Header	2.37	2.37
25	1	Trans	SV7	S2011-36-ND	Cut from Dual Row Straight 72 pin Header	2.37	2.37
26	1	DSP56362TQ	U1				0
27	1	DUALOSC	U10	XC317-ND	ECS 24.576Mhz Dual out Crystal Osc 8-dip. Must buy 35	5.81	5.81
28	1	GS71024T	U2				
29	1	AT29LV01J	U3				
30	1	MAX6314	U4				
31	1	LP3962	U6				
	2		C1,C2	P2017-ND	47uF@6.3V Tant. Cap. EF-Series	0.83	
	1		IC1 alt	296-1070-5-ND	SN74ACT244DW Tri-State Octal Buffer SO-20 pkg.	0.96	
	1		P1 mate	SC1052-ND	Too expensive 2.1mm Power Plug	2.91	
	1		P1 mate	CP-004A-ND	Cheaper but plug too long	0.65	
	4		Spacers	1801BK-ND	2-56x.25" Al round threaded spacers	0.37	0.37
	4		Spacers alt.	1801AK-ND	2-56x.187" Al round threaded spacers	0.374	0.374
	4		Screws	J130-ND	2-56x.25" Slotted Panhead screws	0.0412	0.0412
	1		SV1 mate	A3AAG-1406G-ND	14 Contact 6" Header to Header conn. And ribbon cable assemble	3.36	
The above non number items may be needed for alternative configurations							
Most catalog numbers are from Digi-key, Theif River Falls, MN							

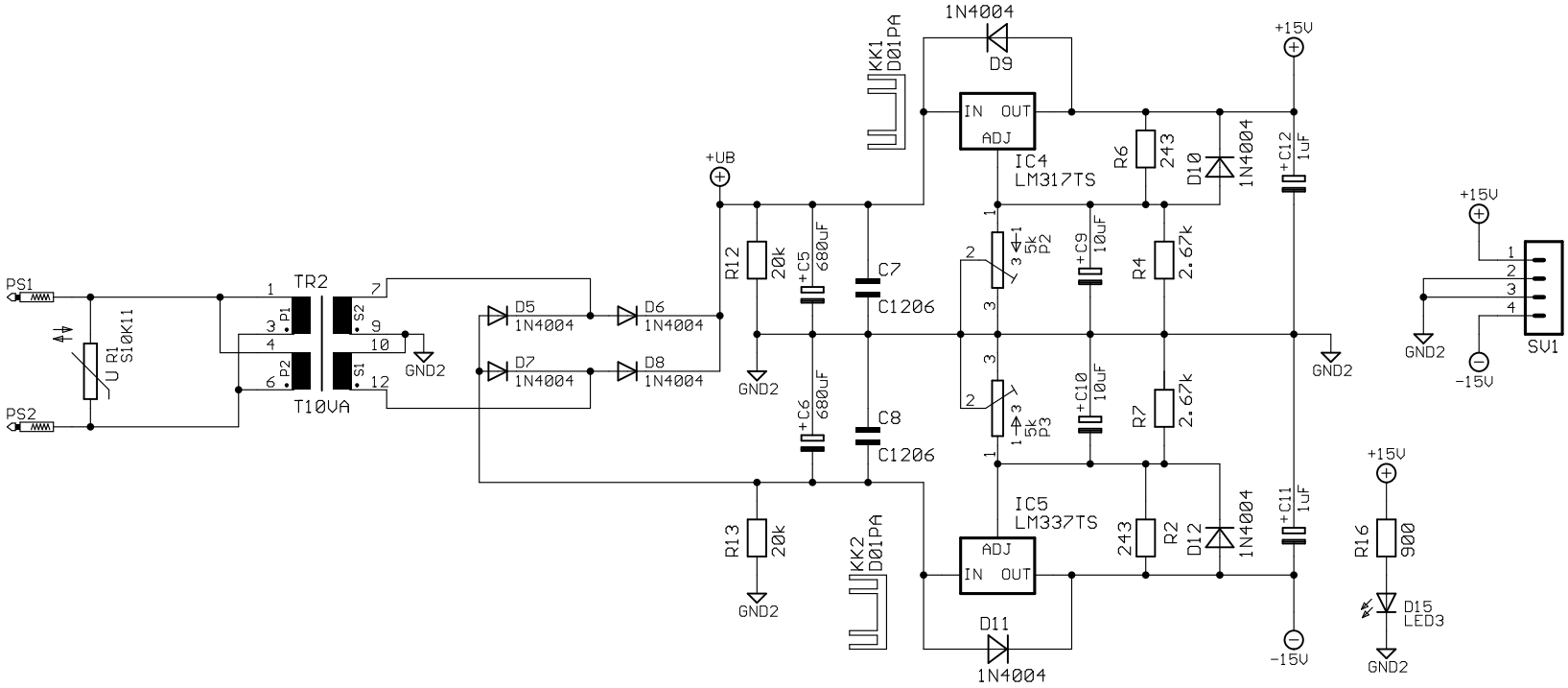

Figure A.34. ± 18 V at 10 VA linear power supply schematic.

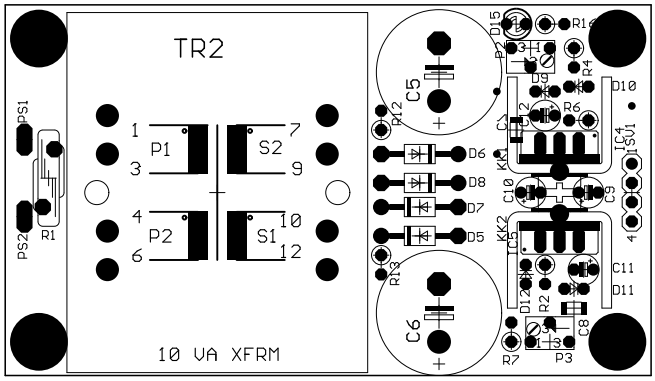

Figure A.35. ±18 V linear power supply top silk-screen (approx. 1:1 scale).

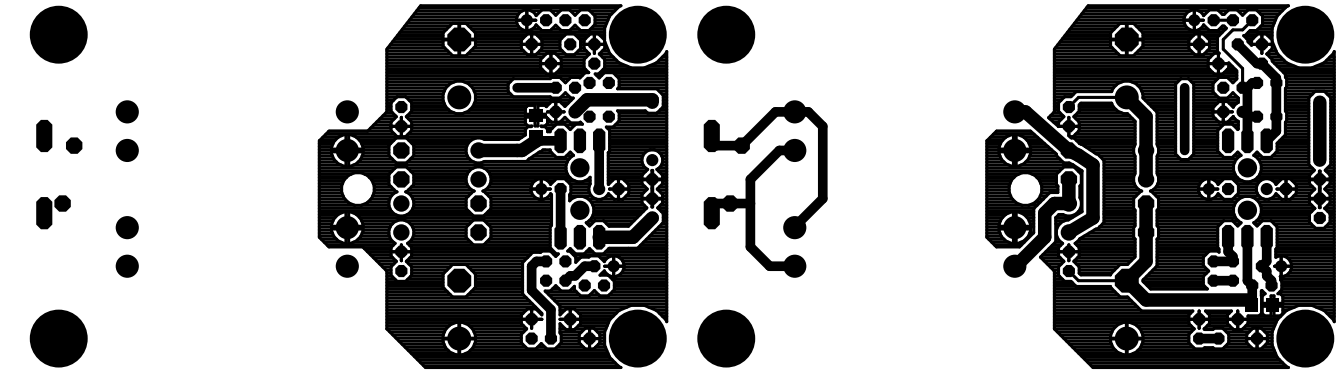

Figure A.36. ±18 V linear power supply top and bottom metallization. Left image is top metallization.

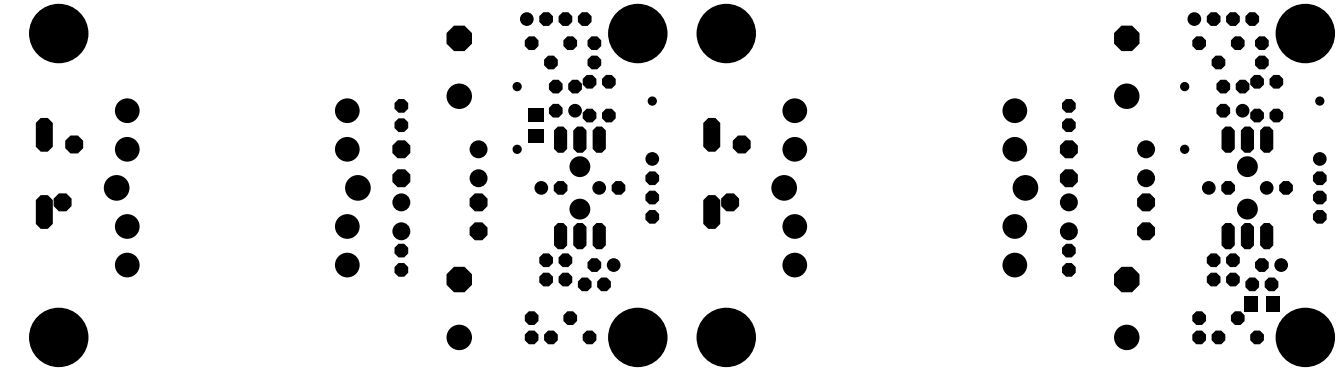

Figure A.37. ±18 V linear power supply top and bottom solder mask. Left image is top solder mask.

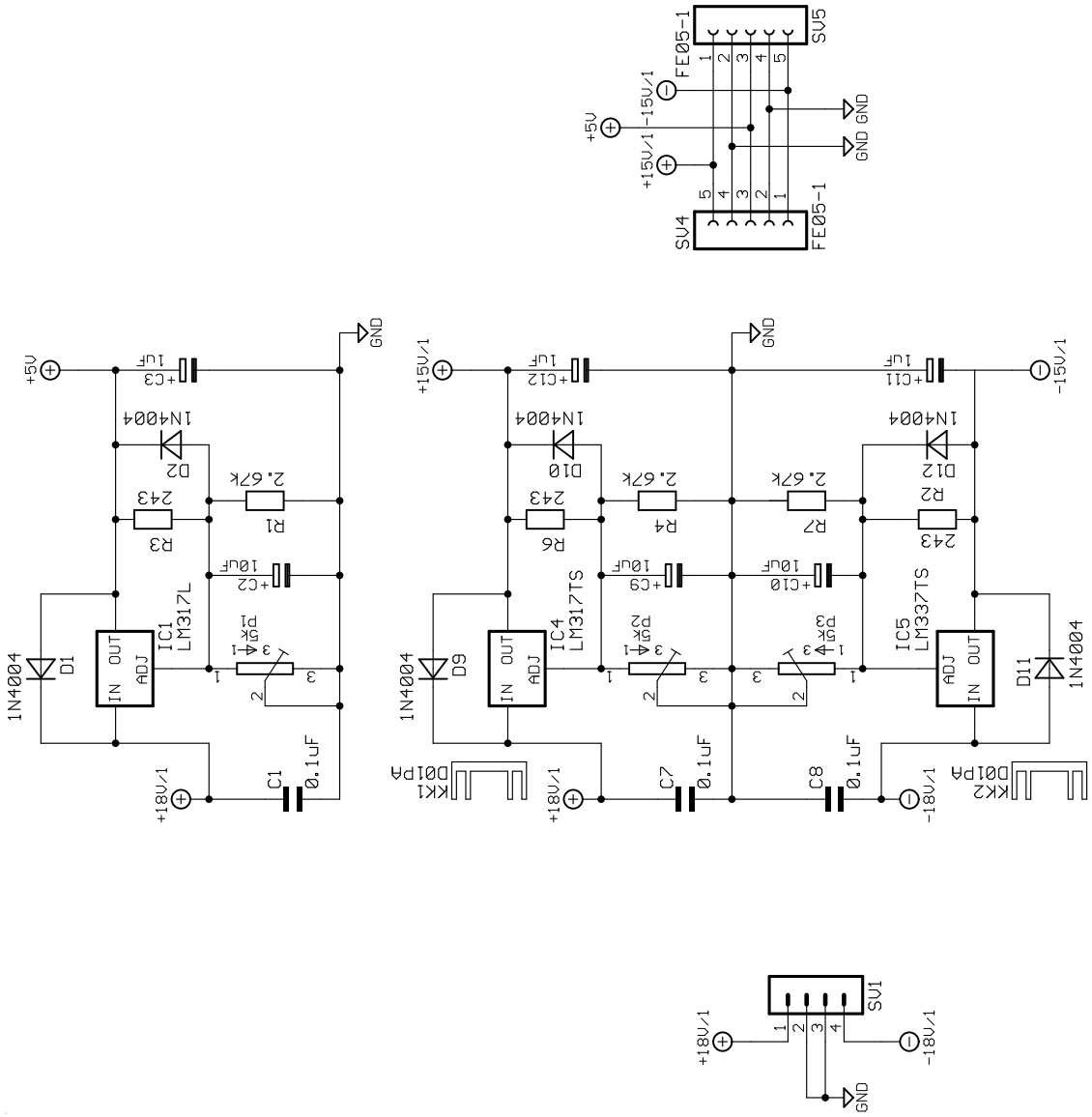

Figure A.38. ±15 V and +5 V regulator board schematic for quad A./D converter circuit power.

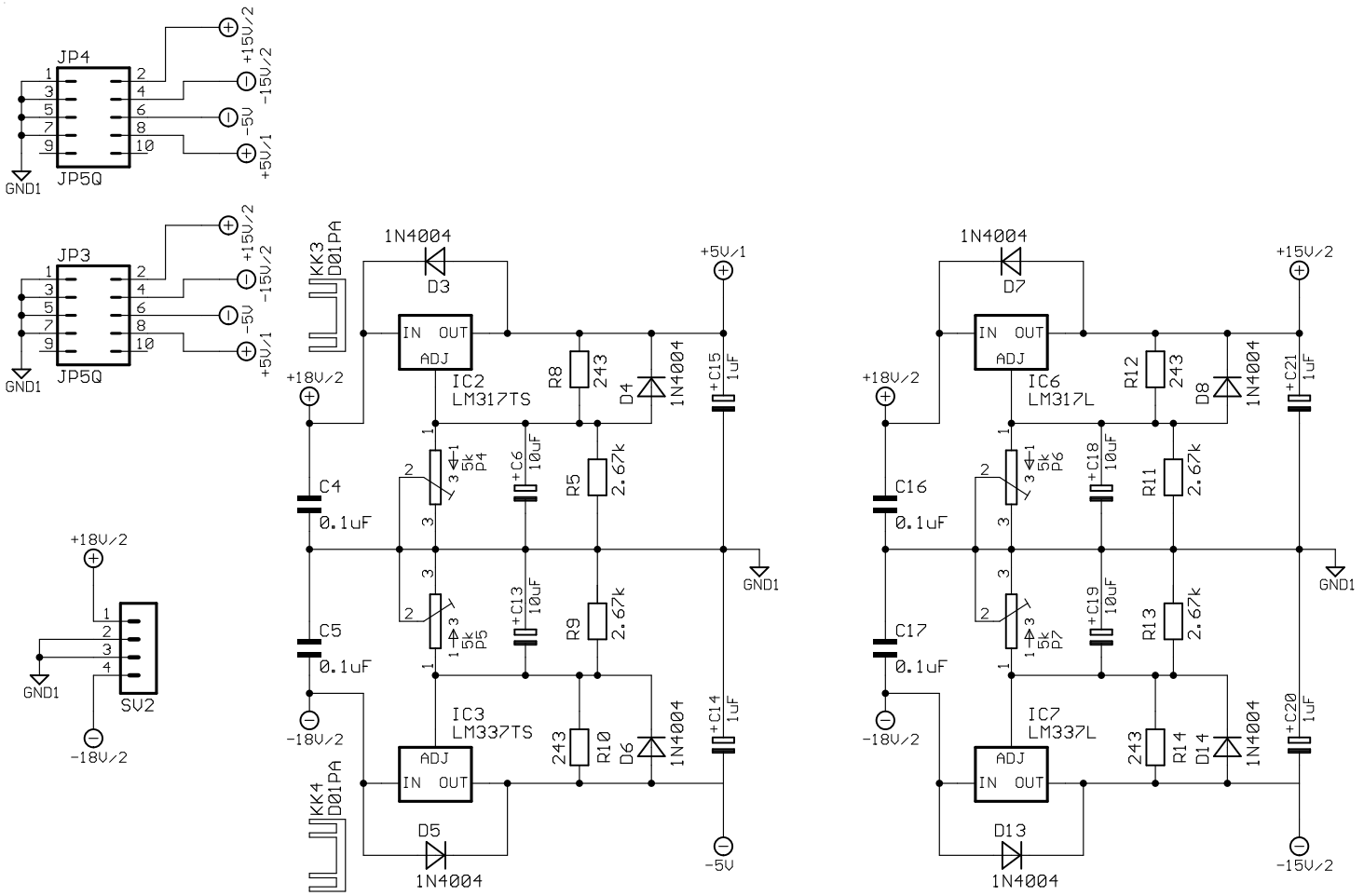

Figure A.39. ±15 v and ±5 V regulator board schematic for D/A converter circuit power.

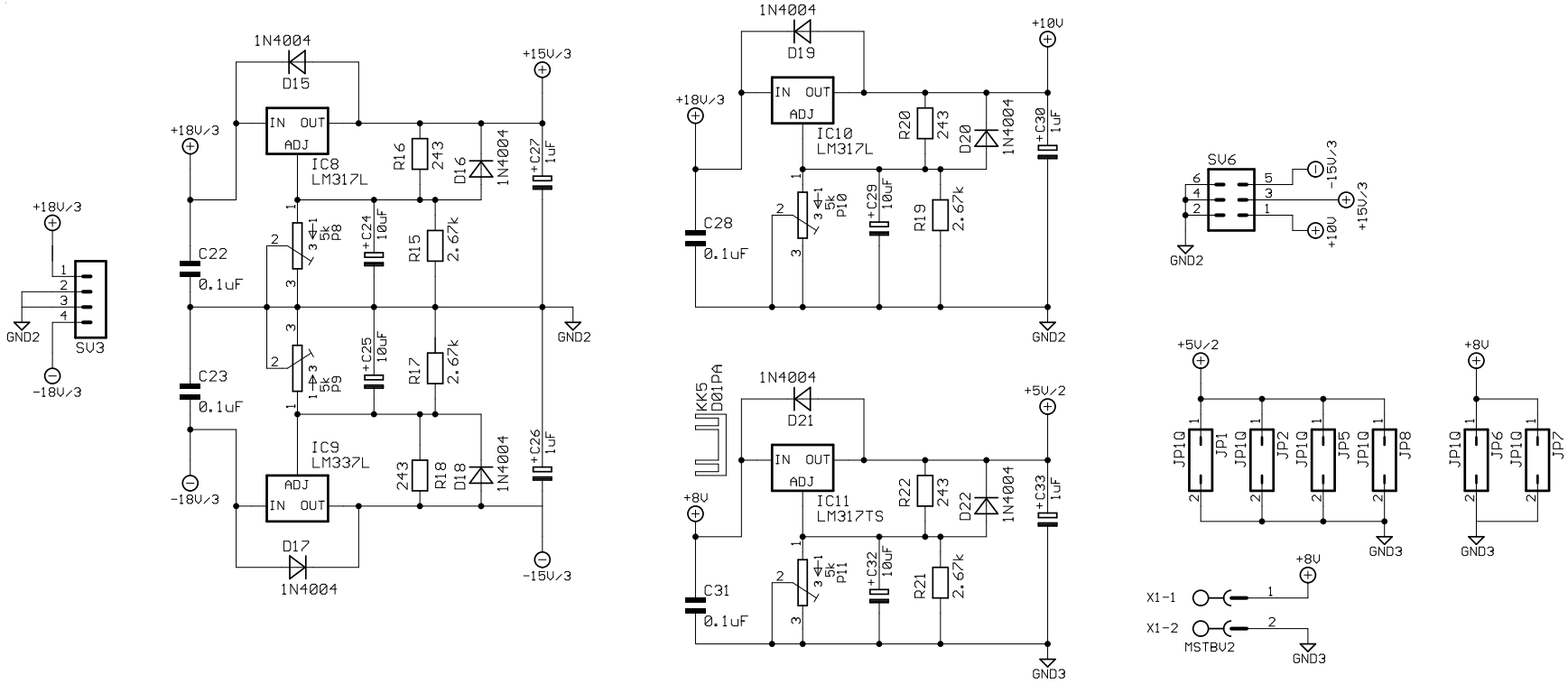

Figuer A.40. ±15 V and +10 V regulator for quad photodiode power and +5V regulator for DSP and ADAT board power schematic.

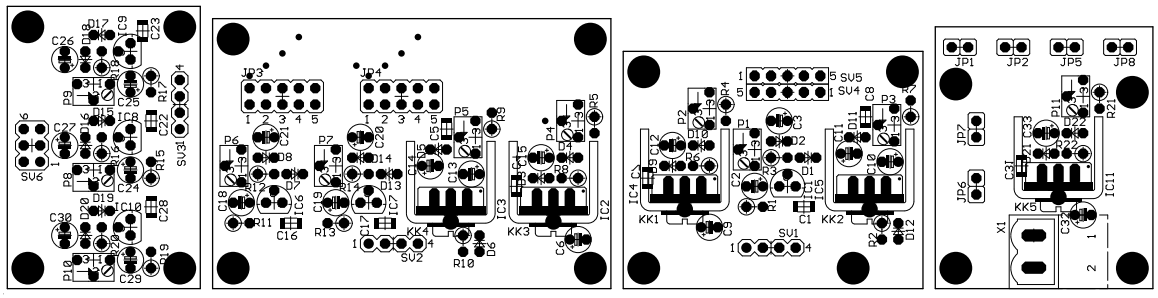

Figure A.41. Multiple regulator board top silk-screen. Starting from the left is the ±15 V, +10V regulator board for the photodiode circuit. Next is the ±15V, ±5 V regulator board for the D/A converter. Next is the ±15V, +5V regulator board for the quad A/D converter. Lastly on the right hand side is the +5 V regulator for the DSP and ADAT boards. Thise layout images have been scaled to fit the page width and should not be scaled.

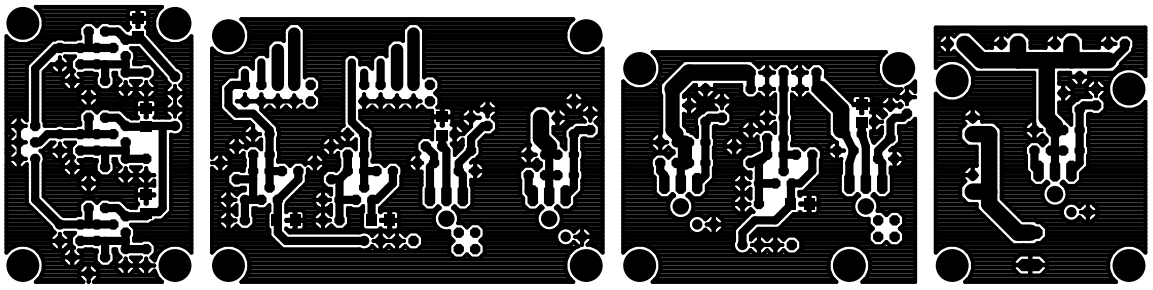

Figure A.42. Multiple regulator board top metallization.

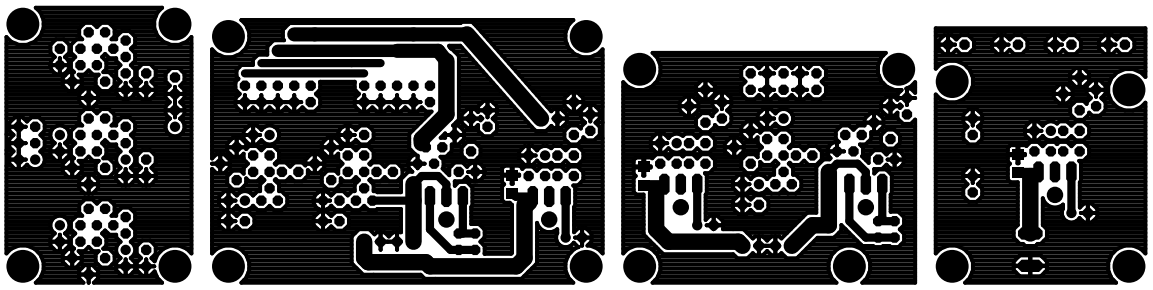

Figure A.43. Multiple regulator board bottom metallization.

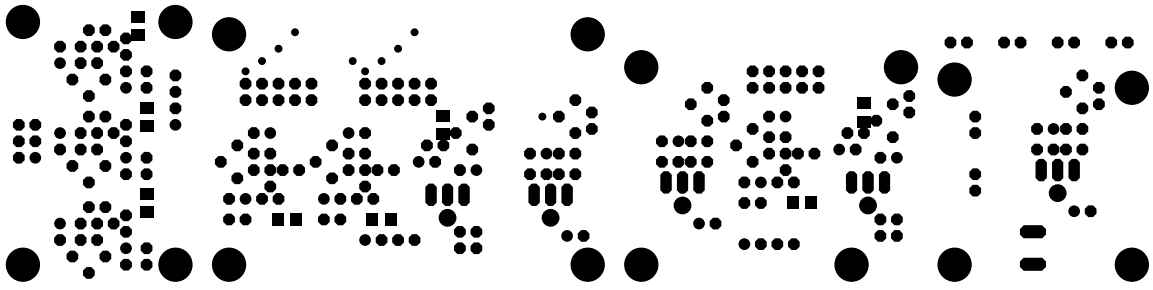

Figure A.44. Multiple regulator board top solder mask.

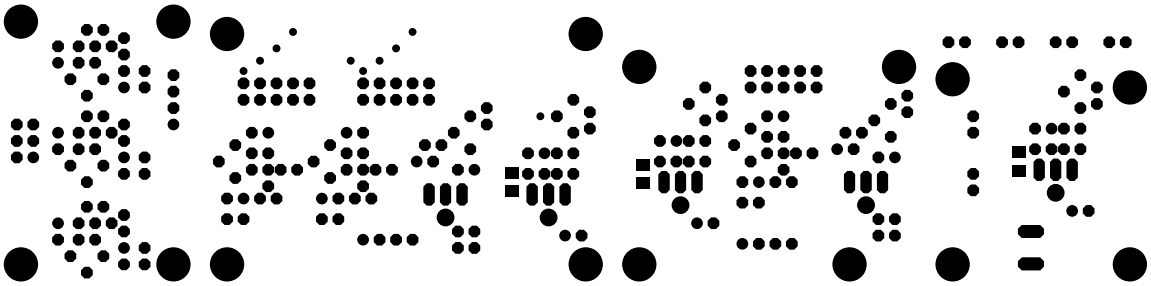

Figure A.45. Multiple regulator board bottom solder mask.

Table A.7. Multiple regulator board parts list

Item	Qty	Value	Parts	Description	Catalog NO.	Price	Subtotal
1	2	2700uF	C1, C5	2700uF@25V FC Series electrolytic	P10286-ND	1.93	3.86
2	18	10uF	C2, C9, C10, C16, C17, C26, C27, C32,C33, C37, C41, C42, C47, C48, C53, C54,C58, C61	10uF@25V EF Series tantalum cap	P2049-ND	0.909	16.362
3	2	330uF	C20, C21	330uF@63V FC Series electrolytic	P10349-ND	1.05	2.1
4	2	680uF	C22, C23	680uF@63V FC Series electrolytic	P10354-ND	1.93	3.86
5	13	0.1uF	C3,C7, C8, C15, C25, C31, C36, C40, C45, C46,C51, C52, C57	0.1uF@100V X7R Ceramic 1206 pkg Cap.	1206B104J101N	0.2	2.6
5b	5	0.1uF	C14, C24, C30, C39, C60	0.1uF@100V X7R Ceramic 1206 pkg Cap.(mounted on solder side of PCB)	1206B104J101N	0.2	1
6	18	2.2uF	C4, C11, C12, C18, C19, C28, C29, C34,C35, C38, C43, C44, C49, C50, C55, C56,C59, C62	2.2uF@35V EF Series tantalum cap.	P2061-ND	0.363	6.534
7	2	100uF	C6, C13	100uF@63V FC Series electrolytic	P10342-ND	0.56	1.12
9	4	1N5402	D1, D2, D3, D4	1N5402 200PIV@3A Rectifier Diode	1N5402DICT-ND	0.204	0.816
10	36	1N4002	D5, D6, D12, D13, D14, D15, D21, D22,D23, D24, D30, D31, D32, D33, D35, D36,D37, D38, D39, D40, D41, D42, D43, D44,D45, D46, D47, D48, D49, D50, D51, D52,D53, D54, D55, D56	1N4002 200PIV@1A Recifier Diode	1N4002DICT-ND	0.043	1.548
11	4	LED3	D7, D16, D25, D34	Do Not Install			0
12	12	1N4002	D8, D9, D10, D11, D17, D18, D19, D20,D26, D27, D28, D29	1N4002 200PIV@1A Recifier Diode	1N4002DICT-ND	0.043	0.516
13	5	LM317L	IC1, IC10, IC13, IC15, IC17	LM317LZ 100mA Pos. adj. Volt reg. TO-92 pkg	LM317LZ-ND	0.3752	1.876
14	6	LM317TS	IC2, IC4, IC6, IC8, IC11, IC18	LM317T 1.5A Pos. adj. Volt reg. TO-220 pkg	LM317T-ND	0.98	5.88

15	3	LM337L	IC3, IC14, IC16	LM337LZ 100mA Neg. adj. Volt reg. TO-92 pkg	LM337LZ-ND	1.82	5.46
16	4	LM337TS	IC5, IC7, IC9, IC12	LM337T 1.5A Neg. adj. Volt reg. T0-220 pkg	LM337T-ND	1.54	6.16
17	6	JP1Q	JP1, JP2, JP5, JP6, JP7, JP8	2 Pin C-Grid Pocket header Molex.	WM4800-ND	0.85	5.1
18	2	JP5Q	JP3, JP4	10 Pin dual row header. Digikey precut version	S2011-05-ND	1.32	2.64
19	1	SK129	KK1	Aavid TO-220 heat sink 529802 w/ solder pins big	HS188-ND	1.55	1.55
20	9	D01PA	KK2, KK3, KK4, KK5, KK6, KK7, KK8, KK9,KK10	Aavid TO-220 heat sink 577202	HS107-ND	0.35	3.15
21	18	5k	P1, P2, P3, P4, P5, P6, P7, P8, P9, P10,P11, P12, P13, P14, P15, P16, P17, P18	5K 1/4" Multiturn Cermet Pot 3266 Series Bourns	3266W-502-ND	3.25	58.5
22	8	P1-17Y	PS1, PS2, PS3, PS4, PS5, PS6, PS7, PS8	Wire solder points no parts to install			0
23	4	S10K11	R1, R22	130VAC Series 10 D-Type Varistor Panasonic	P7205-ND	0.46	1.84
23b	2	S10K11	R6, R11	Do Not Install	P7205-ND	0.46	0.92
24	7	9.76k	R2, R12, R13, R18, R19, R26, R27	9.76K@1/4W 1% Metal Film resistor	9.76KXBK-ND	0.108	0.756
25	18		R3, R7, R9, R14, R17, R23, R25, R30,R32, R34, R36, R38, R40, R42, R44, R46,R48, R50	Do Not Install	3.32KXBK-ND	0.108	1.944
26	18	243	R4, R8, R10, R15, R21, R24, R29, R31,R33, R35, R37, R39, R41, R43, R45, R47,R49, R51	243@1/4W 1% Metal Film resistor	243XBK-ND	0.108	1.944
27	4	2.00K	R5, R16, R20, R28	2.00K@1/4W 1% Metal Film resistor	2.00KXBK-ND	0.108	0.432
28	3		SV1, SV2, SV3	4 Pin C-Grid straight Pocket header Molex **********INSTALL BACKWARDS FROM SILKSCREEN	WM4802-ND	1.045	3.135
28	3		SV6, SV7, SV8	4 Pin C-Grid straight Pocket header Molex	WM4802-ND	1.045	3.135

29	1	FE05-1	SV4, SV5	This is one part. 10 Pin dual row header. Digikey precut version	S2011-05-ND	1.32	1.32
30	1		SV9	6 Pin dual row header. Digikey precut version	S2011-03-ND	1.24	1.24
31	1	T20VA	TR1	10VAC@2A 20VA xfrm. Microtran Worldtran	MT3122-ND	11.41	11.41
32	1	T2,5VA	TR2	36VCT@70mA 2.5VA xfrm Microtran Worldtran	MT3137-ND	7.97	7.97
33	1	T5,0VA	TR3	36VCT@140mA 5.0VA xfrm Microtran Worldtran	MT3138-ND	8.6	8.6
34	1	T10VA	TR4	36VCT@280mA 10VA xfrm Microtran Worldtran	MT3139-ND	9.47	9.47
35	2	MSTBV2	X, X1	Conn. Term Block Plug 2 Pos 5.08mm	277-1011-ND		184.748
				Conn. Header Vert. 2 Pos 5.08mm	277-1128-ND		
				Mica heatsink insulator			
				Mounting screws			
				heatsink grease			
				Insulating mounting shoulder washers			
				Aavid TO-220 heatsink w/ tab shorter 577102	HS213-ND		
				Mouser has 577202B04000 in stock w/ Tabs			
	2	3300uF	C1, C5	3300uF@25V FC Series electrolytic	P10287-ND	2.05	
	18	3.3uF	C4, C11, C12, C18, C19, C28, C29, C34,C35, C38, C43, C44, C49, C50, C55, C56,C59, C62	3.3uF@35V EF Series tantalum cap.	P2062-ND	0.427	
	1	SK129	KK1	Aavid TO-220 heat sink 529902 w/ solder pins big	HS229-ND	1.83	
25	18	15.0K	R3, R7, R9, R14, R17, R23, R25, R30,R32, R34, R36, R38, R40, R42, R44, R46,R48, R50	15.0K@1/4W 1% Metal Film resistor	15.0KXBK-ND	0.108	

	EAGLE Version 3.55r3 Copyright (c) 1988-1999 CadSoft						
	Partlist exported from C:\Program Files\EAGLE\projects\multips.brd at 1/21/2001 02:40:34p						